國立臺灣大學醫學院分子醫學研究所

博士論文

Institute of Molecular Medicine

College of Medicine

National Taiwan University

Doctoral Dissertation

Dynamin-2 在神經肌肉接合處後端所扮演的角色

The Role of Dynamin-2 in Postsynaptic Neuromuscular Junction

林珊珊

Shan-Shan Lin

指導教授： 劉雅雯 博士

Advisor: Ya-Wen Liu, Ph.D.

中華民國 110 年 1 月

Jan 2021

doi:10.6342/NTU202100043

國立臺灣大學博士學位論文
口試委員會審定書

Dynamin-2 在神經肌肉接合處後端所扮演的角色

The Role of Dynamin-2 in Postsynaptic Neuromuscular Junction

本論文係林珊珊君（F04448002）在國立臺灣大學分子醫學研究所完成之博士學位論文，於民國 110 年 1 月 8 日承下列考試委員審查通過及口試及格，特此證明

口試委員：劉雅惠（簽名）

（指導教授）

李昌允　潘俊良

傅琪鈺　李孝

系主任、所長 潘俊良（簽名）

doi:10.6342/NTU202100043

本研究榮獲財團法人罕見疾病基金會
「第22屆罕見疾病博碩士論文獎助學金」獎助
謹於此特別致謝

doi:10.6342/NTU202100043

致謝

在分醫所的這六年裡我學會最重要的事情就是要有耐心。自小我就是個急性子的人，能當天搞定的事我一定不會拖到隔天，這樣的我在進入分醫所後受到很大的衝擊，因為很少有事情是能讓我當天搞定的。舉凡做不出的實驗、看不懂的 paper，或是一改再改、一投再投的期刊論文，沒有事情是能一步到位。在分醫所的每一天我都在練習成為一個對自己有耐心的人。

回憶起碩一那年，每個禮拜的 jorunal club 簡直是我的噩夢，除了上課前必拉肚子外，為了能表現得和其他同學差不多，我每次都在 paper 上寫滿講稿，如此一來，當我的組員可以直接看圖用流暢的英文表達時，輪到我報告我至少也能照稿子讀出來。我深知自己程度落後於其他同學，但也知道懊惱於大學時期的懶散是毫無用處的，想要跟其他人看起來一樣游刃有餘，我只能好好努力。

六年過去，雖仍稱不上厲害，但至少沒有以前弱。不論專業知識、心態、抗壓性都比以前好多了。而能有這些成長都要歸功於一路上遇見的老師、同學、還有許許多多的貴人。

我非常感謝我的指導教授 劉雅雯老師，謝謝您沒有在我說要休學時放棄我，讓我有機會碰觸到那個「我喜歡做研究」的瞬間。謝謝您除了研究外也給我許多精神上的支持，讓時常懷疑自己的我能重整旗鼓、挑戰極限。我還要感謝給予我許多研究上指教的潘俊良老師、李芳仁老師、University of Michigan 的 Allen 老師，各位老師不論是專業、教學，或是為人處事都是我學習的榜樣，謝謝您們曾在我報告後給予鼓勵，這對當時的我而言意義非凡，也成為我一路上進步的動力。謝謝我的口試委員姚季光老師和傅琪鈺老師，不論是進度報告或是個別討論，都給我許多實驗上的指引和建議，有您們的幫忙才能讓這篇研究能成功發表

doi:10.6342/NTU202100043

在好期刊。

感謝台大TechComm的以君和佩穎學姊、顯微影像核心的華蔓、中研院CryoEM core 的慧茹學姊、中研院生化所的瓊雯和香儀學姊、國家實驗動物中心的純芳學姊，謝謝你們實驗上的協助和指導，讓這篇論文能夠完成。

我還要感謝實驗室兩位學姊梅均和嘉雯，謝謝梅均當一隻領頭羊帶大家奔向逕博的旅途，霸氣的為我們這些小羊開路，也謝謝嘉雯，當初因為有妳一起作伴我才勇敢的直升博班，謝謝妳們的陪伴，和你們一起出國開會、自助旅行是我博班期間最美好的回憶，未來不論妳們在哪裡工作，我也會持續做妳們的後盾。謝謝宗霖和佑安，你們的努力上進讓學姊們自愧弗如，謝謝你們帶給實驗室這麼多正能量，相信你們的態度會領你們飛到很高的地方。

最後我想感謝我的家人，謝謝你們對我充滿信心，在我實驗撞牆、心情低落時帶我出門吃好料，在我實驗成功、期刊發表後也陪我吃好料。謝謝你們就算聽不懂我到底在做什麼研究也總是「好酷！」「好厲害！」「太神奇了！」的使勁捧場，無意間成為我做研究的助力。謝謝我的男友韻峯，看著你總是氣定神閒地做好每件事，讓容易緊張焦慮的我也學會放寬心，謝謝(曾經)同為博士生的你百分百理解博士生會遇到的瓶頸和困難，也一直作為我最穩健的支持和依靠。

謝謝所有在這段旅程幫助過我的人。學海無涯，我會帶著感謝的心繼續努力，畢業只是另一個旅程的開始！

doi:10.6342/NTU202100043

中文摘要

Dynamin 是一種大型 GTP 水解酶，因其在胞吞過程中催化膜分裂而聞名。有越來越多研究發現 dynamin 的功能並不侷限於膜上，一些需要機動蛋白重塑的位置，例如足小體、侵襲體、以及板狀偽足上都可以見到 dynamin 的身影。儘管過去研究發現足小體可以調節神經肌肉接合處（neuromuscular junction, NMJ）的發育，且在這些足小體上可以看到 dynamin 的聚集，但 dynamin 是否以及如何調節 NMJ 的發育尚不清楚。在本篇研究中，我們從分子、細胞、及個體的角度來回答這個問題。我們發現廣泛存在於不同細胞的 dynamin 亞型：dynamin-2，具有能被 GTP 水解調控的肌動蛋白綑綁能力，他能聚集在足小體周圍來調控足小體的生長與功能。在動物實驗中，我們還發現 dynamin-2 會影響突觸後細胞骨架以及果蠅的電生理活性。總結來說，我們的研究證實 dynamin-2 能透過調節肌動蛋白骨架重塑，進而促進 NMJ 突觸後發育。

關鍵字：dynamin-2，神經肌肉接合處發育，足小體，肌動蛋白綑綁蛋白質

doi:10.6342/NTU202100043

Abstract

Dynamin is a large GTPase most-known for catalyzing membrane fission during endocytosis. Growing evidence suggests that the function of dynamin is not restricted to membrane but also required at sites where endocytosis-independent actin remodeling occurs: including podosome, invadopodium, and lamellipodium. Although podosome has been shown to regulate NMJ development, and dynamin has been shown enriched at muscle podosomes. Whether and how dynamin regulates NMJ development remained unclear. In this study, we address this question from molecular, cellular, and organismal levels. We revealed that the ubiquitously expressed isoform, dynamin-2, is an actin-bundler with its activity regulated by GTP hydrolysis. It assembles around podosomes to regulate their growth, turnover, and function. On the organismal level, we uncover the impact of dynamin-2 in postsynaptic cytoskeleton and electrophysiological properties. To summarize, our study revealed a novel role of dynamin-2 in actin remodeling, which facilitates the process of postsynaptic NMJ development.

Keywords: dynamin-2, NMJ morphogenesis, podosome, actin-bundling protein

doi:10.6342/NTU202100043

Table of Contents

口試委員會審定書 ..... **i**

致謝財團法人罕見疾病基金會 ..... **ii**

致謝 ..... **iii**

中文摘要 ..... **v**

Abstract ..... **vi**

Table of Contents ..... **vii**

Chapter 1-Introduction **1**

1.1 Dynamin, a well-known catalyzer for membrane fission 1

1.2 The potential function of dynamin at postsynaptic NMJ 3

1.3 Podosome and its role during NMJ development 5

1.4 A tale of dynamin and actin filaments 6

Chapter 2-Material and Methods **8**

2.1 *Drosophila* stocks 8

2.2 Dissecting of *Drosophila* larval body wall muscle 8

2.3 Cell culture 9

2.4 Transfection, lentiviral and adenoviral infection 10

2.5 Immunofluorescent staining 11

2.6 Fluorescence microscopy 12

2.7 Matrix degradation assay 13

2.8 TEM of *Drosophila* NMJs 14

2.9 Electrophysiology of *Drosophila* NMJ 16

2.10 Image analysis 17

2.11 Dynamin expression and purification 17

2.12 F-actin bundle sedimentation assay 18

2.13 Transmission electron microscopy 20

doi:10.6342/NTU202100043

2.14 Quantification and statistical analysis 21

Chapter 3-Results 21

3.1 Dyn2 is enriched at postsynaptic NMJ 21

3.2 Dyn2 affects postsynaptic cytoskeletal organization 22

3.3 CNM-Dyn2 interfere electrophysiological activity of *Drosophila* larval NMJ ..24

3.4 Dyn2 forms belt-shaped structures around the actin core of podosomes 26

3.5 Dyn2 is required for podosome growth 29

3.6 Dyn2 regulates podosome turnover 30

3.7 Actin binding, self-assembly, and GTP hydrolysis activity of Dyn2 are involved in podosome growth 33

3.8 Actin binding, self-assembly, and GTP hydrolysis activity of Dyn2 are involved in podosome turnover 34

3.9 Dyn2 is required for podosome-mediated ECM degradation 36

3.10 Dyn2 regulates AChR cluster perforation through podosome 37

3.11 Dyn2 remodels actin cytoskeleton through actin bundling activity 38

3.12 Actin bundling activity of Dyn2 is regulated by GTP hydrolysis 39

3.13 Dyn2 oligomers assemble around actin filaments 42

3.14 CNM-associated Dyn2 mutant proteins are insensitive to GTP hydrolysis 45

3.15 Dyn2 bundles both linear and branched actin filaments 46

Chapter 4-Discussion.....47

4.1 Dyn2 regulates NMJ development 47

4.2 Dyn2 promotes podosome growth through its actin bundling activity 48

4.3 Dyn2, a novel regulator for podosome turnover 50

4.4 Dyn2 is a bundling protein for actin filaments 51

Chapter 5-Figures and Tables.....53

Figure 1. Structure and assembly of Dyn 53

doi:10.6342/NTU202100043

Figure 2. Structure of podosome 55
Figure 3. Dyn2 enriched at *Drosophila* postsynaptic NMJ 57
Figure 4. Dyn2 affects postsynaptic cytoskeletal organization in *Drosophila* 59
Figure 5. Effects of Dyn2 at *Drosophila* postsynaptic NMJ 61
Figure 6. Dyn2 affects postsynaptic SSR density in *Drosophila* 63
Figure 7. Dyn2 affects electrophysiological activities in *Drosophila* 65
Figure 8. Dyn2 did not affect GluRIIA distribution 67
Figure 9. Endogenous Dyn2 is enriched at mouse postsynaptic NMJ 69
Figure 10. AChR clustering and perforation in C2C12 myotubes on laminin-coated glass coverslips 71
Figure 11. AChR clustering and perforation in C2C12 myotubes 73
Figure 12. Dyn2 formed belt-shaped structure around some podosome core 75
Figure 13. Dyn2-belt localize in between podosome core and the radical actin cables 77
Figure 14. Level of Dyn2 enrichment correlates with podosome size 79
Figure 15. Dyn2 is required for podosome growth 81
Figure 16. Dyn2 forms belt-shaped structure as podosome matures 83
Figure 17. The correlation of Dyn2 enrichment and podosome lifespan 85
Figure 18. Dyn2 is required for podosome turnover 87
Figure 19. Dyn2 GTPase activity is involved in podosome growth and turnover 89
Figure 20. Mutations used in this study 91
Figure 21. Effects of mutant Dyn2 on podosome morphology in wild type myotubes 93
Figure 22. Rescuing effects of mutant Dyn2 on podosome morphology in Dyn2-depleted myotubes 95
Figure 23. Dyn2 is essential for podosome growth 97
Figure 24. Dyn2 is essential for podosome turnover 99

doi:10.6342/NTU202100043

Figure 25. Dyn2 is essential for podosome growth in c-Src transformed NIH3T3 cells 101

Figure 26. Dyn2 is essential for podosome turnover in c-Src transformed NIH3T3 cells 103

Figure 27. Dyn2 regulates podosome lifespan in c-Src transformed NIH3T3 cells 105

Figure 28. Dyn2 regulates podosome-mediated matrix degradation 107

Figure 29. Expressing Dyn2 hyper self-assembly mutant perturbs matrix degradation activity in wild type myotubes 109

Figure 30. Dyn2 mediates AChR cluster organization 111

Figure 31. Expressing Dyn2 hyper self-assembly mutant perturbs AChR perforation 113

Figure 32. Dyn2 bundles in vitro reconstituted actin filaments 115

Figure 33. GTP, GDP, and GTPγS addition reduced Dyn2-bundled actin 117

Figure 34. GTP hydrolysis reduced Dyn2-bundled actin 119

Figure 35. GTP hydrolysis induced disassembly of Dyn2-bundled actin 121

Figure 36. PRD domain of Dyn2 is not required for its actin bundling activity 123

Figure 37. Physical interruption failed to generate single actin bundles 125

Figure 38. Reducing temperature and Dyn2 concentration generated small actin bundles 127

Figure 39. Small actin bundles can be visualized under negative stain and CryoEM activity in wild type myotubes 129

Figure 40. Actin filaments packed inside the Dyn2 helix 131

Figure 41. Actin filaments bundled by hyper self-assembly Dyn2 mutant was less sensitive to GTP 133

Figure 42. Actin filaments bundled by CNM-Dyn2 mutant were less sensitive to GTP 135

Figure 43. Dyn2 bundles branched actin 137

doi:10.6342/NTU202100043

Figure 44. GTP hydrolysis regulates disassembly of branched-actin bundles 139

Figure 45. branched-actin bundled by CNM-Dyn2 were less sensitive to GTP hydrolysis 141

Figure 46. Working model of Dyn2 in podosome turnover and its distinct role in pre- and postsynaptic NMJ 143

Table 1. Plasmids used in this study 145

Table 2. Antibodies used in this study 146

Chapter 6-References 147

doi:10.6342/NTU202100043

Chapter 1-Introduction

1.1 Dynamin, a well-known catalyzer for membrane fission

Dynamin is a large GTPase that plays an essential role in the late step of membrane fission events during clathrin-mediated endocytosis and is critical for synaptic vesicle recycling (Antonny et al., 2016; Ferguson and De Camilli, 2012; Hinshaw, 2000). The function of mammalian dynamin in synaptic membranes was initially uncovered when the *Drosophila melanogaster shibire*, whose mutation resulted in synaptic vesicle depletion in neuron, was mapped to the mammalian dynamin (*DNM*) (Obar et al., 1990; van der Bliek and Meyerowitz, 1991). After decades of study, the function and mechanism of dynamin on synaptic vesicle recycling at the presynaptic membrane has been well characterized and appreciated; however, the function of dynamin at the postsynaptic membrane has less been explored.

Dynamin is a multidomain protein that composed of five functional domains: a G domain that capable of binding and hydrolyzing GTP, a stalk region consisting of middle domain and GTPase effector domain (GED) that mediates dynamin self-assembly and further oligomerization, a pleckstrin homology (PH) domain that binds

doi:10.6342/NTU202100043

phosphoinositide PI(4,5)P_2, and a proline and arginine rich domain (PRD) that binds SH3 domain-containing proteins **(Figure 1A)** (Antonny et al., 2016; Chappie et al., 2010; Chappie et al., 2011). Dynamin forms dimers through the stalk regions, and two dynamin dimers form a tetramer that could further assemble into polymers on membrane tubules with GTPase facing outward and PH domain binding to the membrane **(Figure 1B)**. Upon GTP hydrolysis, dynamin undergoes conformational change thus triggers membrane scission by constriction or tilting mechanism (Antonny et al., 2016).

There are three dynamin isoforms in mammals, including two tissue-specific isoforms, Dyn1 and Dyn3, and one ubiquitously expressed isoform, Dyn2 (Ferguson and De Camilli, 2012). Dyn1 is highly expressed in neuronal tissues, whereas Dyn3 is primarily expressed in the brain and testis. Mice lacking Dyn1 showed abnormal clathrin-coated pits accumulation in neuronal synapses (Ferguson et al., 2007), and this impaired presynaptic vesicle recycling phenotype was even more severe in Dyn1 and Dyn3 double knockout mice (Raimondi et al., 2011). Despite its ubiquitous expression and essential function in mouse embryo development, Dyn2 has been found related to two tissue-specific autosomal-dominant human congenital diseases,

doi:10.6342/NTU202100043

i.e., Charcot-Marie-Tooth (CMT) neuropathy and centronuclear myopathy (CNM) (Bitoun et al., 2005; Romero, 2010; Zhao et al., 2018; Zuchner et al., 2005). The CMT-Dyn2 mutant proteins are hypoactive and cause defects in endocytosis and peripheral neuron myelination, whereas CNM-Dyn2 mutant proteins are hyperactive and elicit fragmentation of muscular plasma membrane invagination and defective triad structures in mice (Chin et al., 2015; Cowling et al., 2011; Gibbs et al., 2014; Sidiropoulos et al., 2012).

1.2 The potential function of dynamin at postsynaptic NMJ

Previously our lab utilized transgenic *Drosophila* with Dyn2 expression to investigate the effects of Dyn2 mutants on muscle structure. We demonstrated that CNM-Dyn2 mutants caused T-tubule fragmentation due to hyper self-assembly properties and slower dissociation rate (Chin et al., 2015). Interestingly, we also observed an enrichment of Dyn2 in the postsynaptic neuromuscular junction (NMJ). It has been reported that Dyn2 is required for proper structured NMJ and that muscle-specific Dyn2-deficient mice have disorganized AChR clustering and enlarged neuromuscular endplates (Tinelli et al., 2013). Also, a CNM-Dyn2 mutant, S619L,

doi:10.6342/NTU202100043

has been reported to cause dispersed AChR clusters and impaired motor behavior in zebrafish, pointing to an important role of Dyn2 in postsynaptic NMJ (Gibbs et al., 2013). However, whether and how Dyn2 involves in the development of postsynaptic NMJ remains unclear.

Postsynaptic NMJ is an elaborated structure that comes from a series of morphological transitions including prepatterning and plague-to-pretzel transition of AChR clusters. The prepatterning occurs during E12.5 to E14.5 of the early mouse embryogenesis with postsynaptic apparatus developing in the absence of motor neuron innervation (Lin et al., 2001; Shi et al., 2012; Yang et al., 2001). These aneurally formed AChR clusters have been shown to confine the innervation of motoneurons (Ferraro et al., 2012; Wu et al., 2010; Yang et al., 2001). After birth, the cluster undergoes a plague-to-pretzel morphology transition to perfectly align with motor neuron axon terminals (Lin et al., 2001; Shi et al., 2012; Yang et al., 2001). This process requires both the motor neuron inputs and the extracellular matrix (ECM), as well as muscle-intrinsic machinery (Bernadzki et al., 2014; Bezakova and Ruegg, 2003; Marques et al., 2000; Shi et al., 2012). Interestingly, in an *in vitro* culture system that grows myotubes aneurally to recapitulate the plaque-

doi:10.6342/NTU202100043

to-pretzel morphological transition of AChR clusters, Dyn2 was found enriched in the perforated region of AChRs clusters where an actin-based structure called podosome was located at (Proszynski et al., 2009).

1.3 Podosome and its role during NMJ development

Podosomes are dynamic structures involved in cell migration and extracellular matrix degradation. They comprise an actin-rich protrusive core that grows vertically utilizing actin polymerization machinery and surrounded by an adhesive ring of integrins and integrin-associated proteins (**Figure 2**) (Linder and Aepfelbacher, 2003; Linder and Kopp, 2005). Unlike the podosomes in motile cells that facilitate cell motility, bone adsorption, and cancer cell metastasis (Linder, 2007; Linder and Aepfelbacher, 2003; Linder and Wiesner, 2016; Luxenburg et al., 2007), podosomes present in postsynaptic apparatus have been shown to play a key role in postsynaptic maturation through promoting NMJ development by redistributing AChR and ECM components in cultured myotubes and mice (Bernadzki et al., 2014; Chan et al., 2020; Kishi et al., 2005; Proszynski and Sanes, 2013). Yet, how these podosomes are regulated and affect NMJ development and why a membrane fission

doi:10.6342/NTU202100043

GTPase, Dyn2, is enriched at postsynaptic podosomes remained ill-defined.

1.4 A tale of dynamin and actin filaments

On top of its ability to catalyze membrane fission, dynamin has also been found to localize and function as an actin remodeling protein at many actin structures, including dorsal membrane ruffles, lamellipodia, and podosomes (Ferguson and De Camilli, 2012; Menon and Schafer, 2013). Dynamin functions as an actin remodeling protein through interacting with actin polymerization regulators such as cortactin or directly bundling actin filaments (Gu et al., 2010; Mooren et al., 2009). Depleting Dyn2 resulted in disorganization of podosomes, while overexpression of the GTPase defective mutant, K44A, lead to a delay of podosome turnover (Destaing et al., 2013; Ochoa et al., 2000). Previously we discovered the mechanical property and function of podosome in myocytes are regulated by Dyn2 (Chuang et al., 2019). Moreover, we discovered that Dyn2 forms spirals around actin filaments and enhance podosome stiffness. Although a recent study reported that the homolog of dynamin in Drosophila, *shibire*, also binds and bundles actin filaments (Zhang et al., 2020), it remains largely unclear which biochemical activities of dynamin is required

doi:10.6342/NTU202100043

for its actin rearrangement ability, especially its remodeling ability to podosomes. Here we hypothesized that Dyn2 might play a distinct role at postsynaptic NMJ comparing to its membrane fission role at the presynapse.

In this study, we investigated the molecular and physiological function of Dyn2 on biochemical, cellular, and organismal levels. We demonstrate that Dyn2 is an actin-remodeling protein that bundles both linear and branched actin filaments, and the bundling activity is regulated by GTP hydrolysis. At the cellular level, we discovered that Dyn2 regulates podosome maturation and turnover by its GTP hydrolysis-dependent actin-bundling activity. Dyn2 forms belt-shaped structures around the actin core as podosomes mature. We revealed that GTPase activity, actin-binding, and self-assembly are crucial to podosome morphology and functional. Most importantly, overexpression of the hyper self-assembly CNM-Dyn2 mutant in myotubes delayed podosome turnover and lead to aberrant AChR clustering. At the organismal level, expressing this mutant in *Drosophila* disorganized its postsynaptic cytoskeleton and electrophysiological properties. Our results suggested a novel role of Dyn2 in actin remodeling, which facilitates the process of postsynaptic NMJ development.

doi:10.6342/NTU202100043

Chapter 2-Material and Methods

2.1 *Drosophila* stocks

Fly stocks and *GAL4* lines were obtained from the Bloomington *Drosophila* Stock Center and maintained on normal food medium. The parental strain ZH-51D was used to generate transgenic flies by injecting the *pUAST*-based constructs into *Drosophila* embryos, thereby integrating them into the attP (second chromosome) landing site.

2.2 Dissecting of *Drosophila* larval body wall muscle

Third-instar larvae were dissected in Ca^{2+}-free buffer (128 mM NaCl, 2 mM KCl, 4 mM MgCl, 5 mM HEPES, 35.5 mM sucrose and 5 mM EGTA) and fixed in either 4% formaldehyde for 20 min or Bouin's fixative (Sigma-Aldrich) for 2 min, and then rinsed in 0.1 M phosphate buffer (pH 7.2) containing 0.2% Triton X-100. After blocking, samples were incubated overnight with indicated primary antibody at 4 °C. After further staining with secondary antibodies, samples were mounted in Fluoromount-G (-01, SouthernBiotech).

doi:10.6342/NTU202100043

2.3 Cell culture

Mouse-derived C2C12 myoblasts (ATCC, CRL-1772) were cultured in growth medium containing DMEM supplemented with 2 mM L-glutamine, 1 mM sodium pyruvate, antibiotics, and 10% FBS (Gibco). To induce cell differentiation, growth medium was replaced with differentiation medium containing DMEM supplemented with 2 mM L-glutamine, 1 mM sodium pyruvate, antibiotics, and 2% horse serum (Gibco) at 90% confluency. This time-point was considered as day 0 of differentiation. c-SrcY527F transformed NIH3T3 cells were cultured in DMEM, 10% FBS and 200 μg/ml Hygromycin B as previously described (Pan et al., 2011).

For immunostaining and time-lapse imaging, coverslips, Permanox slides (#160005, Thermo Fisher Scientific), or glass-bottom dishes (#P35G-1.5-14-C, MatTek) were coated with 10 μg/ml of laminin (#23017-015, Invitrogen) and incubated overnight at 37 °C prior to seeding. The laminin solution was aspirated completely before plating cells. Cells were seeded at 80% confluency one day before differentiation. After differentiation, cells cultured on laminin-coated coverslips or Permanox slides were ready for immunostaining, and cells cultured on laminin-coated glass-bottom dishes were ready for time-lapse imaging.

doi:10.6342/NTU202100043

2.4 Transfection, lentiviral and adenoviral infection

For transfection, cells at 70% confluency were transfected with target DNA using Lipofectamine 2000 (#11668-027, Invitrogen), as recommended by the manufacturer. For Dyn2 knockdown experiments, lentiviruses with or without (pLKO empty vector) targeting shRNA sequences [5'- GCCCGCATCAATCGTATCTTT-3' (#1) and 5'-GAGCTCCTTTGGCCATATTAA-3'] were prepared and used. C2C12 myoblasts at 50% confluency were infected with viruses and selected with 2 μg/ml puromycin for three days. Cells surviving after selection were pooled together to reach 90% confluency for differentiation. For adenoviral infection, prior to the day of infection, day 3-differentiated myotubes were first trypsinized using pre-warmed 1x trypsin with the amount just enough to cover the cell surface for 1 min, follow by using dropper to resuspend the cells in growth medium. Suspended myotubes were diluted 2 times in growth medium and then placed onto either laminin-coated coverslips, gelatin-FITC coated coverslips, or laminin-coated Permanox slides and culture overnight for attachment. On the next day, the day 4-differentiated myotubes are ready for viruse infection in the presence of differentiation medium containing 10 ng/ml tetracyclin overnight. Plasmids used in this study are listed in **Table 1**.

doi:10.6342/NTU202100043

2.5 Immunofluorescent staining

To visualize synaptic podosomes, C2C12-differentiated myotubes were fixed with 4% paraformaldehyde in PBS at 37 °C for 2 min and continued fixation at room temperature for 5 min. After washing with PBS, cells were permeabilized in PBS plus 0.1% saponin for 15 min under room temperature and treated with PBS plus 2% BSA and 5% normal donkey serum for a 1 hr blocking. For visualizing AChR clusters in myotubes, cells were fixed with 3% paraformaldehyde plus 0.1% glutaraldehyde in PBS at 37 °C for 2 min and continued fixation at room temperature for 5 min. After washing with PBS, cells were incubated with 0.2% $NaBH_4$ (#452882, Sigma-Aldrich) for 10 min, twice. Cells were then washed and permeabilized in PBS plus 0.5% triton for 30 min, and treated with PBS plus 2% BSA and 5% normal donkey serum for blocking. Cells were then stained with the indicated primary and secondary antibodies. Antibodies used in this study are listed in **Table 2**.

The *transversus abdominis* (TVA) muscles were dissected from 4-week-old wild-type mice and fixed in 4% paraformaldehyde, as previously described (Au - Murray et al., 2014). To visualize NMJs in mouse TVA muscle, after being permeabilized in 2% Triton X-100 and blocked in 4% BSA plus 1% Triton in PBS, the TVA muscles were

doi:10.6342/NTU202100043

washed in PBS and stained using the indicated antibodies. After washing in PBS, all samples were mounted in Fluoromount-G (-01, SouthernBiotech).

2.6 Fluorescence microscopy

For fixed samples, images were collected using an LSM700 confocal microscope with a 63×, 1.35-NA oil-immersion objective (Carl Zeiss), an LSM780 confocal microscope (Carl Zeiss), or a TSC SP8 X STED 3X (Leica) system with a 100× oil objective 1.4 NA (STED microscopy), acquired with the excitation laser at 488 or 594 nm and the depletion laser at 592 or 660 nm using Hybrid Detector (Leica HyD).

For time-lapse microscopy, cells were seeded on laminin-coated glass-bottom dishes and transfected with target DNA. After 5 days of differentiation, the differentiation medium was replaced with imaging medium (phenol-red free DM with 20 mM HEPES, pH 7.4, 50 μg/ml ascorbic acid, and 10% FBS). Cells were imaged with a Zeiss inverted microscope Axio Observer Z1 at 37 °C.

To image reconstituted actin bundles, 1 μM F-actin solution (20% rhodamine-labeled) was applied to chambers loaded with acid-washed coverslips. Actin polymerization buffer containig Dyn2 and GTP with a final concentration of 0.2 μM

doi:10.6342/NTU202100043

Dyn2 and 0.2 mM GTP was added afterward and imaged under a LSM780 confocal microscope (Carl Zeiss) at room temperature. Another way of visualizing actin bundles is to use fluorescence-conjugated phalloidin to stain the actin filaments. To do this, 1 μM F-actin solution was diluted 20 times in cold staining solution which contains 10 mM HEPES pH7.4, 100 mM KCl, 1mM $MgCl_2$, 0.1 mM EDTA, 1 mM DTT, 0.002% BSA, 0.5% Methylcellulose, 3 mg/ml glucose, and freshly added 50 μl/ml fluorescence-conjugated phalloidin. For imaging under confocal, the actin solution was then placed on acid-washed slides and covered with acid-washed coverslips.

2.7 Matrix degradation assay

To make FITC-gelatin-coated coverslips, acid-washed coverslips were first coated with 0.01% poly-D-lysine (#P7280, Sigma-Aldrich) for 1 h at room temperature and washed three times with PBS. We added 0.5% glutaraldehyde (#G5882, Sigma-Aldrich) to coverslips on ice for 15 min and washed with cold PBS. Pre-warmed coating solution composed of 0.1 mg/ml FITC-gelatin (#G-13187, Invitrogen) and 10 μg/ml laminin (#23017-015, Invitrogen) were added to the coverslips, which were

doi:10.6342/NTU202100043

then placed in the dark for 10 min at room temperature. After washing with PBS, 5 mg/ml $NaBH_4$ (#452882, Sigma-Aldrich) was added for 15 min to inactivate residual glutaraldehyde. The FITC-gelatin-coated coverslips were washed with PBS and stored in 70% ethanol. Remove all the ethanol and wash the coverslips with PBS prior to use.

Day 3-differentiated C2C12 myotubes were plated on FITC-gelatin-coated coverslips with or without adenovirus induction. After 16 h, the cells were fixed, stained for F-actin and HA-Dyn2, and imaged by confocal microscopy. The thresholding feature in Metamorph software (Molecular Devices) was used to analyze matrix degradation areas and cell-containing areas.

2.8 TEM of *Drosophila* NMJs

Larval fillets were dissected in calcium-free HL-3 medium (70 mM NaCl, 5 mM KCl, 10 mM $MgCl_2$, 10 mM $NaHCO_3$, 5 mM HEPES, 115 mM sucrose, 5 mM Trehalose, pH 7.2) at room temperature and were fixed for 12 h in 4% paraformaldehyde/1% glutaraldehyde/0.1 M cacodylic acid (pH 7.2) solution and then rinsed with 0.1 M cacodylic acid (pH 7.2) solution. They were subsequently fixed

doi:10.6342/NTU202100043

in 1% OsO_4/0.1 M cacodylic acid solution at room temperature for 3 h. The samples were subjected to a series of dehydration steps, i.e., from 30% to 100% ethanol. After the 100% ethanol dehydration step, the samples were incubated in propylene, a mixture of propylene and resin, and then in pure resin(Van Audenhove et al., 2015). Lastly, they were embedded in 100% resin. The images of type Ib boutons were captured using a Tecnai G2 Spirit TWIN system (FEI Company) and a Gatan CCD Camera (794.10.BP2 MultiScan) at ≥4,400× magnification. We identified type Ib boutons by the multiple layers of subsynaptic reticulum, and the size and layers of SSR of type Ib boutons were measured using Image J (NIH) accordingly to previous reports (Budnik et al., 1996; Lee and Schwarz, 2016). In brief, SSR thickness was measured in ImageJ as follows: (1) the center of mass was determined by drawing a region of interest around the periphery of a bouton; (2) four lines were drawn 90 degrees apart from one another emanating from the center of mass; (3) SSR thickness was then determined based on the average length between SSR edge and bouton edge along each line. SSR layers were determined by the plot profile feature in ImageJ across the segment of SSR on each line.

doi:10.6342/NTU202100043

2.9 Electrophysiology of *Drosophila* NMJ

Evoked excitatory junctional potential (EJP) was recorded as previously described (Peng et al., 2019). Briefly, third instar larvae were dissected in calcium-free HL3 buffer at room temperature, followed by incubation in 0.5 mM Ca^{2+} HL3 solution for 5–10 min prior to recording. The mean resistance value for the recording electrode was ~40 MΩ when 3 M KCl solution was used as the electrode solution. All records were obtained from muscle 6 in the A3 hemisegment. Resting membrane potentials of muscles were held at less than −60 mV. EJPs were amplified using an Axoclamp 900A amplifier (Axon Instruments) under bridge mode and filtered at 10 kHz. EJPs were analyzed using pClamp 10.6 software (Axon Instruments). Averaged EJP amplitude was calculated from the amplitudes of 80 EJPs in one consecutive recording. Miniature EJP recordings were performed in HL3 solution containing 0.5 mM Ca^{2+} and 5 μM tetradotoxin (TTX) and also analyzed using pClamp 10.6 software.

doi:10.6342/NTU202100043

2.10 Image analysis

Immunostained images were analyzed in Metamorph (Molecular Devices) and ZEN (Carl Zeiss) software. Podosome diameter and height were analyzed manually in xz orthogonal view in ZEN. Cell area and *Drosophila* NMJ area were selected manually and the area and signal intensity were measured in Metamorph. Matrix degradation area as well as GluRIIA and AChR cluster area were selected using threshold features in Metamorph and quantified automatically using the same software. Spectrin thickness was quantified by drawing a line across the center of a bouton and analyzing the width between two edges of the spectrin signal at one side of the bouton. Ghost bouton index was defined as the percentage of ghost bouton number divided by total bouton number in the same synapse, whereas NMJ branch points were analyzed by counting axonal branches with more than two type Ib boutons. For all immunostained *Drosophila* NMJ image analysis, only NMJ in muscle 6/7 in A2 or A3 hemisegments were examined.

2.11 Dynamin expression and purification

For the expression of Dyn2, human Dyn2 was constructed into pIEX6 vector

doi:10.6342/NTU202100043

(Novagen) and transfected into Sf9 insect cell for 48 hours at 28°C. Dyn2 transfected insect cells were harvested by transferring the cells into 50 mL centrifuge tubes and centrifuged at 3500 rpm for 5 minutes. Finally, insect cells pellets were stored at -80°C refrigerator for long term storage.

For Dyn2 purification, GST-SH3 proteins were inducted and purified from BL21 and then incubated with glutathione beads. Subsequently, Dyn2 was purified from insect cells by GST-SH3 affinity column. Finally, Dyn2 was eluted , dialysis into buffer composed of 20 mM HEPES, pH 7.4, 150 mM, 1 mM DTT, 1 mM EGTA with 10% glycerol and was snap-frozen and stored at -80°C.

2.12 F-actin bundle sedimentation assay

Dynamin proteins were expressed in Sf9 cells, purified as previously described, then snap-frozen in buffer containing 20 mM HEPES, 150 mM KCl, 1 mM EGTA, 1 mM DTT and 10% glycerol (Liu et al., 2011). The actin bundling assay was performed as described previously (Chuang et al., 2019; Lin et al., 2019). Briefly, 10 μM purified rabbit skeletal muscle actin (#AKL99-C, Cytoskeleton) was diluted in general actin buffer (5 mM Tris pH 7.4, 0.2 mM ATP, 0.2 mM $CaCl_2$, and 0.5 mM DTT) and

doi:10.6342/NTU202100043

incubated at 4 °C for 1 h and then centrifuged at 20,000 *g* for 15 min to remove aggregated proteins. The G-actin was polymerized in actin polymerization buffer comprising 2.5 mM Tris pH 7.4, 0.1 mM $CaCl_2$, 0.25 mM DTT, 50 mM KCl, 2 mM $MgCl_2$, and 1 mM ATP for 1 h at room temperature to generate actin filaments. To reconstitute branched actin, 160 nM WASP VCA domain protein (#VCG03, Cytoskeleton) and 60 nM Arp2/3 protein complex (#RP01P, Cytoskeleton) were also added to the actin polymerization buffer. To generate Dyn2-actin bundles, 5 μM polymerized F-actin was incubated with the indicated concentrations of Dyn2, resulting in a final KCl concentration of 75 mM. After 30-min incubation at room temperature, the mixture was centrifuged at 14,000 *g* for 20 min at room temperature. Protein in supernatants and pellets was solubilized in SDS sample buffer and subjected to SDS-PAGE. Proteins were visualized by Coomassie blue staining, and band intensities were quantified using ImageJ. The actin bundling activity is calculated by analyzing the proportion of sedimented actin in the presence of dynamin.

doi:10.6342/NTU202100043

2.13 Transmission electron microscopy

To visualize actin bundles with negative stain TEM, 5 μM filamentous actin was incubated with or without 1 μM Dyn2 at room temperature for 30 min. The mixture was then diluted 2 to 5-fold and adsorbed 6 μl onto carbon-coated grids for 30 sec and stained with 2% uranyl acetate for 30 sec. Airdry the grid before observation. For CryoEM sample preparation, 10 μM G-actin was polymerized in actin polymerization buffer for 30 min at room temperature, and then diluted in actin polymerization buffer to reach 1 μM and incubate another 30 min at room temperature. Dyn2 was first centrifuged at 20,000 *g* for 15 min to remove aggregated proteins. 0.5 μM filamentous actin was then incubated with 1 μM Dyn2 on ice for 30 min. Add 3 μl actin solution to the grid wait for 2 to let water volatilize and repeat this step for 3 times before putting onto Vitrobot. CryoEM samples were imaged under Tecnai F20.

For negative stain TEM, images were collected using a Hitachi H-7650 electron microscope at 75 kV and a nominal magnification of 120,000. To image Dyn2-actin bundles upon addition of GTP, the actin mixture was placed on parafilm before GTP addition. GTP was added to the actin mixture with a final concentration of 1 mM. The carbon-coated grids were placed on top of the mixture one min before being subjected

doi:10.6342/NTU202100043

to 2 % uranyl acetate staining. Negative-stained samples of actin bundles in the presence of other nuceotides were prepared and captured by TEM as described above.

2.14 Quantification and statistical analysis

Quantitative data are expressed as mean ± SD of at least three independent experiments. All data were analyzed with one-way ANOVA followed by Dunnett's or Tukey's (Figures 5D, 5F. S5G and S5H) multiple comparisons test, Student's *t* test, or Pearson correlation analysis. Statistical significance was defined using GraphPad Prism 8.0. $P < 0.05$ was considered statistically significant, indicated as *, $P < 0.05$; **, $P < 0.01$; or ***, $P < 0.001$.

Chapter 3-Results

3.1 Dyn2 is enriched at postsynaptic NMJ

According to literatures, Dyn2 has been shown to regulate NMJ morphology and function in living organisms. Patients with CNM-Dyn2 mutations were found to show abnormal neuromuscular transmissions (Gibbs et al., 2013). Mice lacking Dyn2 exhibit enlarged neuromuscular endplates while zebrafish carrying CNM-

doi:10.6342/NTU202100043

Dyn2 mutations display dispersed AChR clusters (Gibbs et al., 2013; Tinelli et al., 2013). However, how exactly does Dyn2 involve in NMJ development remained unclear.

To address this question, here we used the *MHC-Gal4* promoter to specifically express human Dyn2 in *Drosophila*'s muscle cells and utilized presynaptic and postsynaptic markers to visualize the localization of Dyn2 in third instar larvae. We firstly found that Dyn2 was enriched at postsynaptic NMJ and colocalized with the postsynaptic NMJ compartments, including the subsynaptic reticulum (SSR) scaffolding protein, discs large (DLG), and the actin cytoskeleton-associated protein, spectrin **(Figure 3A)**.

3.2 Dyn2 affects postsynaptic cytoskeletal organization

Due to the considerable colocalization between Dyn2 and spectrin, we next examine whether Dyn2 is involved in postsynaptic cytoskeleton organization. To examine if the membrane fission activity is involved, we expressed $Dyn2^{WT}$ and two disease-associated mutants including $Dyn2^{A618T}$, a hypermorphic CNM mutant that has hyper self-assembly activity, and $Dyn2^{G537C}$, a hypomorphic Charcot-Marie-

doi:10.6342/NTU202100043

Tooth neuropathy mutant that has membrane fission defect. The expression of Dyn2 in postsynaptic NMJ was confirmed by immunofluorescence staining and western blot **(Figure 3B, C)**. We found that overexpression of $Dyn2^{WT}$ does not affect the distribution of spectrin, which generally appeared as a sharp enrichment at the periphery of the presynaptic motor neuron labeled with an anti-HRP antibody **(Figure 4A)**. Interestingly, in larvae expressing the hyper-assembly mutant, $Dyn2^{A618T}$, but not the membrane fission defective mutant, $Dyn2^{G537C}$, the distribution of spectrin became disorganized. We could see a clear difference under line scan of a single bouton that spectrin formed two abrupt peaks at the outer edge of HRP in control, $Dyn2^{WT}$, and $Dyn2^{G537C}$ expressing larvae but not in $Dyn2^{A618T}$ expressing larvae (**Figure 4A**). The quantification result showed that the thickness of spectrin was significantly increased in $Dyn2^{A618T}$ expressing larvae (**Figure 4B)**, while overall protein expression of α-spectrin remained constant among expression of different Dyn2 proteins **(Figure 3C)**. Comparing the spectrin intensity of $Dyn2^{WT}$ and $Dyn2^{A618T}$ expressing larvae alone showed a significant reduction effect from $Dyn2^{A618T}$ flies in spectrin intensity (**Figure 4C)**. These results suggest that Dyn2

doi:10.6342/NTU202100043

may partake in regulating postsynaptic cytoskeletal organization through a membrane fission-independent manner.

We next extend our observations to other NMJ compartments. Unlike the disrupted pattern of spectrin in Dyn2^{A618T}-expressing NMJs, other NMJ components or maturation phenotypes were not significantly affected, including the SSR marker DLG, active zone marker Brp, ghost bouton number, as well as NMJ branch points **(Figure 5A-D)**. These results showed that the proper assembly of Dyn2 is critical for the cytoskeleton organization at postsynaptic NMJ.

3.3 CNM-Dyn2 interfere electrophysiological activity of *Drosophila* larval NMJ

In *Drosophila*, α-and β-spectrins are highly associated with postsynaptic plasma membrane and are critical for NMJ development. Spectrins form complex with actin filaments to establish cytoskeleton network that involved in postsynaptic subsynaptic reticulum (SSR) formation (Pielage et al., 2006). It has been shown that RNAi knockdown of α- or β-spectrin altered cytoskeleton organization as well as SSR membrane organization and synaptic transmission (Pielage et al., 2006). Next,

doi:10.6342/NTU202100043

we examined the ultrastructure of SSR using transmission electron microscopy **(Figure 6A)** (Van Audenhove et al.). We observed that expression of $Dyn2^{WT}$ or $Dyn2^{A618T}$ did not cause significant change in bouton SSR area and thickness **(Figure 6B, C**). However, expression of $Dyn2^{A618T}$ led to the reduction of the SSR density, resulting in loose membrane structure (**Figure 6A, D**). To assess whether the structural change may also alter synaptic transmission, we performed electrophysiology analysis. Expression of $Dyn2^{A618T}$ but not $Dyn2^{WT}$ increased the amplitude of miniature excitatory junction potential (mEJP) (**Figure 7A**), while the mEJP frequency was not altered under these manipulations (**Figure 7B**). As a result, expression of $Dyn2^{A618T}$ caused larger evoked EJP than those in control or expression of $Dyn2^{WT}$ (**Figure 7C**), meanwhile quantal content (QC) among different genotypes was similar (**Figure 7D**). The large mEJP size could be a consequence from the increment of either the level or activity of postsynaptic glutamate receptors, or both. However, we noted that there was no observable difference regarding the morphology or distribution of Glutamate receptor IIA (GluRIIA) clusters (**Figure 8A)**, the major subunit of glutamate receptors (Marrus et al., 2004). Neither the cluster area, intensity, nor the cluster size of GluRIIA was

doi:10.6342/NTU202100043

altered by expression of Dyn2^{A618T} (**Figure 8B-D**). Hence, above ultrastructural and electrophysiological results suggest that the hyper self-assembly activity of Dyn2^{A618T} can alter actin-dependent cytoskeleton organization thus cause abnormal SSR structure and electrophysiological function of postsynaptic compartment in *Drosophila* NMJ.

3.4 Dyn2 forms belt-shaped structures around the actin core of podosomes

In addition to demonstrating the structural effect of Dyn2 *in vivo*, we also wanted to ask how Dyn2 regulates the development of NMJ. It has been reported that one of the CNM-Dyn2 mutant, S619L, causes aberrant AChR cluster distribution in zebrafish (Gibbs et al., 2013), and the plaque-to-pretzel morphological maturation of AChR clusters in mice is regulated by an actin-enriched structure called podosome (Chan et al., 2020; Proszynski et al., 2009; Proszynski and Sanes, 2013). Since dynamin was reported to enriched at synaptic

doi:10.6342/NTU202100043

podosomes (Proszynski et al., 2009), we thus hypothesize that Dyn2 may partake in AChR clusters morphogenesis through regulating podosomes.

To explore the function of Dyn2 at muscle podosomes, we first examine the localization of endogenous Dyn2 in mice NMJ and in myotubes. We found that endogenous Dyn2 not only enriched in the NMJ of young-adult mouse (**Figure 9A, B)** but also enriched in cultured myotubes (**Figure 9C)**, in line with precious report (Proszynski et al., 2009). After confirming the enrichment of Dyn2 in the postsynapse, we differentiated myotubes from C2C12 myoblasts on laminin-coated glass coverslip to develop postsynaptic apparatus aneurally at the contacting surface. However, although podosomes could be found under this culture condition, the AChR clusters looked less organized **(Figure 10)**. We thus seek help from Dr. Prosynski in Nenki Institute who developed the aneural culturing system to improve our culture condition (Pęziński et al., 2020). With his suggestions including optimized fixation method as well as switching glass coverslip to Permanox plastic slides, we were then able to promote the formation of AChR clusters in C2C12-derived myotubes as reported (Kummer et al., 2004; Proszynski et al., 2009) (**Figure 11A)**. Consistent with the previous report (Proszynski et al., 2009),

doi:10.6342/NTU202100043

podosomes were found present in the perforated region of AChR clusters. We then used immunostaining and z-sectioning confocal microscopy to determine the spatial distribution of the endogenous Dyn2 at synaptic podosomes of myotubes. Podosome is an actin-based protrusive structure composed of an actin core, an actin cable network, and an adhesive ring (Linder and Aepfelbacher, 2003; Linder and Wiesner, 2016; Luxenburg et al., 2007). The actin core is enriched with branched actin polymerization machinery with actin cable network emanates from the actin core to bridge with the adhesive ring composed of integrin and adaptor proteins (**Figure 2)**.

By co-staining with phalloidin and the specific podosome scaffold protein, Tks5 (Seals et al., 2005), we observed that Dyn2 is highly enriched at the edge of the actin core (**Figure 12A)**. The orthogonal view of a single podosome from a reconstructed z-stack image showed that Dyn2 forms a belt-shaped structure in the middle region of the podosome, and is tightly associated with the actin core (**Figure 12A**). The belt-shaped Dyn2 distribution was further confirmed by stimulated emission depletion (STED) microscopy (**Figure 12B, C**). In contrast, the actin polymerization machinery, Arp2/3 and cortactin, were mostly in the core and only partially colocalized with Dyn2-enriched belt (**Figure 13A**), whereas both the actin

doi:10.6342/NTU202100043

cable network labeled by myosin IIA and the adhesive ring labeled by vinculin were located outside of the Dyn2-enriched belt, with myosin IIA closely located outside the Dyn2 belt (**Figure 13A-C**). Therefore, despite the direct interaction between Dyn2 and cortactin (McNiven et al., 2000), their differential localization at podosome and limited colocalization between Dyn2-belt and cortactin suggests that Dyn2 may play an direct role in the podosome formation through actin bundling activity.

3.5 Dyn2 is required for podosome growth

While Dyn2 localizes distinctly to the outer edge of actin core in podosome, we noticed that not every podosome is decorated with a Dyn2 belt: some podosomes are partially surrounded by Dyn2, and some have no Dyn2 belt (**Figure 12A, B)**. To investigate the role of belt-like Dyn2 enrichment in podosomes, we quantified the height of podosome cores after categorizing them into three groups – podosomes equipped with full, partial, or no Dyn2 belt. Statistical analysis showed that there was no significant difference in the population percentage of these three types of podosomes (**Figure 14A)**. Interestingly, podosomes with Dyn2 belt have higher and

doi:10.6342/NTU202100043

larger actin core (2.83 ± 0.20 μm in height and 1.46 ± 0.25 μm in width) than those with partial Dyn2 surrounding (2.19 ± 0.22 μm in height and 1.02 ± 0.19 μm in width) or no Dyn2 surrounding (1.65 ± 0.28 μm in height and 0.79 ± 0.17 μm in width) (**Figure 14B, C**).

To investigate the importance of Dyn2 on podosome growth, we downregulated Dyn2 by lentiviral shRNAs in C2C12-derived myotubes (**Figure 15A**) and then examined the morphogenesis of podosomes. In the projected z-stack images, the enrichment of Dyn2 at the actin cores was evident in control cells (**Figure 15B)**. Strikingly, Dyn2 knockdown abolished Dyn2 enrichment and significantly reduced both the height and width of the podosome cores (**Figure 15C**), but not the density of podosomes (**Figure 15D)**. These findings showed that Dyn2 contribute to the growth but not initiation of podosomes.

3.6 Dyn2 regulates podosome turnover

Next, we performed live-cell imaging to investigate the temporal distribution of Dyn2 together with other critical podosome components in myotubes. Consistent with the kinetics of podosome components in other cell types (Luxenburg et al.,

doi:10.6342/NTU202100043

2012), F-actin and cortactin accumulated synchronously during the initiation of synaptic podosome (**Figure 16A)**, whith the recruitment of Tks5 slightly lagged behind (**Figure 16B**). This result supports the role of cortactin in podosome initiation and Tks5 in podosome maturation. On the other hand, Dyn2-belt appeared only for a short period of time (**Figure 16C)**. Distinct from the short-lived podosome in macrophage and osteoclasts which is less than 15 min (Destaing et al., 2002; Guiet et al., 2012), the lifespan of podosomes in myotubes is heterogeneous, with more than 85 % had a lifetime longer than 15 min (**Figure 17A**) and more than 30% had a lifespan longer than one hour. By tracking the time course of individual podosomes (**Figure 17B**), we found that the time of Dyn2 enrichment covers ~ 48 % of the podosome lifespan (**Figure 17C**). Moreover, by analyzing the accumulation of Dyn2 on each podosome, we found there was a high correlation (Pearson's r = 0.753) between Dyn2 enrichment at podosome and the podosome lifespan (**Figure 17B, D)**. The transient appearance of Dyn2 enrichment explained why only part of the podosomes possessed Dyn2 belt at a given time (**Figure 14A**). We also noticed that, after Dyn2 belt disappeared, the actin core gradually dissembled and eventually vanished (**Figure 16C)**, suggesting a regulatory role of Dyn2 in podosome turnover.

doi:10.6342/NTU202100043

To validate whether Dyn2 regulate podosome turnover, again we downregulated Dyn2 in myotubes and performed live-cell imaging to analyze the podosome lifespan. Consistent with the defect in podosome growth, podosome lifespan was also significantly diminished in Dyn2-depleted myotubes (**Figure 18A, B**), with majority of the lifespan fall within 30 min. On the flip side, treatment of the dynamin GTPase inhibitor, dynasore, caused accumulation of Dyn2 at podosomes (**Figure 19A**). This manipulation produced elongated actin core in a time-dependent manner (**Figure 19B**), suggesting that Dyn2 is important for podosome core maturation, and the GTP hydrolysis-induced disassembly of Dyn2 is likely required for podosome turnover. However, we noted that prolonged dynasore incubation led to the accumulation of Dyn2 at plasma membrane and the reduction of podosome in myotubes, which might be due to indirect effect from the bloackage of dynmin-mediated endocytic pathways (**Figure 19C**).

Taken together, these results demonstrate that Dyn2 indeed plays an essential role in podosome growth and turnover.

doi:10.6342/NTU202100043

3.7 Actin binding, self-assembly, and GTP hydrolysis activity of Dyn2 are involved in podosome growth

To understand which biochemical activity of Dyn2 regulates podosome growth, we utilized adenovirus to transiently overexpress different dominant-negative mutants of Dyn2 in wild-type or Dyn2-depleted myotubes. These mutants included a hyper-assembly CNM mutant A618T, a membrane fission defective CMT mutant G537C, a mutant with lower actin binding ability K/E or with higher actin binding activity E/K, as well as a GTP binding defective mutant K44A(Chin et al., 2015; Gu et al., 2010; Kenniston and Lemmon, 2010) (**Figure 20A, B**).

Overexpression of $Dyn2^{WT}$ and the membrane fission defective mutant, $Dyn2^{G537C}$, were able to form normal belt-like enrichment in wild type myotubes (**Figure 22A**). The cells expressing both proteins displayed normal podosome morphology and density (**Figure 22B-D**), and both of them could rescue the size of podosome actin cores in Dyn2-depleted myotube (**Figures 23 & 23B-C**).

However, when the mutant proteins altering the activity of either GTP hydrolysis, actin binding, or self-assembly were expressed, the morphology of podosomes became aberrant. Firstly, expression of $Dyn2^{K44A}$ led to the most

doi:10.6342/NTU202100043

dramatic impact on podosomes, including reduction in podosomes density and size (**Figure 21B-D)**, which phenocopied the effect of prolonged dynasore treatment (**Figure 19C**). Similarly, expression of the Dyn2$^{K/E}$ mutant also exhibited reduced podosome width (**Figure 21D)**. In Dyn2-depleted myotubes, neither Dyn2$^{K/E}$ nor K44A could rescue the size of podosome cores (**Figure 23B, C)**. On the contrary, both hyper actin-binding Dyn2$^{E/K}$ and hyper self-assembly Dyn2^{A618T} mutants did not affect typical enrichment around the actin core (**Figure 21A)**, and both of them showed a rescuing ability to podosome height in Dyn2-depleted myotubes (**Figure 23B**). In wild type myotubes, the height of the podosome in the Dyn2^{A618T}-expressing myotubes was increased when compared to Dyn2^{WT}-expressing cells (2.43 ± 0.84 μm and 1.94 ± 0.67 μm, respectively) (**Figure 21C)**, suggesting that hyper self-assembly ability of Dyn2 can result in abnormal podosome morphology.

3.8 Actin binding, self-assembly, and GTP hydrolysis activity of Dyn2 are involved in podosome turnover

To examine the effect of Dyn2 on podosome turnover, we co-expressed LifeAct-GFP and mCherry-tagged Dyn2 mutants to measure the lifespan of

doi:10.6342/NTU202100043

podosomes. While overexpressing Dyn2^{G537C}-mCherry, Dyn2$^{K/E}$-mCherry, and Dyn2$^{E/K}$-mCherry do not cause significant alteration in podosome lifespan, overexpression of Dyn2^{A618T}-mCherry result in prolonged Dyn2-belt and abnormal podosome lifetime, resulting a drastic increase of the long-lived podosomes (> 2 hr) (**Figure 24A**). Moreover, unlike the temporal enrichment of Dyn2^{WT}-belt in muscle podosome (**Figure 16C**), Dyn2^{A618T}-belt was very stable throughout the lifetime of podosomes (**Figure 24B**). **Figure 24B** shows one example of podosomes that is decorated with Dyn2^{A618T} belt for more than 10 hr and has a lifetime longer than 15 hr. This result suggests that the CNM-associated, hyper-assembly mutant Dyn2^{A618T} results in the delay of podosome turnover.

Unfortunately, we were unable to analyze the effect of Dyn2^{K44A}-mCherry on podosome lifetime in myotubes due to its strong dominant-negative effect on myoblast differentiation (Chuang et al., 2019), which prevented us from getting myotubes expressing Dyn2^{K44A}-mCherry. For this reason, we then analyzed the effect of Dyn2 mutants on podosome rosettes in cSrc-transformed NIH3T3 fibroblasts. Similar to the enrichment of Dyn2 around podosomes in myotubes, Dyn2 also found enriched around the podosome resettes in cSrc-transformed

doi:10.6342/NTU202100043

NIH3T3 fibroblasts (**Figure 25A)**. Akin to the phenotype in myotubes, we observed an increase in podosome height and lifespan in Dyn2^{A618T}-expressing cells (**Figures 25B)**. Intriguingly, we also observed a notable decrease in podosome size (**Figures 25B, C)** and lifespan (**Figures 26 & 27**) in Dyn2$^{K/E}$- and Dyn2^{K44A}-expressing cSrc-transformed NIH3T3 fibroblast.

In sum, these results showed that the actin binding, self-assembly, and GTP hydrolysis, but not the membrane fission activity of Dyn2 are required for the growth and turnover of podosome.

3.9 Dyn2 is required for podosome-mediated ECM degradation

Podosome is featured by its ECM degradation ability (Linder, 2007). To assess the functionality of podosomes in the situation when specific activity of Dyn2 is perturbed, we performed ECM degradation assay in wild type and Dyn2-depleted myotubes expressing different Dyn2 mutants. In Dyn2-depleted myotubes, only Dyn2$^{K/E}$ and Dyn2^{K44A} could not restore the ECM degradation ability (**Figure 28A, B)**. In wild-type myotubes, only expression of Dyn2^{A618T} (6.82 ± 4.85 %) but not other mutants resulted in a significant difference in the degradation area compared

doi:10.6342/NTU202100043

with Dyn2^{WT} (4.13 ± 2.71 %) (**Figure 29A, B**). Since the podosome density in Dyn2^{A618T}-expressing myotubes remained unchanged (**Figures 21B & 23A**), the increase in the ECM degradation may be a result from delayed turnover of podosomes (**Figure 24**). Our results demonstrate that Dyn2 promotes podosome maturation and turnover, and that podosome surrounded by CNM-associated Dyn2^{A618T} exhibit a greater ECM degradation activity.

3.10 Dyn2 regulates AChR cluster perforation through podosome

It has been shown that the perforation/maturation of AChR cluster is linked to the activity of podosome (Proszynski et al., 2009; Proszynski and Sanes, 2013). We therefore examined the contribution of Dyn2 to AChR distribution by staining the myotubes with Alexa488-conjugated bungarotoxin (BTX). The overall actin cytoskeleton organization in day-5 differentiated myotube was not altered by expressing different Dyn2 mutants. However, the area of the AChR cluster was smaller and with less cluster area remained in Dyn2^{A618T}, but not Dyn2^{WT} and Dyn2^{G537C}-expressing myotubes, compared to the control cells (**Figure 30A-C**). We reasoned that decreased AChR area in Dyn2^{A618T}-expressing myotubes might be

doi:10.6342/NTU202100043

due to prolonged podosome lifespan and excessive ECM degradation that lead to hyper AChR cluster perforation. Thus we also examined the effect of $Dyn2^{A618T}$ expression on myotubes during initial plaque-to-pretzel transition. In agreement with our hypothesis, we found much more AChR cluster perforation in $Dyn2^{A618T}$-expressing day-4 myotubes, compared to control, $Dyn2^{WT}$ and $Dyn2^{G537C}$ myotubes (**Figure 31**). This result shows that proper self-assembly of Dyn2 is critical for podosomes to regulate the plaque-to-pretzel transition during AChR cluster maturation.

3.11 Dyn2 remodels actin cytoskeleton through actin bundling activity

Although Dynamin has been shown to regulate many actin structures like podosomes through interacting with actin polymerization regulators or directly bundling actin filaments (Ferguson and De Camilli, 2012; Gu et al., 2010; Menon and Schafer, 2013; Mooren et al., 2009), it remains unclear which biochemical activities of Dynamin is required for its actin remodeling ability.

To better understand how Dyn2 regulates actin cytoskeleton. we reconstituted

doi:10.6342/NTU202100043

actin filaments *in vitro* followed by co-sedimentation assay and imaging to directly investigate how Dyn2 remodels actin filaments. Consistent with previous reports (Chuang et al., 2019; Gu et al., 2010), we observed that Dyn2 has prominent F-actin bundling activity that is comparable with Dyn1 (**Figure 32A, B**) and the bundling activity increases in a dose-dependent manner (**Figure 32C, D)**.

3.12 Actin bundling activity of Dyn2 is regulated by GTP hydrolysis

Next we wanted to understand how Dyn2's assembly on actin filaments is regulated. It is known that GTP hydrolysis induces conformational change of Dyn2 and its disassociation from the membrane templates (Bashkirov et al., 2008; Chin et al., 2015; Pucadyil and Schmid, 2008). To test whether the assembly of Dyn2 on actin bundles is affected by GTP analogs and also disassociates after GTP hydrolysis, we added GTP, GDP, or the non-hydrolyzable GTP analog, GTPγS. Similar to its assembly on mebrane, the presence of GTP reduced the amount of Dyn2-bundled actin. **(Figure 33A)**. Addition of GDP also reduced the bundling, which later found to be an effect of disorganized Dyn2 ring assembly **(Figure 35A)**. However, we also noticed that in the presence of GTPγS, the bundled actin reduces **(Figure 33A)**,

doi:10.6342/NTU202100043

suggesting that Dyn2 were disassembled upon GTPγS addition. We hypothesized that Dyn2 may still hydrolyze GTPγS, thus we test the actin bundling activity with different incubation time. With 30 min of incubation, both GTP and GTPγS seemed to reduce the amount of bundled actin. Interestingly, when we shorten the incubation time to 5 min, there seemed to be less reduction in the GTPγS group **(Figure 33B)**, raising the possibility that Dyn2 hydrolyze GTPγS slower than GTP. Indeed, GTPγS has been reported to be a slowly-hydrolyzable GTP analog (Jameson, 2014). We thus replace GTPγS with GMPPCP, a less controversial, non-hydrolyzable GTP analog. As expected, Dyn2-actin bundles were significantly reduced upon the addition of GTP, but not the non-hydrolyzable GTP analog, GMPPCP **(Figure 34A, B)**. The Dyn2-mediated actin bundling and the disassembly induced by GTP could be observed in real-time by imaging the dynamics of rhodamine-labeled actin under fluorescence microscopy **(Figure 34C)**.

To visualize in more detail of how Dyn2-actin bundle responds to GTP addition, we utilized negative stain TEM to image the Dyn2-actin bundle with or without nucleotides. We found that distinct from the aligned and bundled actin filaments surrounded by ordered Dyn2 rings in the absence of GTP, the Dyn2 rings were

doi:10.6342/NTU202100043

disassembled and the actin bundles became dispersed upon the addition of GTP, but not GMPPCP **(Figure 35A**). We also analyzed the effect of other GTP analogs including GDP and GDP: AlF_4^-, which act as a transition state analog during GTP hydrolysis. We found that actin bundles remained intact, yet Dyn2 assembles less orderly in the presence of GDP, which might be the reason for less actin bundles observed after sedimentation (**Figure 33A)**. The width of minimum actin bundle was slightly bigger than twice of the width of single actin filaments, suggesting that the minimum actin bundles were composed of two actin filaments. Additionally, the actin bundles dissociated and became dispersed in the presence of GTPγS, similar to the result observed in GTP addition. This result is consistent with our co-sedimentation data that bundled actin was reduced in the presence of GTPγS **(Figure 33)**, in line with the report that GTPγS can be slowly hydrolyzed by Dynamin (Jameson, 2014).

Together, these results indicate that Dyn2 has prominent bundling activity towards filamentous actin, which is terminated by GTP hydrolysis.

doi:10.6342/NTU202100043

3.13 Dyn2 oligomers assemble around actin filaments

To understand how Dyn2 assembles on actin filaments and whether the way it assembles on actin is similar to how it assembles on membrane, we purified truncated mutant protein lacking the PRD domain ($Dyn2^{\Delta PRD}$), the domain that is not essential for Dyn2's assembly on membrane. Similar to the domain requirement for Dyn2 assembly on the membrane, $Dyn2^{\Delta PRD}$ still has prominent actin bundling ability **(Figure 36A, B**), and the size of actin-$Dyn2^{\Delta PRD}$ bundles was comparable to that of actin-$Dyn2^{WT}$ bundles **(Figure 36C)**.

The structure of Dyn2 on membrane has been well-described by CryoEM (Kong et al., 2018). The greatest advantage of CryoEM compared with TEM is that it does not involve chemical fixation or staining, which made the specimen remained in native physiological environment. With the goal to get 3D reconstruction of Dyn2-actin bundles to see how Dyn2 assembles on actin filaments under native conditions, we tried different conditions to get the smallest unit of Dyn2-actin bundles with least protein aggregates in the background. First, we test whether extracting different fractions of bundled actin after sedimentation, or using sonication or freeze-and-thaw to physically disrupt bundled actin could provide or generate smaller actin

doi:10.6342/NTU202100043

bundles. However, neither of these methods worked. The collected fractions from actin solution after centrifugation showed different amount instead of the size of bundled actin (**Figure 37)**. On the other hand, sonication did not cause significant effect on the bundles, while freeze-and-thaw caused fragmentation but not separation of actin bundles (**Figure 37)**.

Next, we tried modifying the ratio of Dyn2 versus actin, as well as the incubation temperature and time to see whether reducing Dyn2 concentration and reaction speed could get smaller bundles. We found that reducing Dyn2 concentration and lower the temperature could generate small actin bundles under negative stain TEM (**Figure 38A)**. However, when the same sample was used for CryoEM, we found that most of the Dyn2 did not attach to the filaments but formed aggregates, resulting a noisy background with most of the filamentous actin unbundled (**Figure 38B, C)**. There were two concerns, one is the bundled actin were lost on Vitrobot (the machine for cryo-fixation) due to brief and vertical incubation, the other is the quality of Dyn2. To solve this issue, we came up with two adjustments: to remove the Dyn2 aggregates prior to use via centrifugation and to horizontally incubate the sample solution on grid before putting it on to Vitrobot. We

doi:10.6342/NTU202100043

successfully remove the Dyn2 aggregates in the background and also increased the density of actin filaments on grids (**Figure 38D, E)**. Unfortunately, we see very few Dyn2 attached to the actin filaments. We then think from another angle—increase Dyn2 concentration while reducing the density of actin filaments. To achieve this, we first polymerize the actin, dilute the filaments five times during the half way of polymerization and then add Dyn2 to induce actin bundling. Finally, this method successfully captured the small Dyn2-actin bundles under negative stain TEM (**Figure 39A, B)**. and under CryoEM (**Figure 39C)**. Although we failed to get a clear 2D classified image of Dyn-actin bundles by CryoEM due to low sample number and heterogeneity of each bundle (**Figure 39D)**, we could see from the classification results of single actin filaments (**Figure 39E)** and side-by-side actin filaments (**Figure 39F)** that the organization of small Dyn2-actin bundles looked completely different from actin-only structures. Fortunately, we could still collect tomographic micrographs under negative stain TEM. We observed some partially packed Dyn2-actin bundles which may represent the intermediate stage of the bundling process (**Figure 40A**). Furthermore, the 3D tomography clearly shows that Dyn2 assembles around actin filaments to form a packed actin bundle (**Figure 40B**).

doi:10.6342/NTU202100043

3.14 CNM-associated Dyn2 mutant proteins are insensitive to GTP hydrolysis

Given that only CNM-Dyn2 but not CMT-Dyn2 mutations lead to abnormal NMJ organization and podosome function, we then examined whether these disease-assiciated Dyn2 mutant proteins behave differently on actin bundles. We purified the membrane fission defective CMT-Dyn2 mutant protein, G537C, and the hyper self-assembly CNM-Dyn2 mutant protein, A618T, to analyze their actin bundling activities. We found both $Dyn2^{A618T}$ and $Dyn2^{G537C}$ have comparable actin bundling activities; however, while actin filaments bundled by $Dyn2^{WT}$ and $Dyn2^{G537C}$ dissociated upon GTP hydrolysis, those bundled by $Dyn2^{A618T}$ were resistant to GTP addition and remained bundled (**Figure 41A, B**). Importantly, both the CMT mutant, $Dyn2^{G537C}$, and CNM-associated Dyn2 mutants, A618T, R465W and S619L, showed prominent actin-bundling activity (**Figure 42A-C**). Like $Dyn2^{A618T}$, the $Dyn2^{R465W}$ and $Dyn2^{S619L}$-bundled actin filaments were also insensitive to GTP hydrolysis (**Figure 42D, E**).

doi:10.6342/NTU202100043

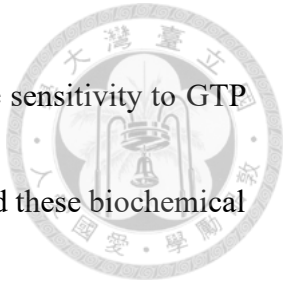

Altogether, these results indicate that the assembly and the sensitivity to GTP hydrolysis of Dyn2 play a decisive role in actin organization, and these biochemical features are critical for the regulation of actin cytoskeleton.

3.15 Dyn2 bundles both linear and branched actin filaments

Since branched actin exists in most of the actin-based structure that Dyn2 was found to locate at (Ferguson and De Camilli, 2012; Menon and Schafer, 2013), we thus repeated the actin sedimentation assays with branched-actin reconstituted by Arp2/3 complex and the VCA domain of neural Wiskott-Aldrich syndrome protein (N-WASP) to examine the bundling ability of Dyn2 on branched actin. We found that Dyn2 has prominent bundling activity on branched actin that is also GTP hydrolysis-dependent (**Figure 43A, B**). The bundled branched-actin looked spiky compared with the bundled linear actin (**Figure 43C**). Disassembly of these branched-actin bundles is also regulated by GTP hydrolysis (**Figure 44A-C**). Moreover, similar to linear actin bundles, CNM-associated Dyn2 mutants including A618T, R465W and S619L, also showed GTP insensitivity on branched actin bundles (**Figure 45A-D**).

doi:10.6342/NTU202100043

Chapter 4-Discussion

4.1 Dyn2 regulates NMJ development

In this study, we reveal that Dyn2 plays critical roles in regulating postsynaptic actin organization to facilitate NMJ development. We provide, to our knowledge, the first evidence of Dyn2 enrichment and direct function at NMJs. In living organism, we found that Dyn2 is enriched at postsynaptic NMJ in mice and *Drosophila* and is involved in regulating postsynaptic cytoskeleton organization of *Drosophila* larvae. In cultured myotubes, we found that Dyn2 regulates podosome maturation and mediates AChR cluster morphogenesis.

We demonstrate that Dyn2 contributes to the maintenance of postsynaptic spectrin organization and proper electrophysiological activities. Disruption of postsynaptic spectrin has been reported to lead to NMJ abnormality, including aberrant SSR integrity, active zone spacing, glutamate receptor clustering, and electrophysiological activities (Blunk et al., 2014; Pielage et al., 2006; Proszynski et al., 2009). Similarly, when we express $Dyn2^{A618T}$ in the muscle cells, the organization of postsynaptic spectrin became disorganized, showing a milder phenotype than spectrin knockdown flies.

doi:10.6342/NTU202100043

CNM-associated Dyn2 mutations such as A618T are hypermorphic alleles resulted from their loss of autoinhibitory regulation thus enhanced self-assembly abilities (Faelber et al., 2013; Hohendahl et al., 2016). Here we demonstrated that with hyper-assembly activity, CNM-Dyn2 is resistant to GTP hydrolysis-induced disassembly thus becomes hyperactive. Furthermore, it is known that podosomes plays essential role in postsynaptic NMJ morphogenesis via mediating AChR perforation. Our data showed that CNM-Dyn2 could cause excessive podosome-mediated matrix degradation and reduced AChR clusters. Taken together, our finding elaborately supports and explains previous findings of NMJ abnormalities in CNM-Dyn2 expressing mouse or zebrafish, supporting that Dyn2 has versatile and critical functions in muscle development and disease.

4.2 Dyn2 promotes podosome growth through its actin bundling activity

The essential role of Dyn2 in actin organization has been demonstrated in several studies (Bruzzaniti et al., 2005; Destaing et al., 2013; Ochoa et al., 2000). It was generally assumed that Dyn2 functions to promote actin polymerization due to

doi:10.6342/NTU202100043

its abilities to remove capping proteins and directly interact with cortactin, Nck, and profilin (Gu et al., 2010; Mooren et al., 2009; Schafer, 2004). Here we discover a regulatory function of Dyn2 in controlling podosome growth and turnover through its direct interaction with actin. Based on our data, we propose that Dyn2 is recruited to the podosome to bind and assemble around the actin core for strengthening the podosome and finally license the turnover of podosome through GTP hydrolysis-induced disassembly (**Figure 46A**). According to our previous lab member, Tsung-Lin Hsieh's work on Src-mediated phosphorylation on Dyn2 (Lin et al., 2020), we learned that Src kinase phosphorylates Dyn2 at residue Y597 to mediate its targeting to podosome. Hsieh reported that myotubes expressing the phosphor-deficient Dyn2 mutant reduced the targeting of Dyn2 to podosomes. He also found that the phospho-mimetic Dyn2 mutant protein showed a slower dissociation rate in the presence of GTP on actin bundles, and had less affinity for liposomes composed of plasma membrane-like lipid components, raising the possibility that Src controls the translocation of Dyn2 from plasma membrane to podosomes.

Together, we propose that upon phosphorylation, Dyn2 oligomerizes around the actin core and forms a belt to facilitate the growth and strengthen the stiffness of

doi:10.6342/NTU202100043

the podosome. Once Dyn2 oligomers undergo GTP hydrolysis-induced disassembly, the podosome proceeds to dissolve. The actin-remodeling activity of Dyn2 partakes in organizing postsynaptic NMJ structure via regulating synaptic podosome turnover and postsynaptic cytoskeleton organization.

4.3 Dyn2, a novel regulator for podosome turnover

Many actin polymerization machinery and motor protein have been discovered to mediate podosome initiation and maturation (Cervero et al., 2018; Labernadie et al., 2014; van den Dries et al., 2014; van den Dries et al., 2013); however, it is unclear how the actin core of podosome remains its cylindrical shape under mechanical stress during protrusion. Given that Dyn2 assembles at the edge of actin core and is required for the maturation of podosome, we hypothesize that Dyn2 functions as a molecular girdle to maintain its structure while podosome encounters physical strain. By contrast to the understanding of podosome formation, relatively little is known about how podosome turnover is regulated. To date, only myosin II, Supervillin and fascin have been reported to regulate podosome turnover. Myosin II and Supervillin enable podosome turnover by increasing the actomyosin contractility, whereas

doi:10.6342/NTU202100043

fascin facilitates podosome disassembly by inhibiting Arp2/3-mediated actin branching. Here we reveal that the GTP hydrolysis-induced Dyn2 disassembly is a key regulator for podosome turnover in both C2C12-derived myotubes and c-Src transformed NIH3T3 fibroblasts. Mutations had aberrant sensitivity to GTP hydrolysis on actin could in turn alter podosome lifespan and perturb its turnover. These observations demonstrate Dyn2 as a novel regulator not only for the formation also for the turnover of podosomes in different cell types.

4.4 Dyn2 is a bundling protein for actin filaments

The structure of dynamin oligomers around membrane template has been beautifully solved: it binds to membrane via PH domain and self-assembles into helixes with its stalk region (Antonny et al., 2016; Kong et al., 2018). Interestingly, our negative stain TEM images also revealed similar ring-like Dyn2 oligomers surrounding actin filaments. Although we failed to get clear 3D reconstructed image from our preliminary CryoEM data, the native CryoEM image and its 2D classification results (**Figure 39**) supported our hypothesis that actin filaments were packed inside the Dyn2 oligomers. Similar to Dyn2 spirals on lipid templates, these

doi:10.6342/NTU202100043

Dyn2 oligomers on actin filaments are also responsive to GTP hydrolysis, which induces its disassembly. Altogether, these data demonstrate that Dyn2 is a unique actin binding protein that aligns and packs actin filaments together by forming ring-like oligomers around them. But how exactly does Dyn2 assemble around actin? Given the actin binding sequence is located at the stalk region of Dyn2 (Gu et al., 2010), the binding and assembly of Dyn2 around actin might be different from its assembly around membrane template. Further structural study of Dyn2 and actin complex is needed.

In summary, we revealed that Dyn2 is an actin bundler that controls podosome dynamics and postsynaptic cytoskeleton organization during NMJ development. There are still many interesting questions remained regarding how Dyn2 binds and assembles on actin filaments, how Dyn2 affect the kinetics for branched actin assembly, and whether Dyn2 contribute to synaptic maturation in synapses other than NMJ. Our results suggest a differential function and localization of dynamin at pre-and postsynaptic membranes (**Figure 46B)** and paved the way for further studies in synapse development, podosome kinetics, and mechanical properties.

doi:10.6342/NTU202100043

Chapter 5-Figures

Figure 1. Structure and assembly of Dyn

(A) Domain structure of Dyn. **(B)** Crystal structure of the Dyn dimer and tetramer, showing the interfaces required for assembly. Below shows a schematic diagram revealing how Dyn tetramers further assemble into a helical structure on the membrane.

doi:10.6342/NTU202100043

A

B

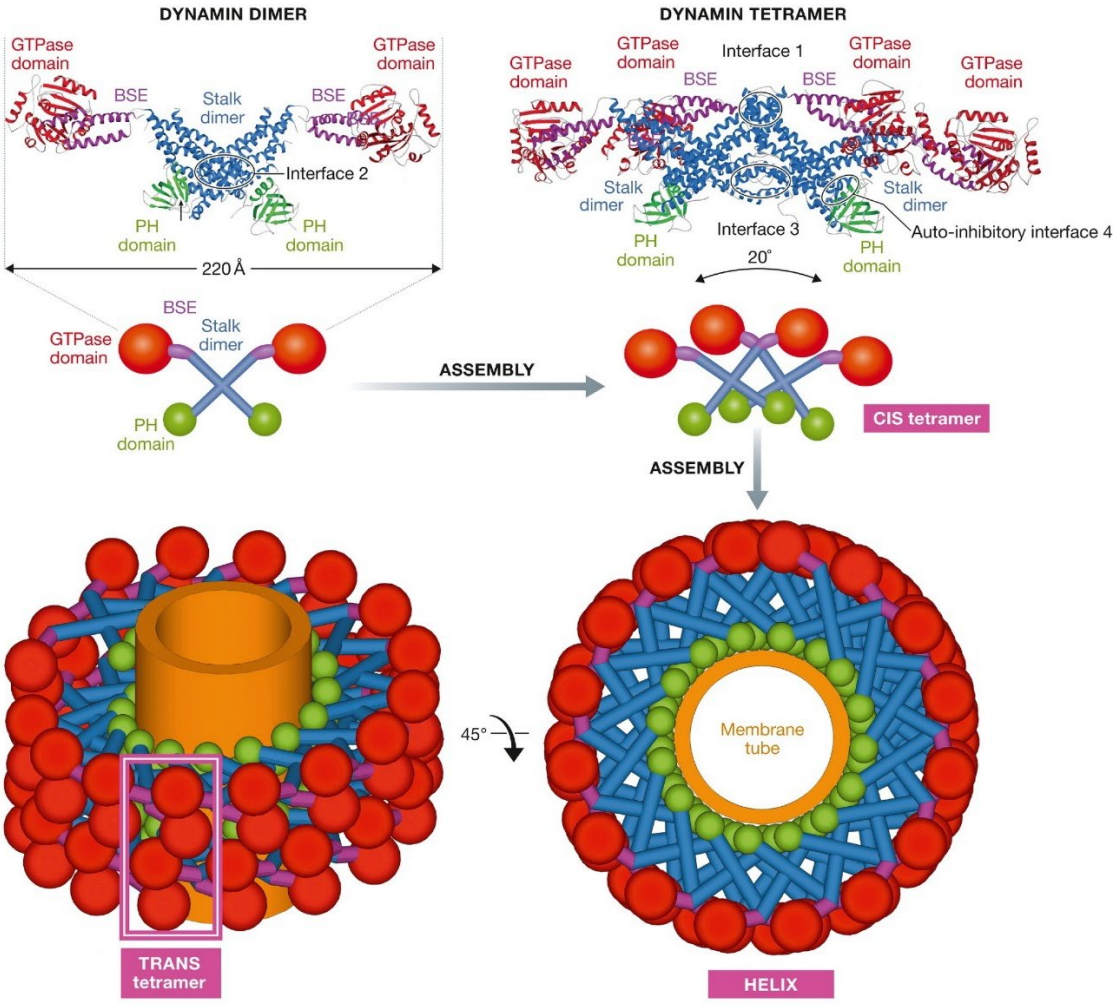

The EMBO Journal (2016) **35**: 2270–2284

doi:10.6342/NTU202100043

Figure 2. Structure of podosome

Podosomes are actin-enriched structures comprising an actin core, a radial actin cable network, and an integrin-based adhesive ring. The actin core is enriched with branched actin polymerization machinery including cortactin and Arp2/3 complex. The cable network contains myosin IIA and emanates from the actin core to link with the adhesive ring composed of integrin and adaptor proteins

doi:10.6342/NTU202100043

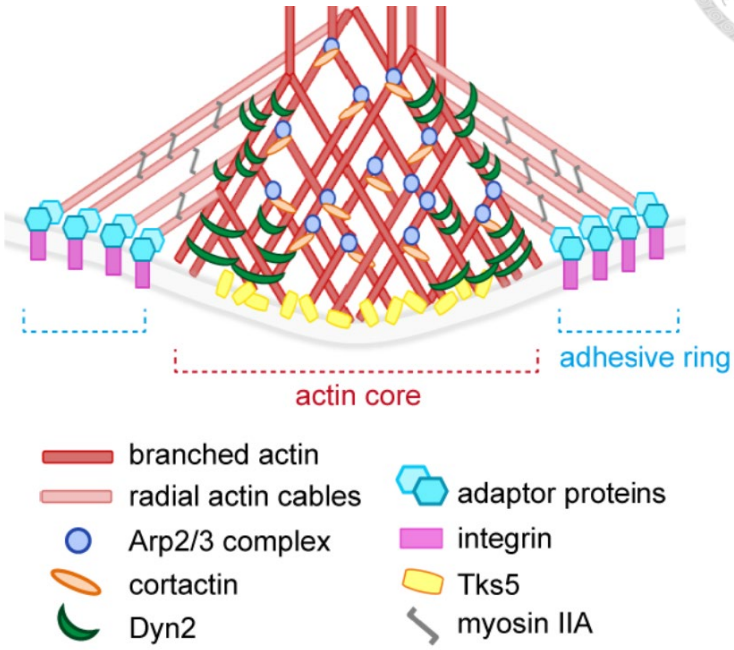

doi:10.6342/NTU202100043

Figure 3. Dyn2 enriched at *Drosophila* postsynaptic NMJ

(A) HA-Dyn2^{WT} was enriched at *Drosophila* NMJ. Distribution of HA-Dyn2^{WT}, DLG, and α-spectrin are shown by immunostaining. **(B)** Immunostaining of third-instar larval NMJs with anti-α-spectrin and anti-HA antibodies was performed as described in Methods. Images were taken from z-stack confocal microscopy and presented as z-stack projections. **(C)** Immunoblotting analysis of *Drosophila* third instar larvae shows the expression levels of α-spectrin, tubulin, and HA-Dyn2. Scale bars, 10 μm.

doi:10.6342/NTU202100043

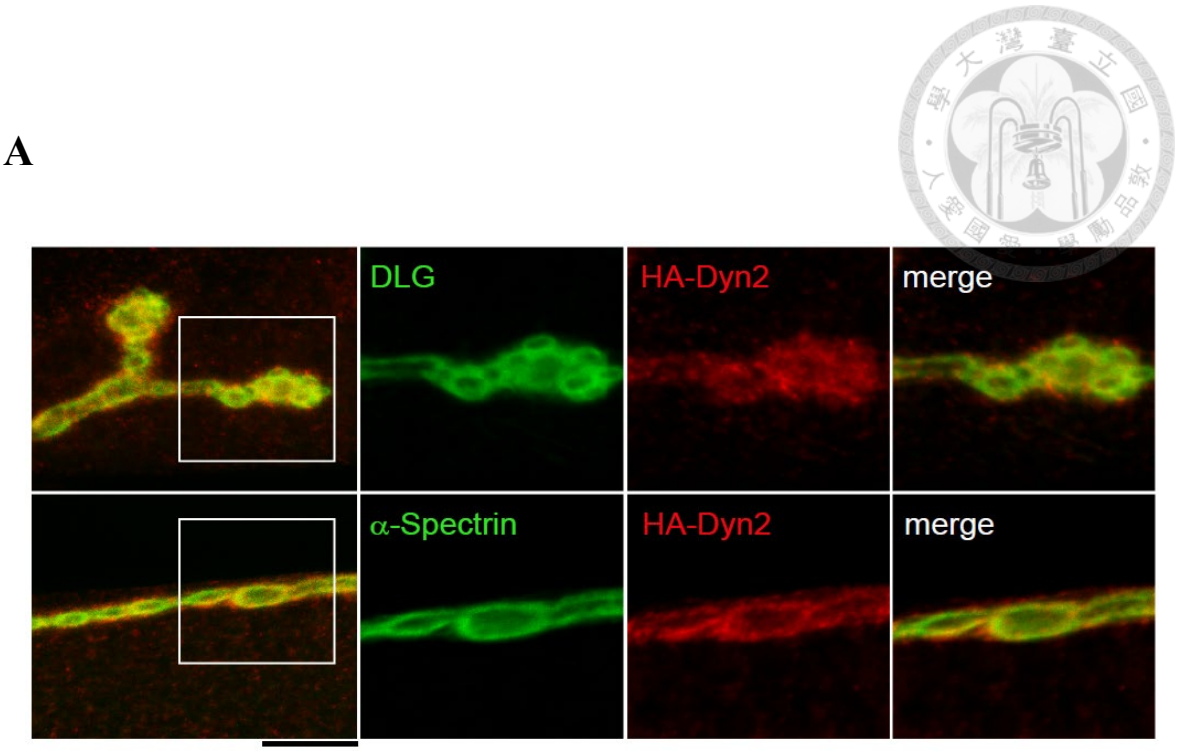

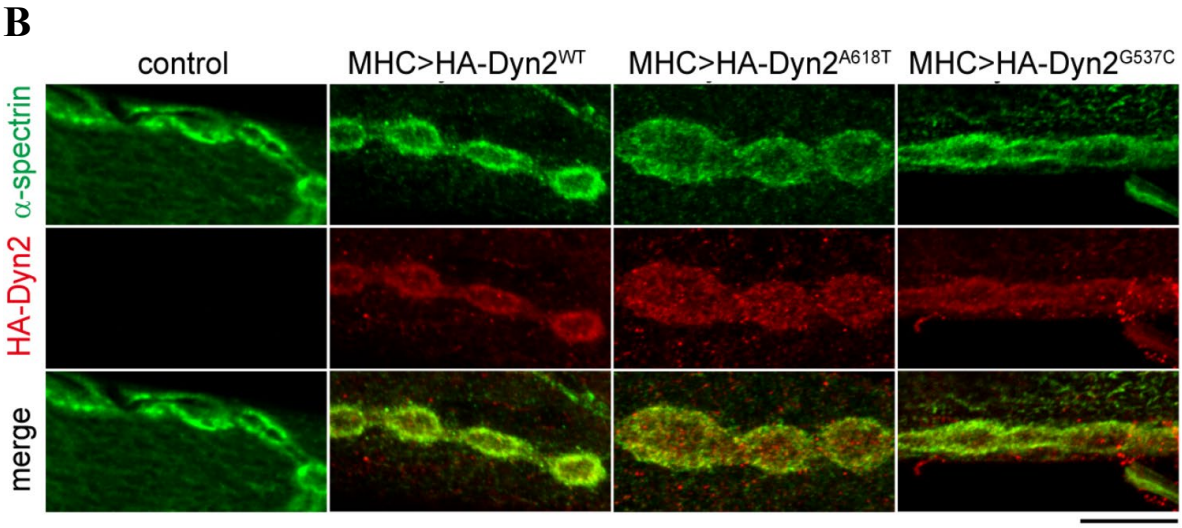

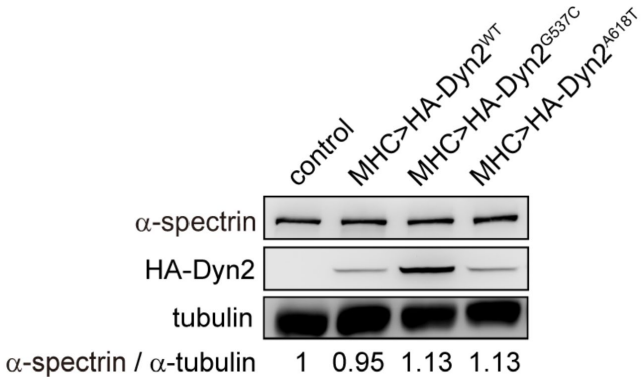

doi:10.6342/NTU202100043

Figure 4. Dyn2 affects postsynaptic cytoskeletal organization in *Drosophila*

(A) Immunostaining with anti-α-spectrin and HRP antibodies showed the distribution of α-spectrin and horseradish peroxidase (HRP) in third-instar larval NMJs. The enrichment of α-spectrin and HRP around single bouton was shown by line scan analysis. Images were taken by z stack confocal microscopy and are presented as z stack projections. Scale bar, 10 μm. **(B)** Thickness of α-spectrin. Each dot represents the spectrin thickness in one bouton. For each mutant, at least 5 NMJs were analyzed. **(C)** Intensity of α-spectrin. Each dot represents the spectrin intensity in one NMJ. For each mutant, 9 NMJs were analyzed.

doi:10.6342/NTU202100043

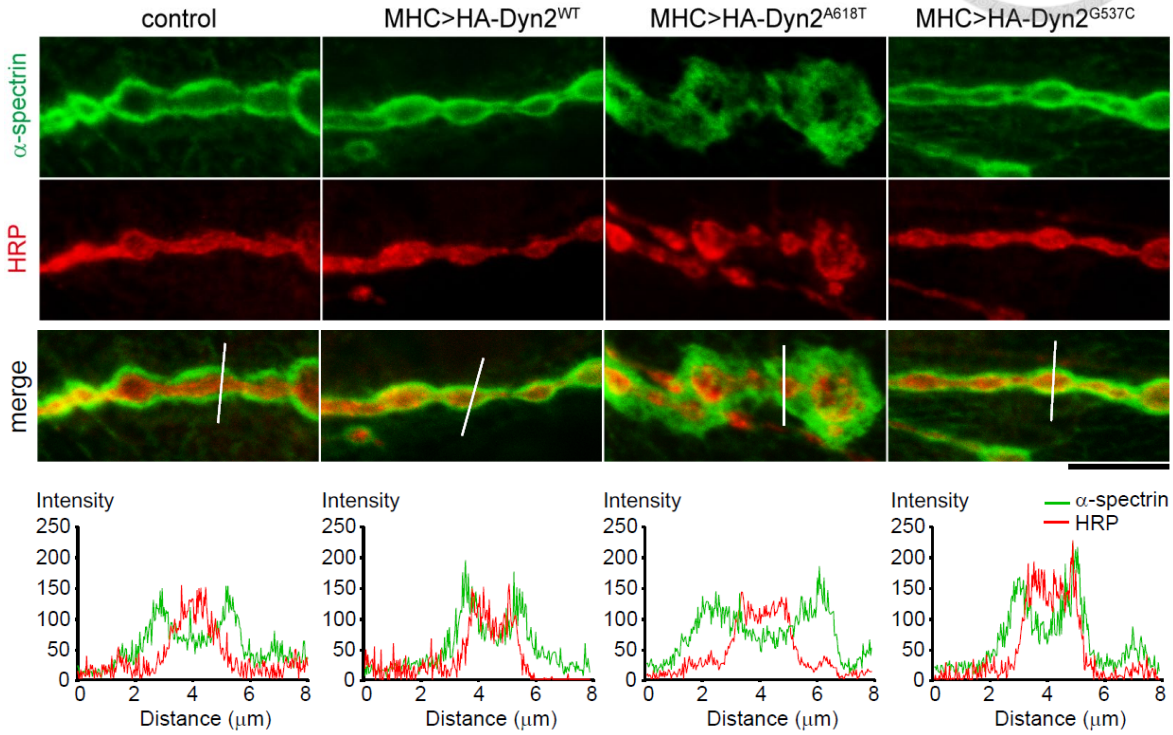

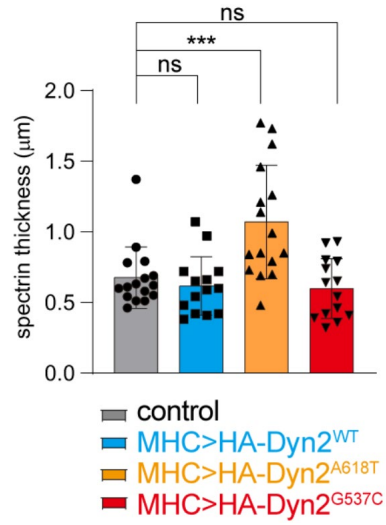

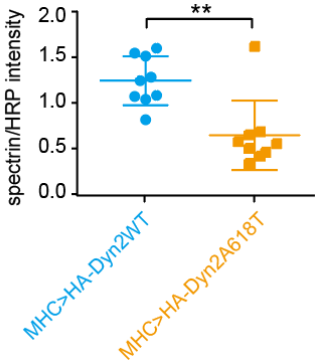

doi:10.6342/NTU202100043

Figure 5. Effects of Dyn2 at *Drosophila* postsynaptic NMJ

(A-B) Distribution of DLG **(A)**, Brp **(B)** and HRP in third-instar larval NMJs in indicative Dyn2 mutant expressing flies. **(C-D)**, Quantification of ghost bouton index and number of branch points per NMJ in wild type and flies expressing indicative Dyn2 mutants. ns, not significant.

doi:10.6342/NTU202100043

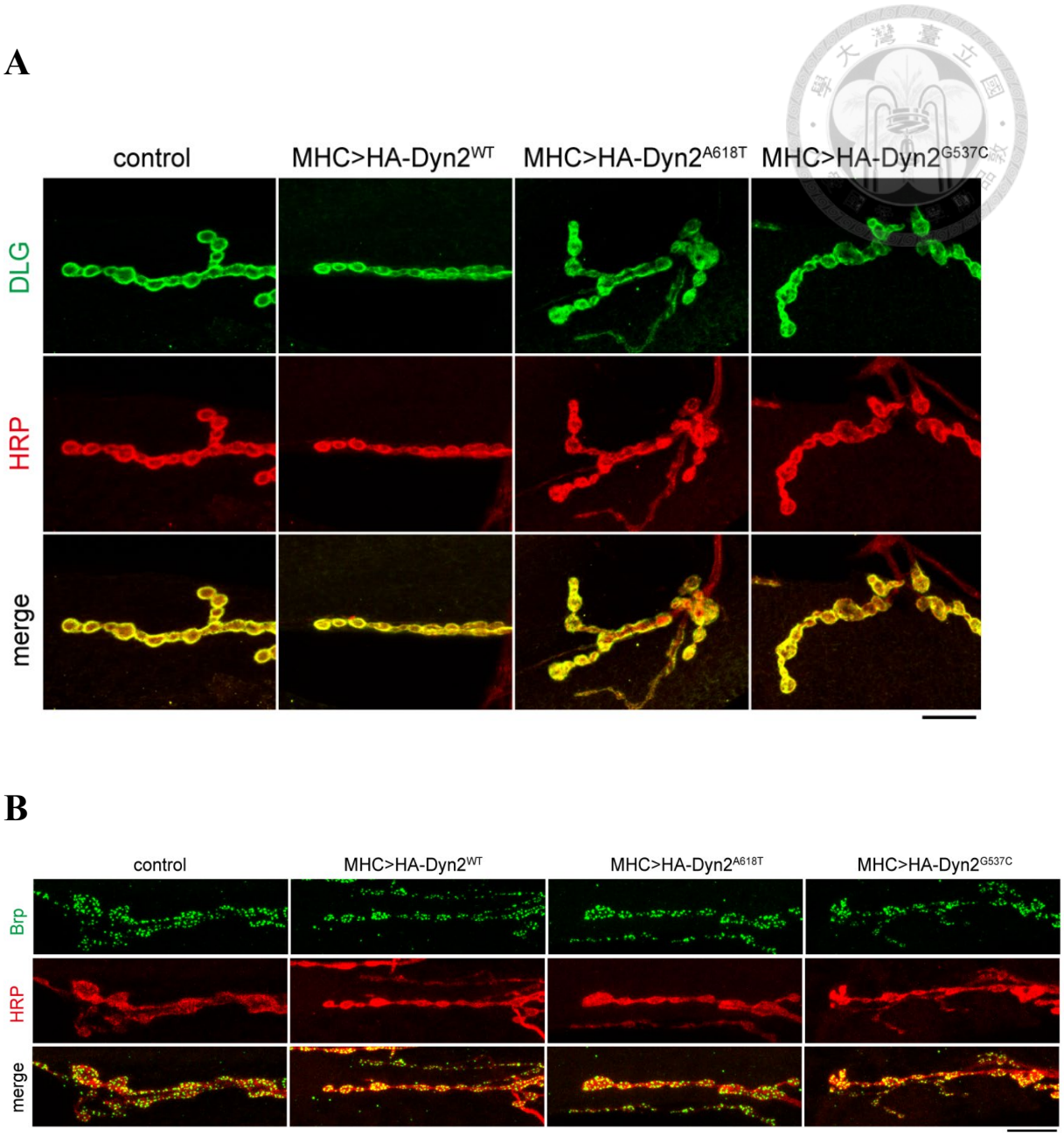

doi:10.6342/NTU202100043

Figure 6. Dyn2 affects postsynaptic SSR density in *Drosophila*

(A) TEM images of NMJ boutons from wild-type and $Dyn2^{WT}$- and $Dyn2^{A618T}$-expressing *Drosophila*. Boxed areas (within yellow dashed lines) are magnified and shown alongside. Scale bar, 500 nm. The SSR is pseudo-colored in green, and parameters of SSR morphology were quantified and are shown in **(B–D)**. All data in this work are expressed as mean ± SD of at least three independent experiments. ns, not significant; $^{**}p < 0.01$; $^{***}p < 0.001$.

doi:10.6342/NTU202100043

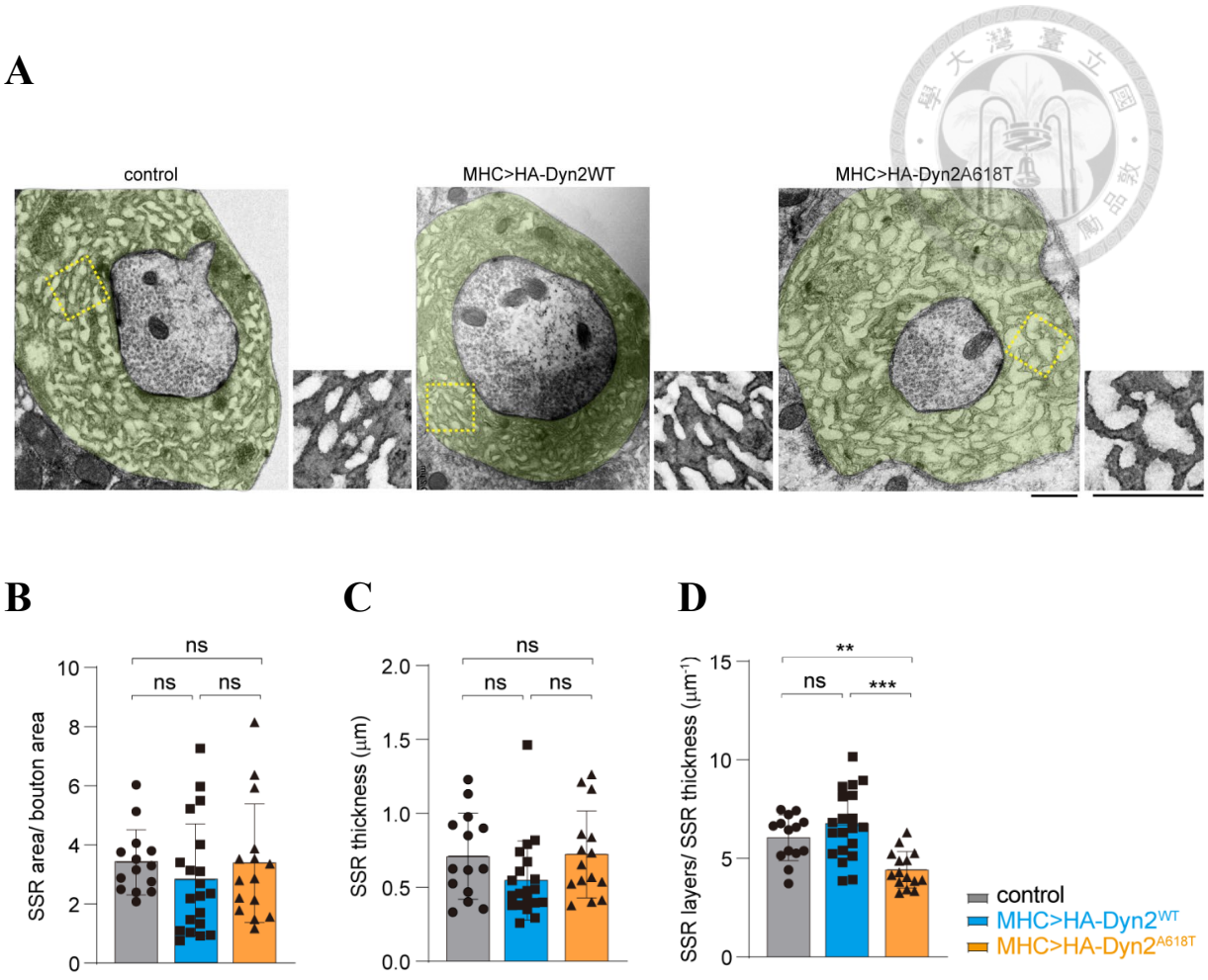

doi:10.6342/NTU202100043

Figure 7. Dyn2 affects electrophysiological activities in *Drosophila*

(A) Representative traces and quantification of the mEJP amplitude of wild-type and *Drosophila* expressing $Dyn2^{WT}$, $Dyn2^{A618T}$, and $Dyn2^{G537C}$ in their body wall muscle. **(B)** Quantification of the mEJP frenquency of wild-type and *Drosophila* expressing $Dyn2^{WT}$, $Dyn2^{A618T}$, and $Dyn2^{G537C}$ in their body wall muscle. **(C)** Representative traces and quantification of the EJP amplitude of wild-type and *Drosophila* expressing $Dyn2^{WT}$, $Dyn2^{A618T}$, and $Dyn2^{G537C}$ in their body wall muscle **(D)** Quantification of the quantal content of wild-type and *Drosophila* expressing $Dyn2^{WT}$, $Dyn2^{A618T}$, and $Dyn2^{G537C}$ in their body wall muscle. ns, not significant; $^{*}p < 0.05$.

doi:10.6342/NTU202100043

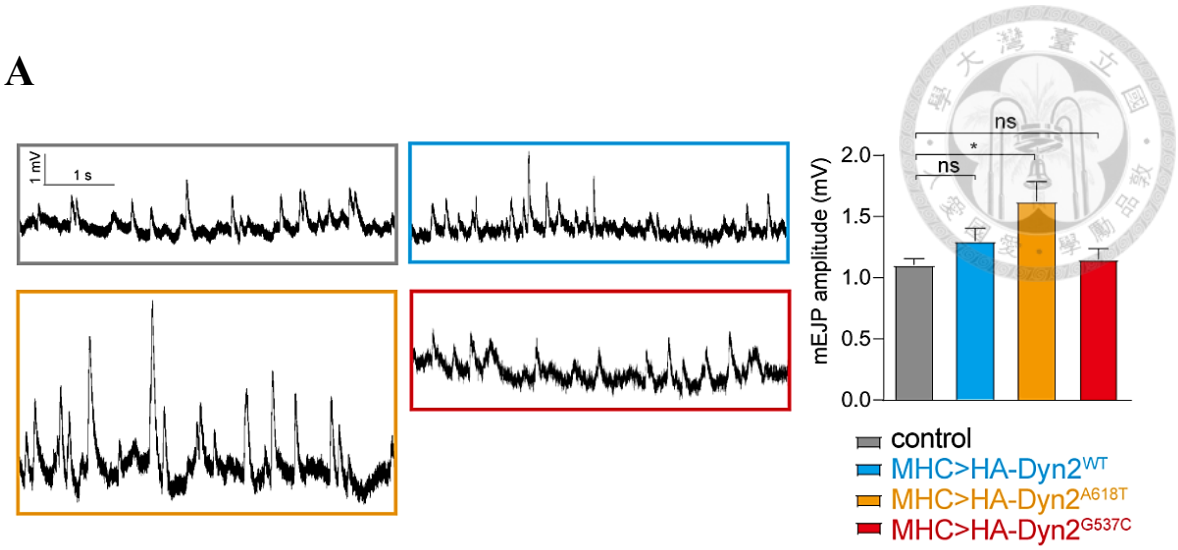

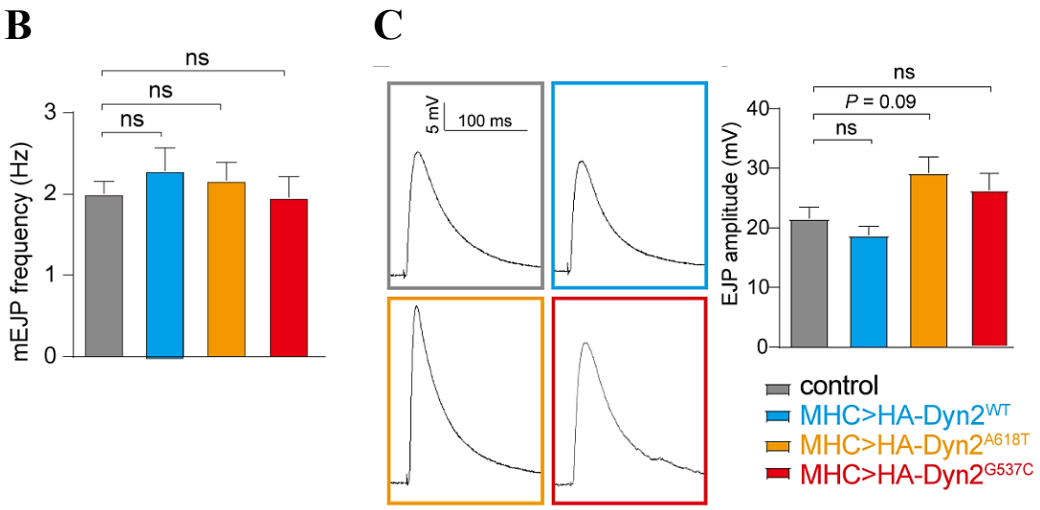

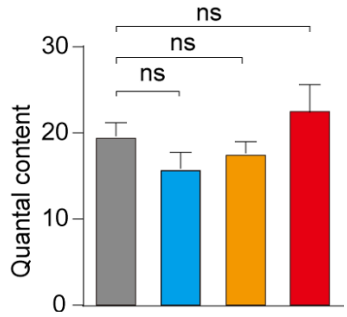

doi:10.6342/NTU202100043

Figure 8. Dyn2 did not affect GluRIIA distribution

(A) Distribution of GluRIIA and HRP in third-instar larval NMJs in $Dyn2^{WT}$ and $Dyn2^{A618T}$ expressing flies. **(B-D)** Quantification results of GluRIIA distribution. **(B)** GluRIIA area is normalized to HRP area and presented as percentages. **(C)** GluRIIA intensity is normalized to HRP intensity. At least 12 NMJs were analyzed in each mutant and each dot represents the normalized area and intensity in one NMJ. **(D)** Size of GluRIIA clusters. At least 90 clusters in each mutant were analyzed. ns, not significant. Scale bars, 10 μm.

doi:10.6342/NTU202100043

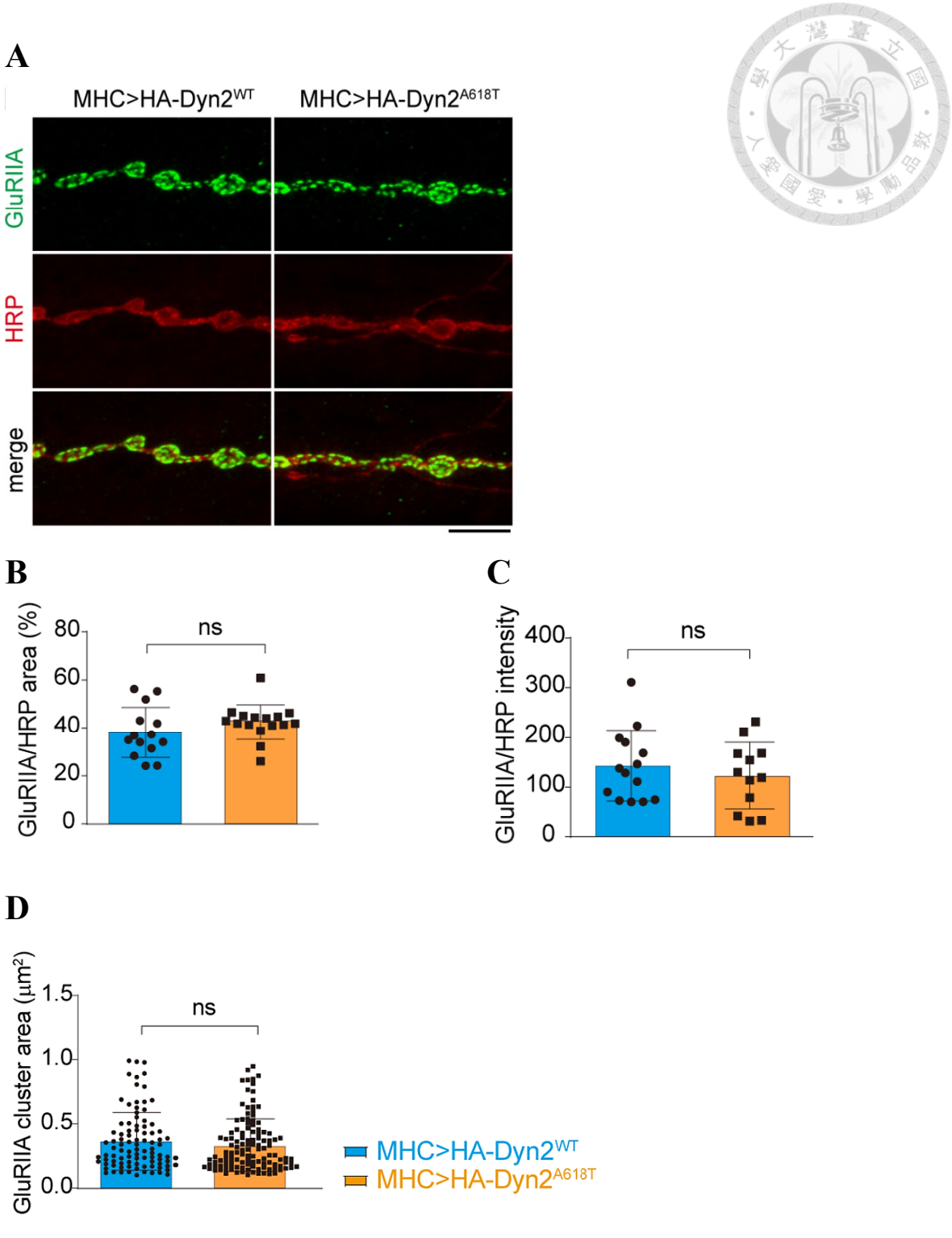

doi:10.6342/NTU202100043

Figure 9. Endogenous Dyn2 is enriched at mouse postsynaptic NMJ

(A-B), *Transverse abdominis* (TVA) muscles from 4-week-old mice were isolated, fixed, and stained to visualize endogenous Dyn2. Postsynaptic AChRs were labeled by Alexa-488 bungarotoxin (BTX) and presynaptic neuron was labeled by synaptophysin. The boxed area is amplified to show the z-projection and orthogonal view of part of the NMJ. Scale bar, 10 μm. **(B)**, Line scan analysis of Dyn2, BTX, and synaptophysin intensity along the yellow line in B. was plotted. **(C)** Day 6-differentiated myotubes cultured on Permonox slides were stained to visualize endogenous Dyn2, F-actin, and AChR (labeled by Bungarotoxin) under z-stack confocal microscopy. Scale bar, 10 μm.

doi:10.6342/NTU202100043

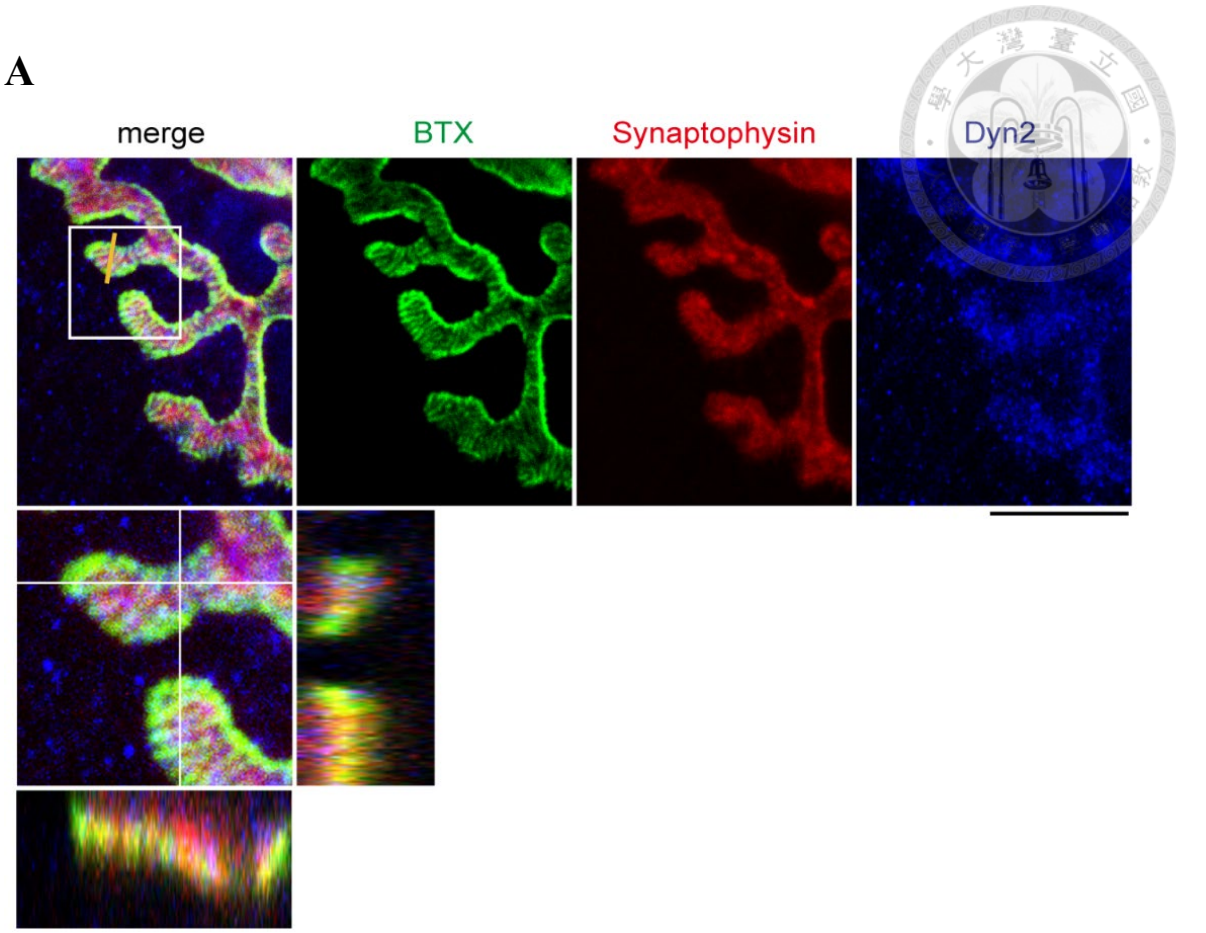

doi:10.6342/NTU202100043

Figure 10. AChR clustering and perforation in C2C12 myotubes on laminin-coated glass coverslips

Myoblasts were seeded on laminin-coated glass coverslips and subjected to differentiation. Day 5-differnetiated myotubes were fixed and stained to visualize AChR cluster and synaptic podosomes. Images were acquired from z-stack confocal microscopy. Boxed areas were magnified and shown in lower panels. Scale bar, 10 μm.

doi:10.6342/NTU202100043

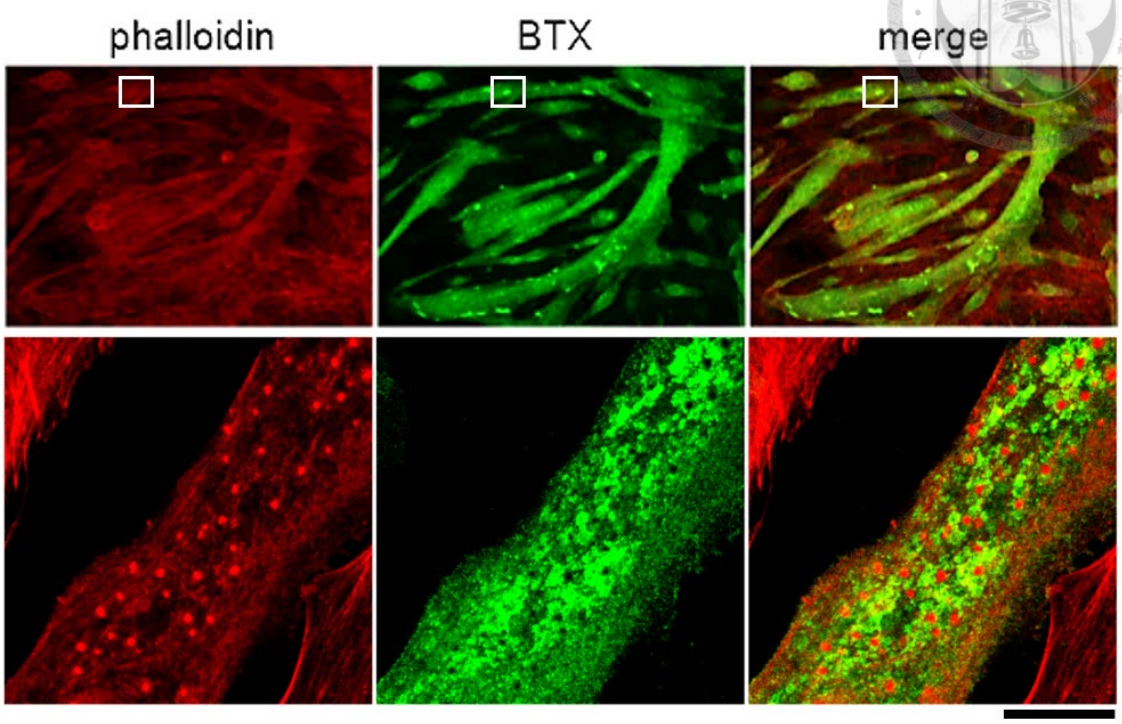

doi:10.6342/NTU202100043

Figure 11. AChR clustering and perforation in C2C12 myotubes

Myoblasts were seeded on laminin-coated Permanox slides and subjected to differentiation. Day 3- to Day 6-differnetiated myotubes were fixed and stained to visualize AChR cluster and synaptic podosomes. Images were acquired from z-stack confocal microscopy. Boxed areas were magnified and shown in lower panels. Scale bar, 10 μm.

doi:10.6342/NTU202100043

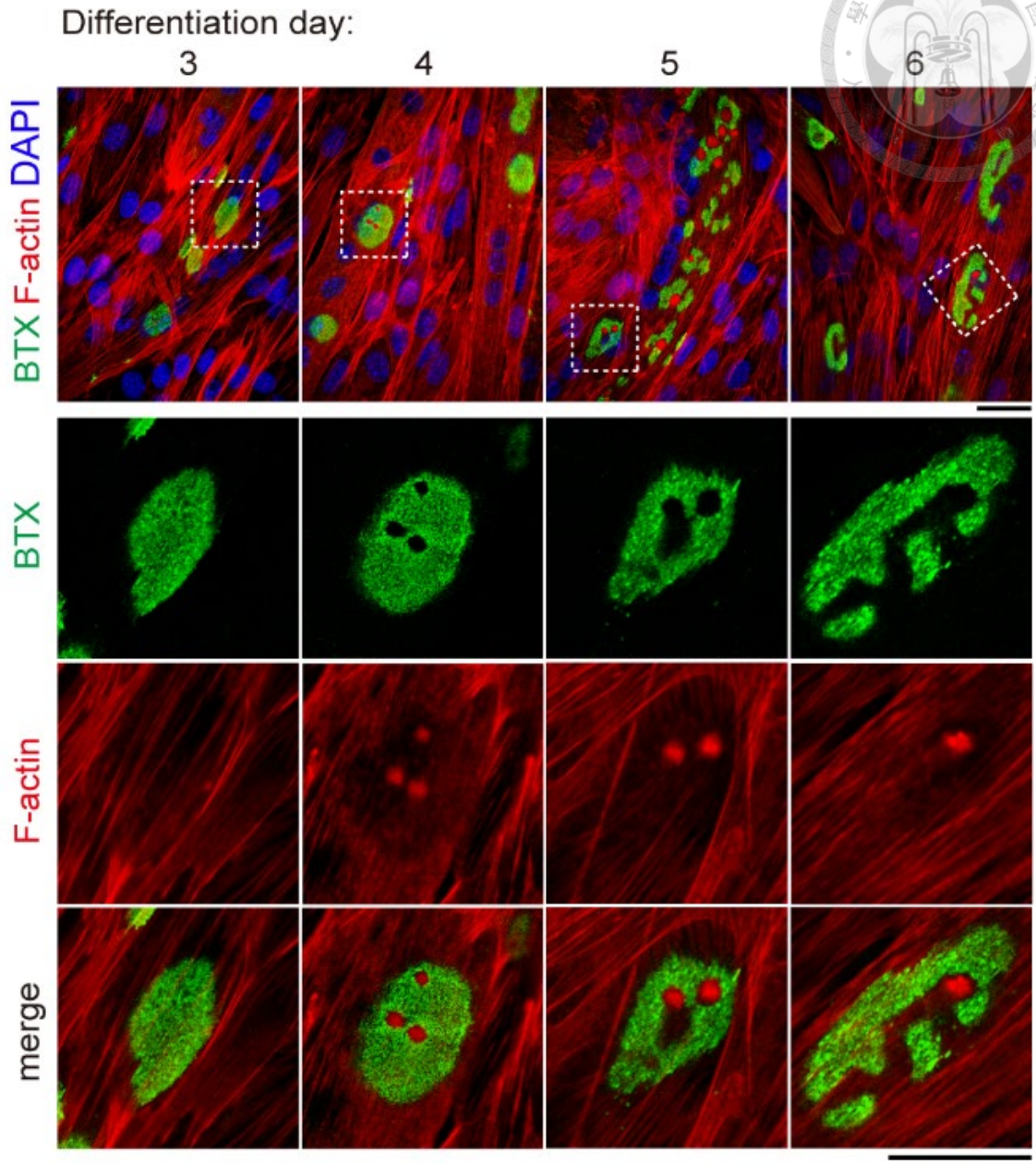

doi:10.6342/NTU202100043

Figure 12. Dyn2 formed belt-shaped structure around some podosome core

(A-B) Dyn2 forms belt-like structures around the actin cores of podosomes. Differentiated myotubes were fixed and stained to visualize endogenous F-actin, Dyn2, and Tks5. Images were acquired from z stack confocal microscopy. Boxed areas in **A** were magnified and shown in lower panels to display the z projection and orthogonal view of a single podosome. Arrowhead, podosome with a Dyn2 belt; open arrow, podosome with partial Dyn2 belt; arrow, podosome without a Dyn2 belt. Scale bar in **A**, 2 μm, Scale bar in **B**, 10 μm. **(C)** Z-projection and orthogonal view of a single podosome from STED microscopy. Scale bars, 10 μm.

doi:10.6342/NTU202100043

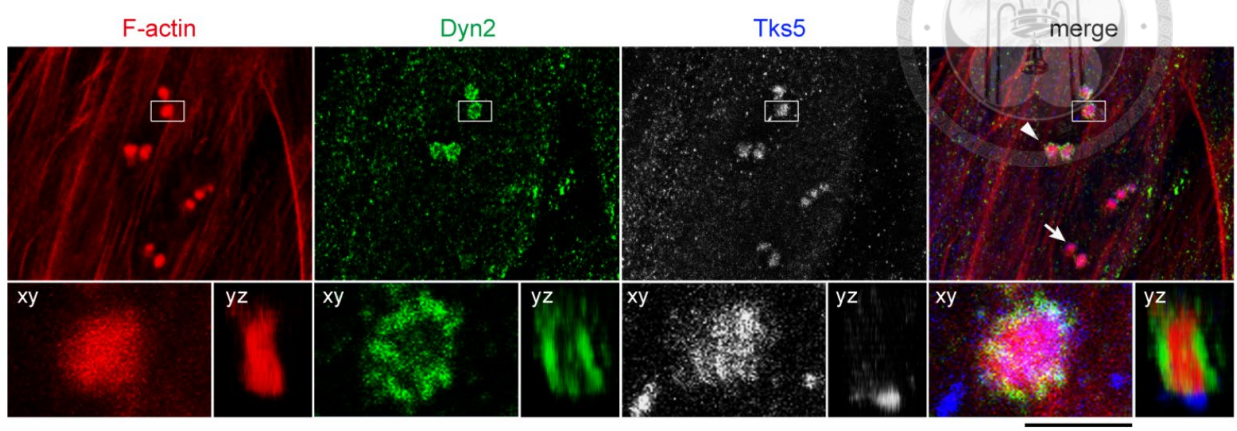

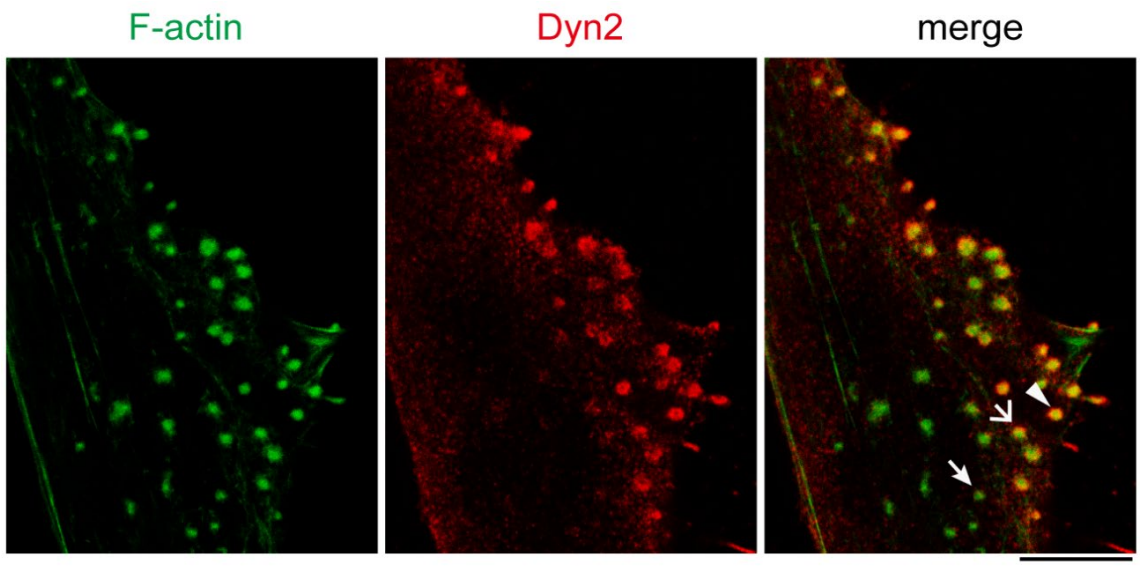

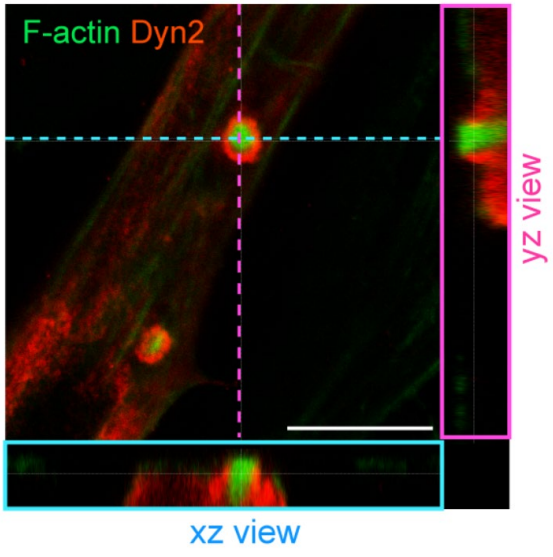

doi:10.6342/NTU202100043

Figure 13. Dyn2-belt localize in between podosome core and the radical actin cables

(A) Dyn2 localizes differently from other podosome components. Differentiated myotubes were fixed and stained to visualize endogenous F-actin, Dyn2, Arp2, cortactin, vinculin, and myosin IIA. Scale bar, 2 μm. **(B)** 3D reconstructed image of single podosome in myotubes derived from z-stack confocal microscopy. **(C)** Line scan analysis of the Dyn2 and Myosin IIA intensity along the white line in **B** was plotted.

doi:10.6342/NTU202100043

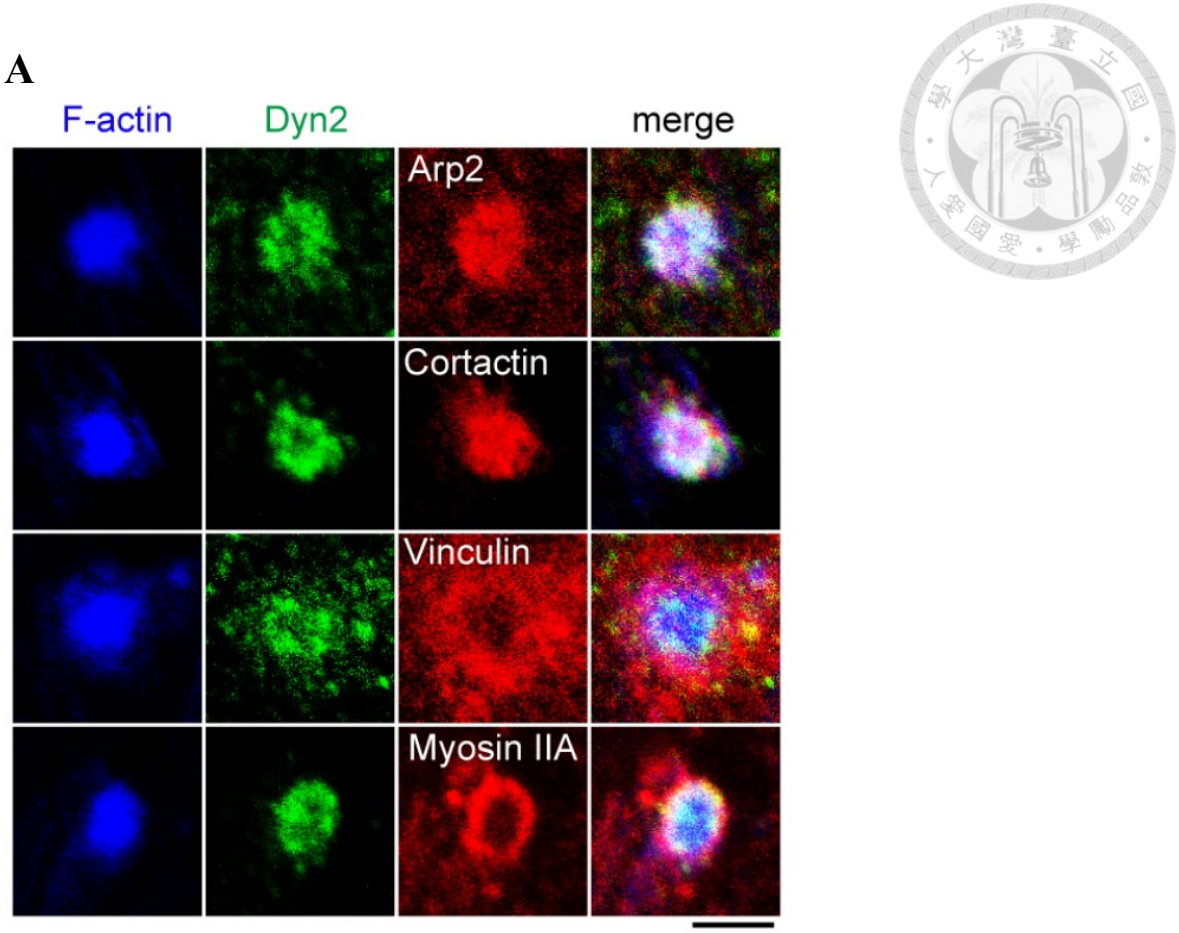

doi:10.6342/NTU202100043

Figure 14. Level of Dyn2 enrichment correlates with podosome size

(A) Population of podosomes with different levels of Dyn2 belts. **(B-C)** Level of Dyn2-belt decoration is correlated with podosome height and width. Podosomes were grouped into three categories according to the amount of Dyn2 surrounding the actin core. Each dot represents one podosome. At least 40 podosomes in 10 cells were analyzed. The representative images are shown in the lower panels, with Dyn2 in green and F-actin in red. $^{**}p < 0.01$; $^{***}p < 0.001$.

doi:10.6342/NTU202100043

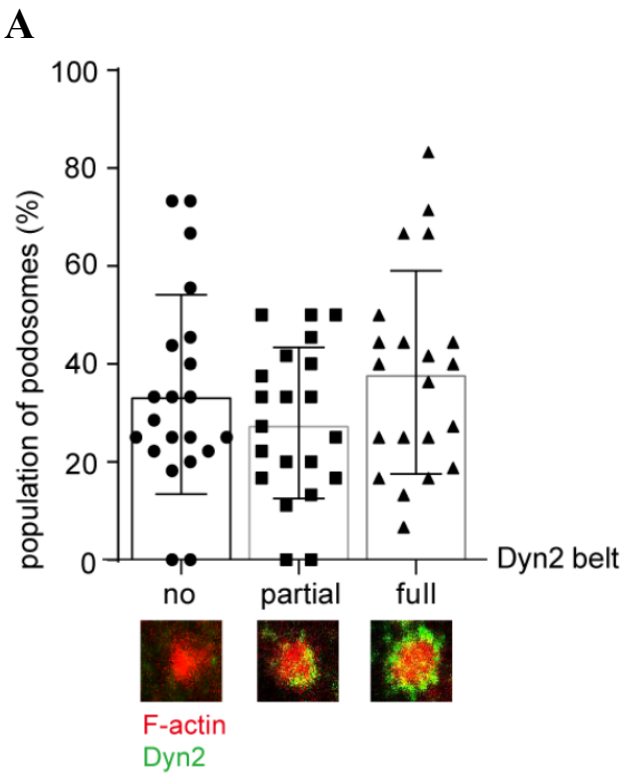

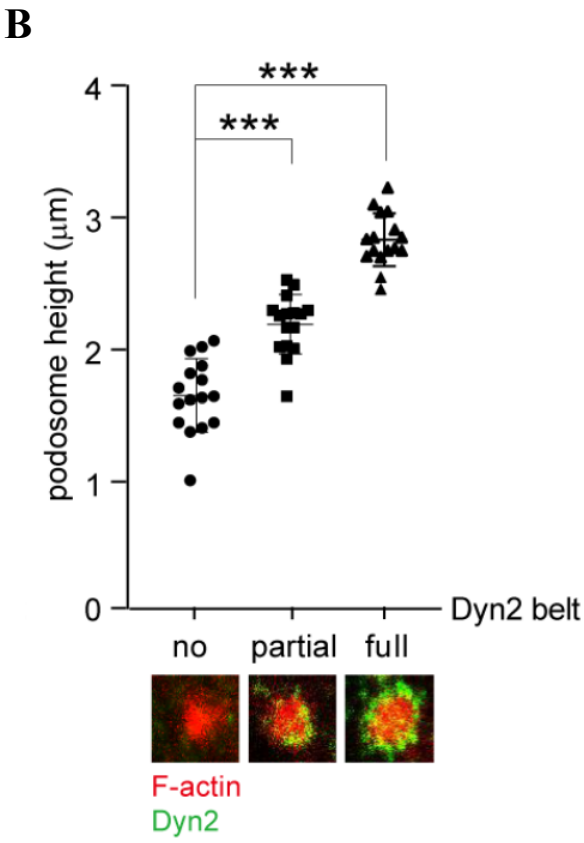

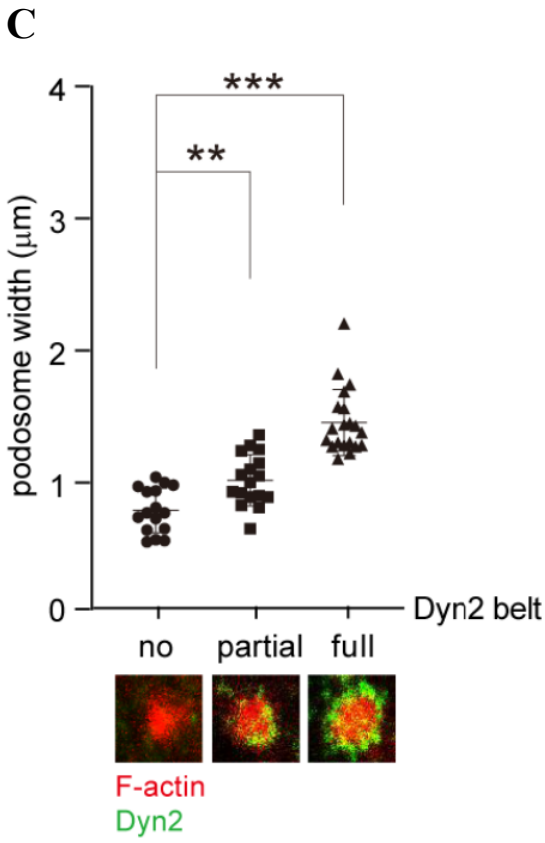

doi:10.6342/NTU202100043

Figure 15. Dyn2 is required for podosome growth

(A) A Knockdown efficiency of *DNM2* shRNA. Dyn2 was depleted by two lentiviral shRNAs and selected with puromycin for 3 days followed by 3 days of differentiation. Cells were subjected to immunoblotting, and the knowkcodown efficiency was quantified and labeld on the bottom of the gel. **(B)** Podosomes in Dyn2-depleted myotubes. Podosomes were labeled with the podosome marker Tks5. Day-5-differentiated myotubes were fixed and stained to visualize endogenous F-actin, Dyn2, and Tks5. Images were acquired by z stack confocal microscopy. Insets represent enlarged views of z projection (upper) and orthogonal views (lower) of a single podosome. Scale bars, 2 μm. **(C)** Height and width of podosomal actin cores are reduced in Dyn2-depleted myotubes. Each dot represents one podosome. **(D)** Podosome density in Dyn2-depleted myotubes. Each dot represents one myotube.

doi:10.6342/NTU202100043

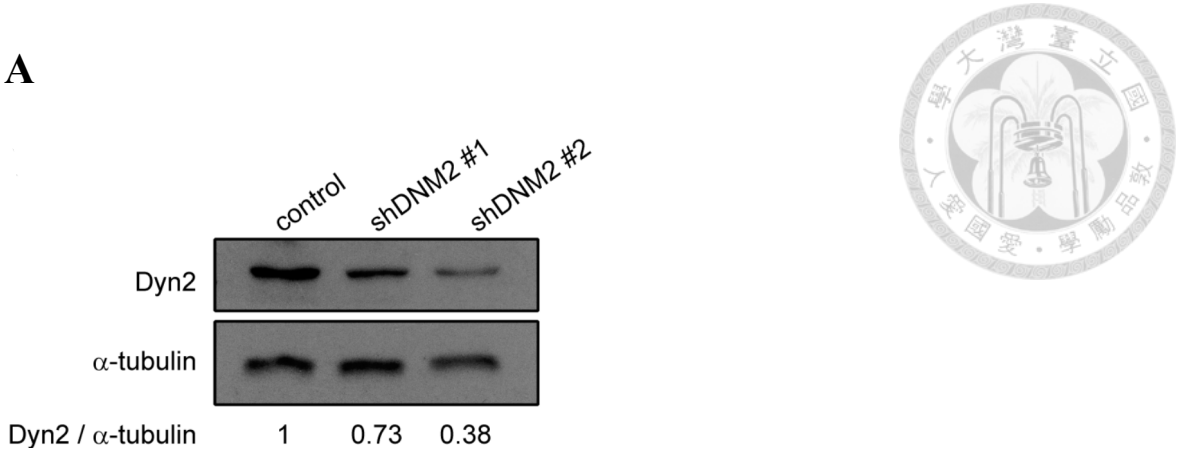

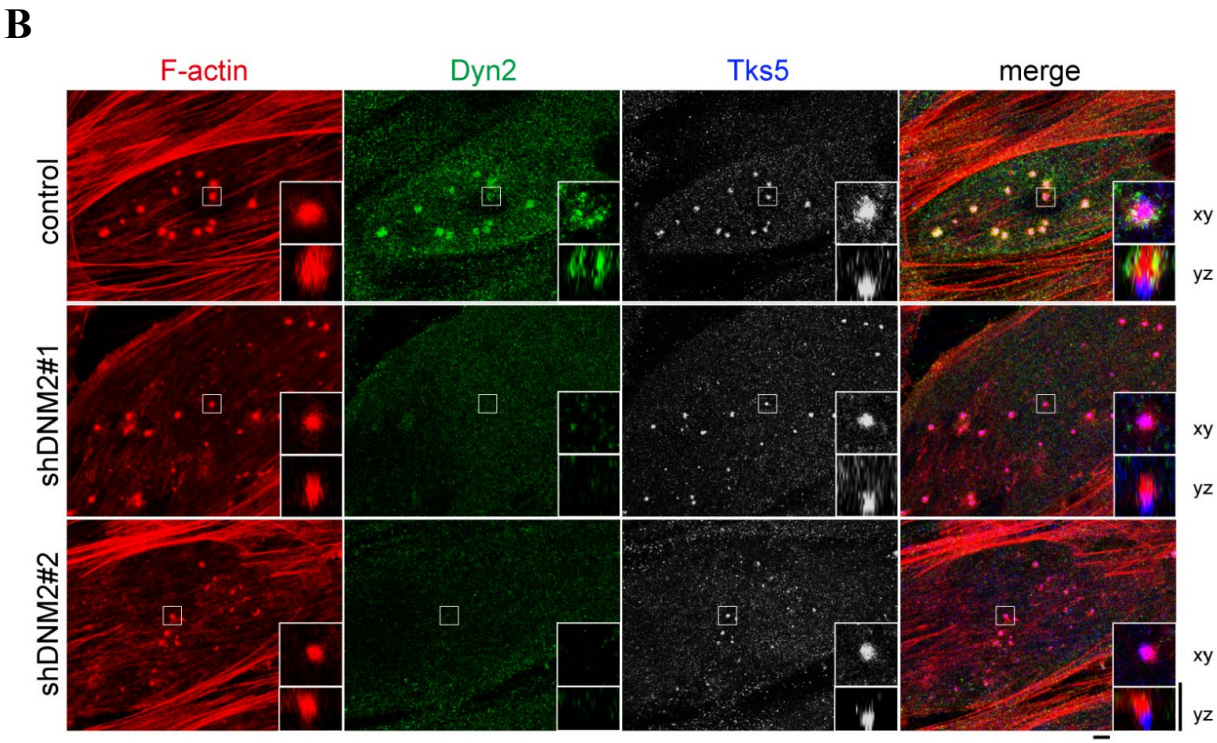

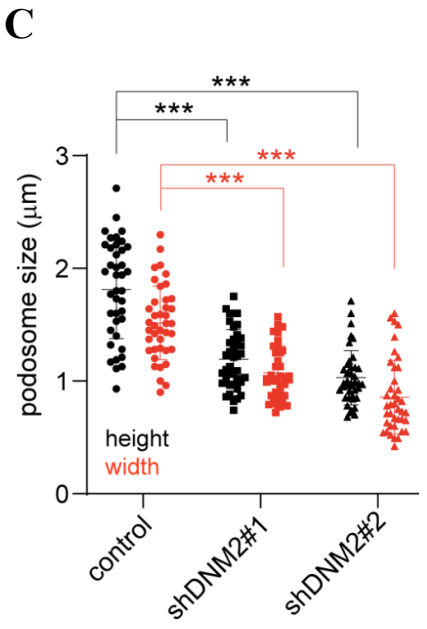

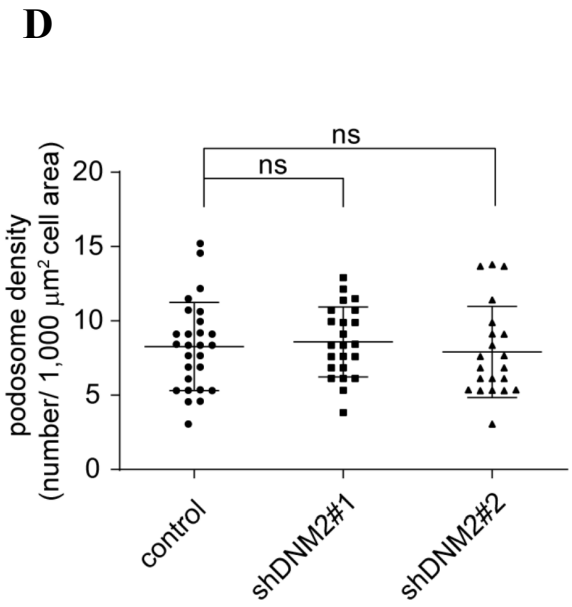

doi:10.6342/NTU202100043

Figure 16. Dyn2 forms belt-shaped structure as podosome matures

(A-C) Snapshots of time-lapse images of a single podosome showing the temporal distribution of Cortactin, Dyn2, and Tks5 in myotubes. Myotubes expressing Lifeact-GFP and Cortactin-mCherry **(A),** Lifeact-RFP and Tks5-EGFP **(B)**, or Lifeact-GFP and $Dyn2^{WT}$-mCherry **(C)** were imaged by inverted fluorescence microscopy at 37°C with 1 min frame intervals. Scale bars in **A, C**, 5 μm. Scale bar in **B**, 2 μm.

doi:10.6342/NTU202100043

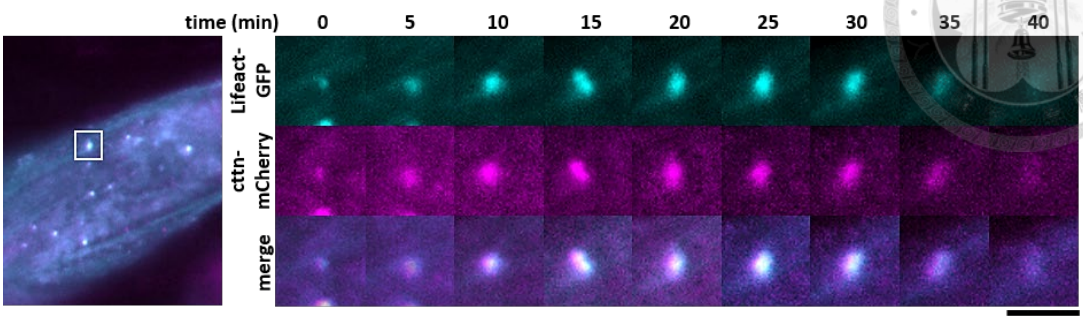

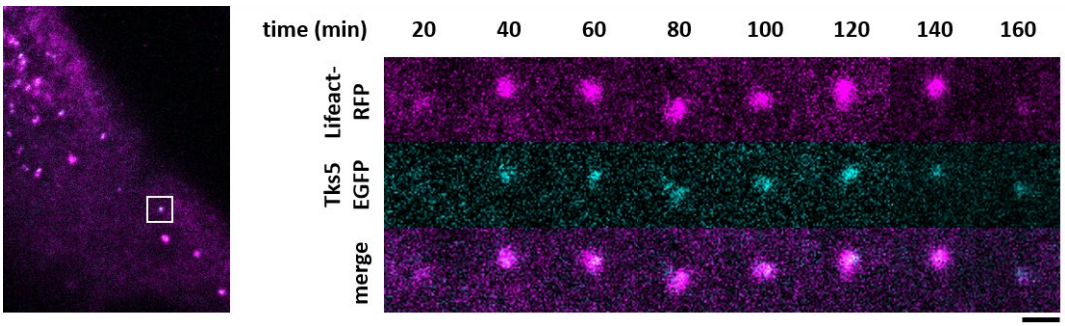

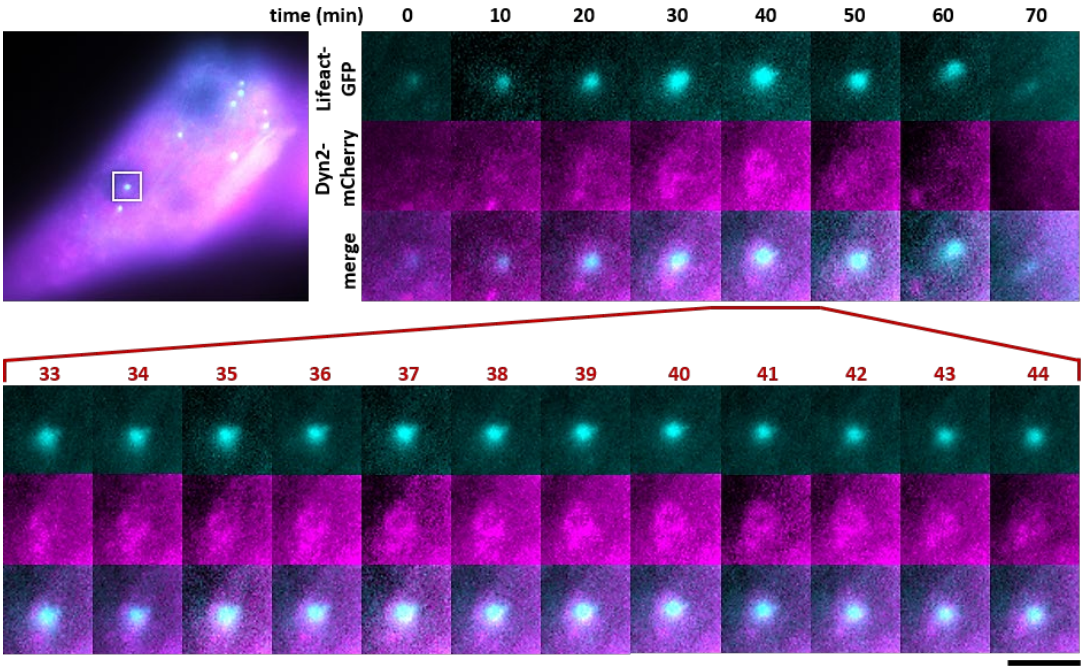

doi:10.6342/NTU202100043

Figure 17. The correlation of Dyn2 enrichment and podosome lifespan

(A) Frequency distribution of podosome lifespan in myotubes (n = 37 podosomes). **(B)** Time course of individual podosomes were plotted from short to long in cyan. Regions colored in magenta represent the appearance of Dyn2. **(C)** Percentage of Dyn2 appearance during podosomes lifespan in myotubes. Each dot represents one podosome. **(D)** Correlation between podosome lifespan and Dyn2 enrichment.

doi:10.6342/NTU202100043

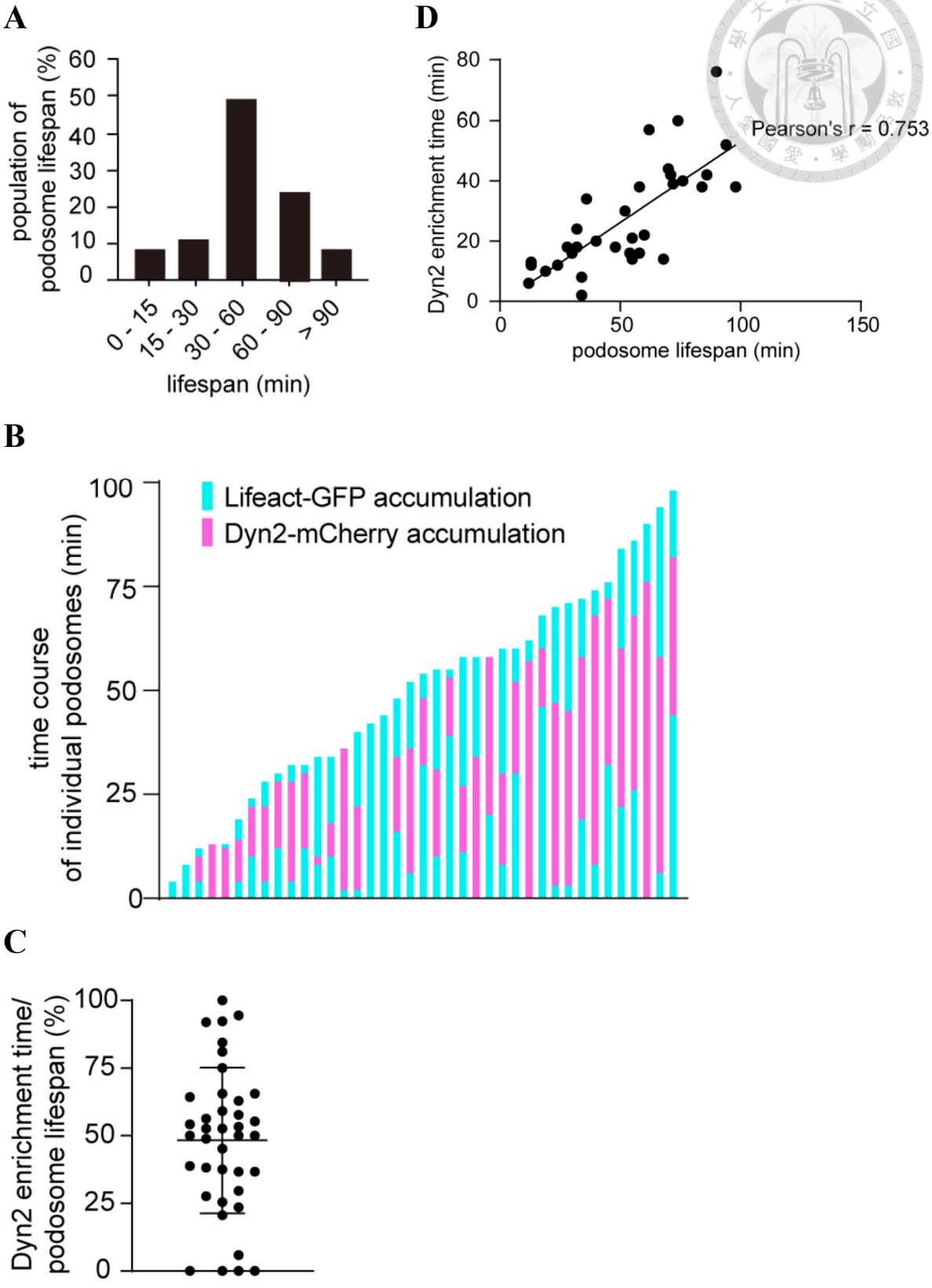

doi:10.6342/NTU202100043

Figure 18. Dyn2 is required for podosome turnover

(A-B) Podosomes in Dyn2-depleted myotubes have shorter lifespans. Podosome lifespan was quantified by the duration of the podosome core, as labeled by Lifeact-GFP, and the data were divided into five cohorts as shown. Scale bars, 2 μm.

doi:10.6342/NTU202100043

A

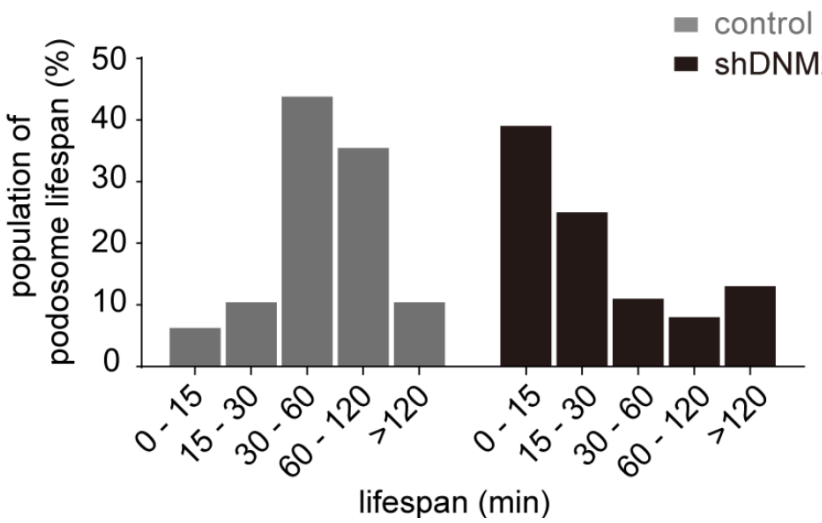

B

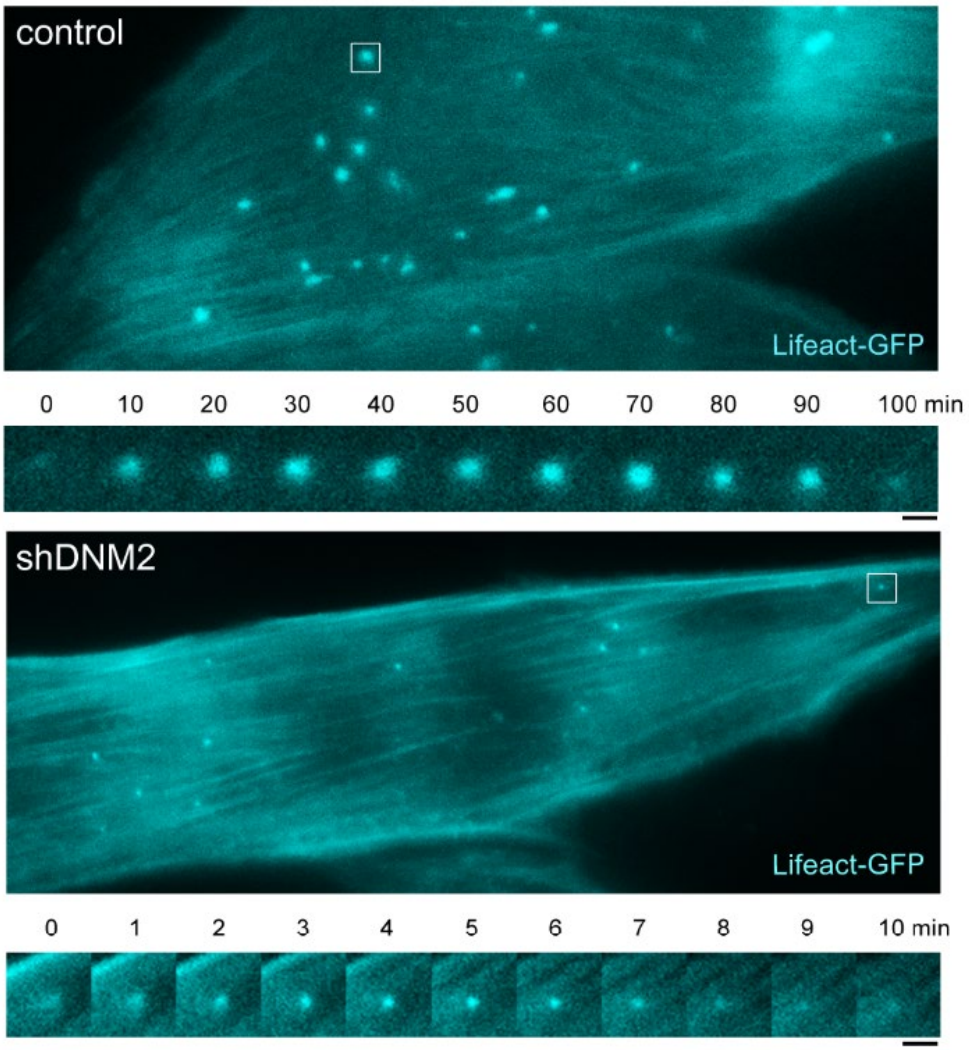

doi:10.6342/NTU202100043

Figure 19. Dyn2 GTPase activity is involved in podosome growth and turnover

(A-B) Acute treatment of 100 μM dynasore increases podosome height in myotubes. Day 4-differentiated myotubes were fixed and stained to visualize endogenous F-actin and Dyn2 after 2 or 4 hrs of dynasore treatment. Scale bar, 10 μm. The height of podosome was quantified from the orthogonal images on the right panel, analyzed and shown as in **B**. Each dot represents one podosome. **(C)** Prolonged treatment of 100 μM dynasore reduced podosome number. In each condition, at least 40 podosomes in 10 different cells were analyzed. 12 h of 100 μM dynasore treatment showed disruptive effects on muscle podosomes. Scale bar, 10 μm. ***$P < 0.001$.

doi:10.6342/NTU202100043

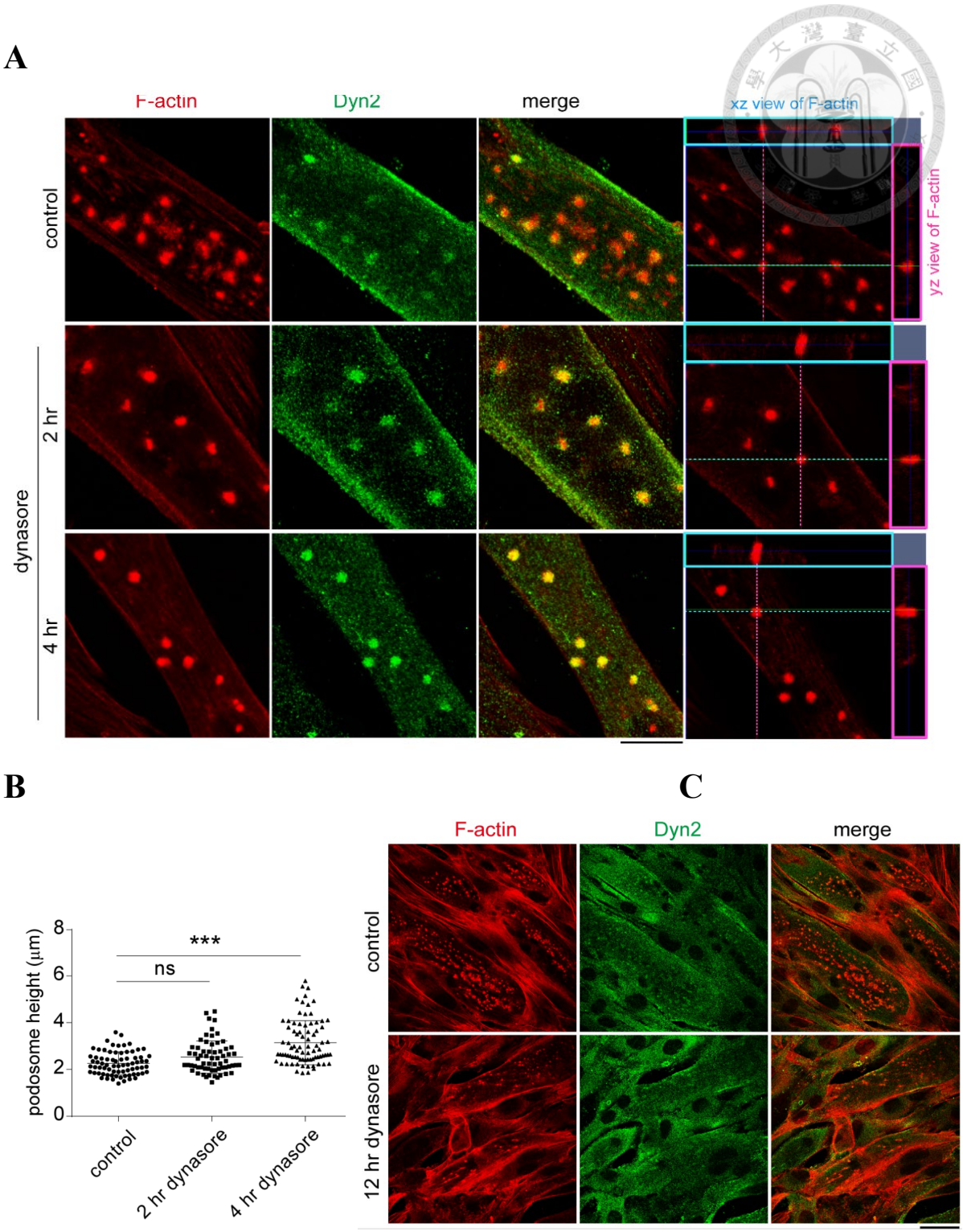

doi:10.6342/NTU202100043

Figure 20. Mutations used in this study

(A) Domain structure of Dyn2 and the mutations used in this experiment. **(B)** References of Dyn2 mutants and their biochemical properties.

doi:10.6342/NTU202100043

A

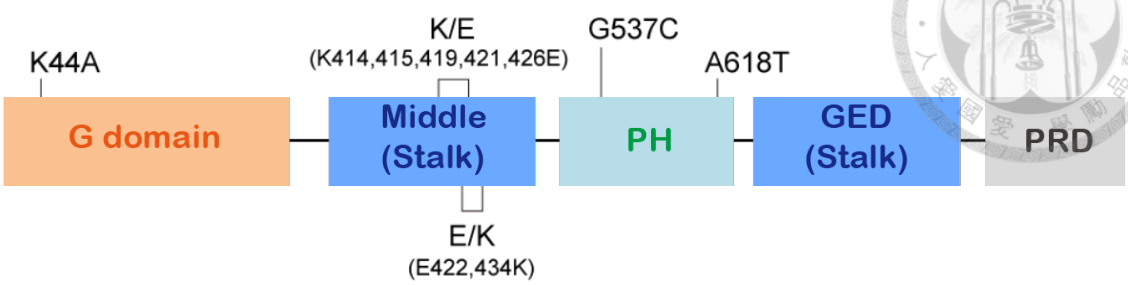

B

Dynamin Mutations	Basal GTPase activity	liposome-stimulated GTPase activity	Membrane fission activity	Actin bundling ability (in vitro or in vivo)	Endocytosis activity	Reference
A618T	Increased	Increased	Increased	Increased	Normal or Increased	(Chin, Lee et al., 2015, Kenniston & Lemmon, 2010); in this study
G537C	Normal	Decreased	Decreased	Normal	Decreased	(Chin et al., 2015), in this study
K/E	Normal	Normal	ND	Decreased	Normal	(Chuang, et al., 2019, Gu, et al., 2010)
E/K	Normal	Normal	ND	Increased	Normal	(Chuang et al., 2019, Gu et al., 2010)
K44A	Decreased	Decreased	Defected	ND	Decreased	(DamkE, Binns et al., 2001, Gu et al., 2010, Sundborger, Fang et al., 2014)

ND: not determined

doi:10.6342/NTU202100043

Figure 21. Effects of mutant Dyn2 on podosome morphology in wild type myotubes

(A) Subcellular localization of different HA-tagged Dyn2 mutants in wild-type myotubes. Scale bar, 10 μm. **(B)** Podosome density in myotubes. Each dot represents the podosome density in one cell. **(C-D)** Morphological effects of different HA-tagged Dyn2 mutants on podosome in wild type myotubes. Each dot represents one podosome (n = 22~109 podosomes per mutant). ns, not significant; $^{**}p < 0.01$; $^{***}p < 0.001$.

doi:10.6342/NTU202100043

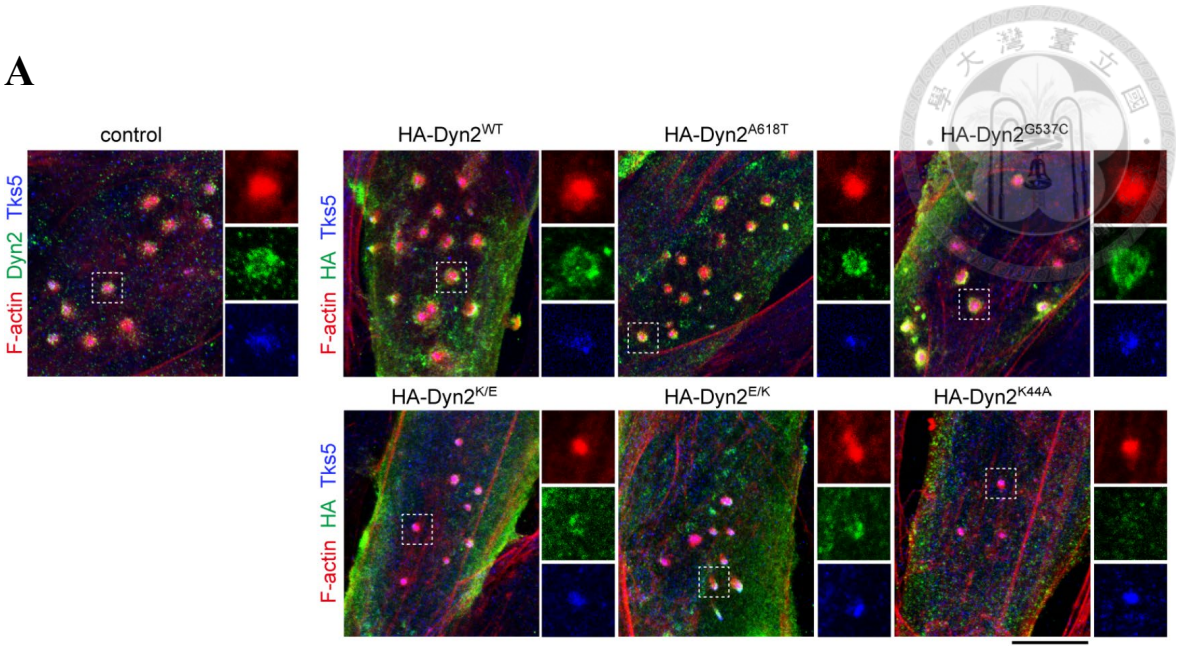

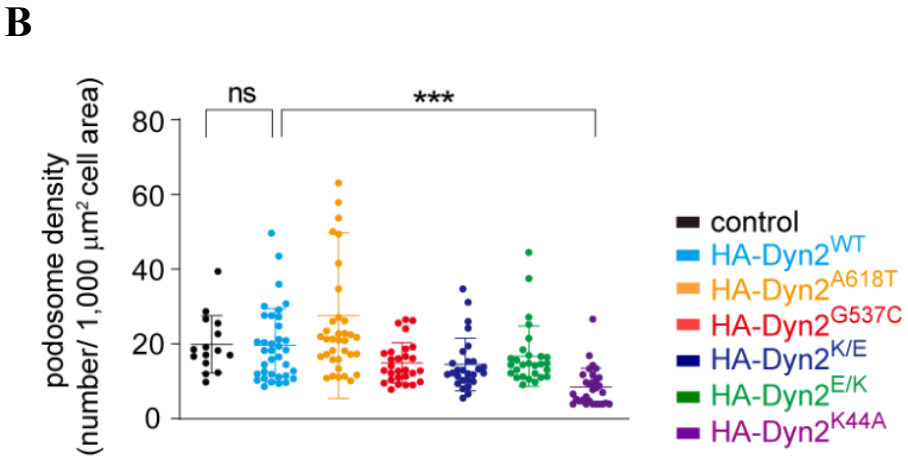

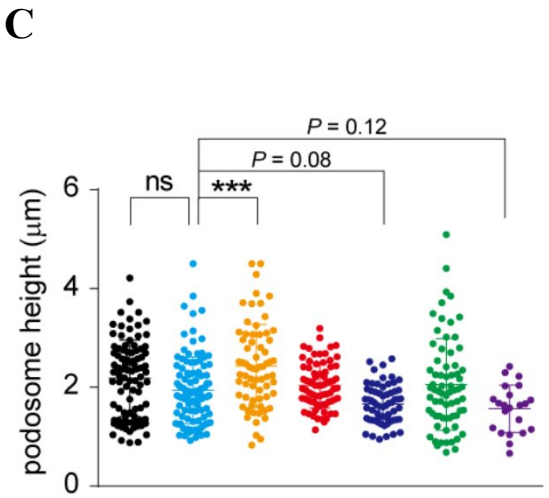

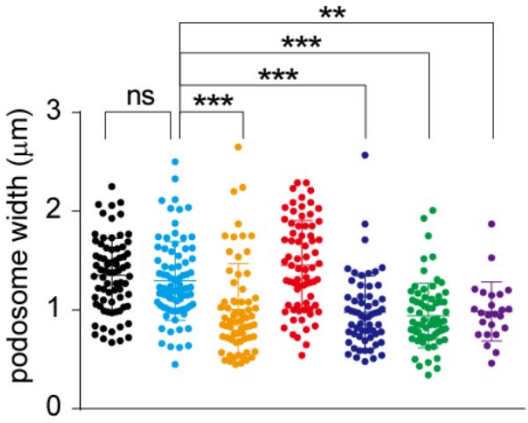

doi:10.6342/NTU202100043

Figure 22. Rescuing effects of mutant Dyn2 on podosome morphology in Dyn2-depleted myotubes

Rescuing effects of different HA-tagged Dyn2 mutants in Dyn2 knockdown myotubes. Endogenous Dyn2 was stained in control cells. HA-tagged Dyn2, F-actin, and Tks5 were stained and imaged under z stack confocal microscopy after 16 h of induction. Scale bar, 10 μm.

doi:10.6342/NTU202100043

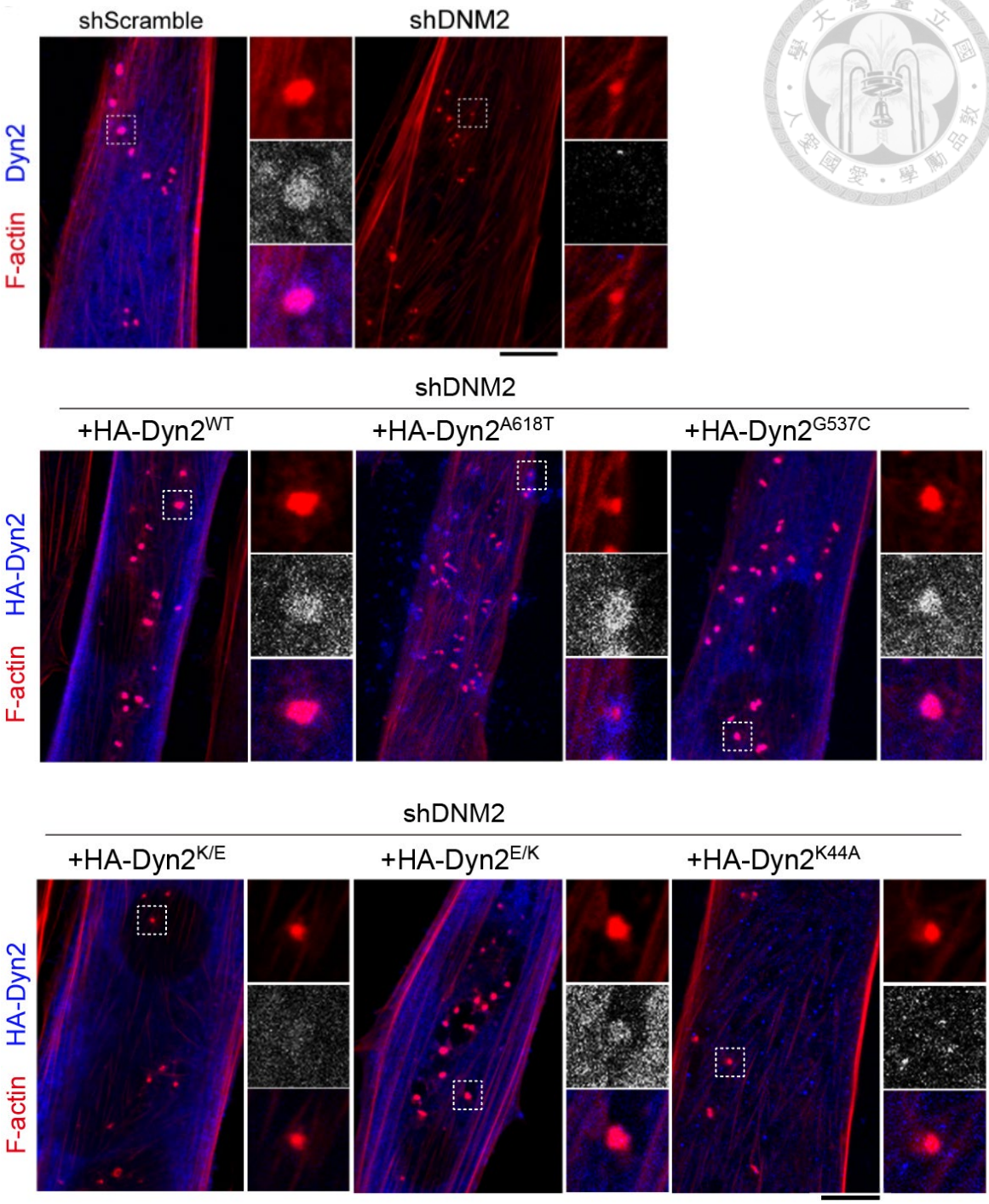

doi:10.6342/NTU202100043

Figure 23. Dyn2 is essential for podosome growth

(A) Podosome density in myotubes. Each dot represents the podosome density in one cell.

(B-C) Height and width of podosomes. Each dot represents one podosome (n = 16 to ~32 podosomes per mutant). For each mutant, 6 to ~9 cells were analyzed. ns, not significant; $^{**}p < 0.01$; $^{***}p < 0.001$.

doi:10.6342/NTU202100043

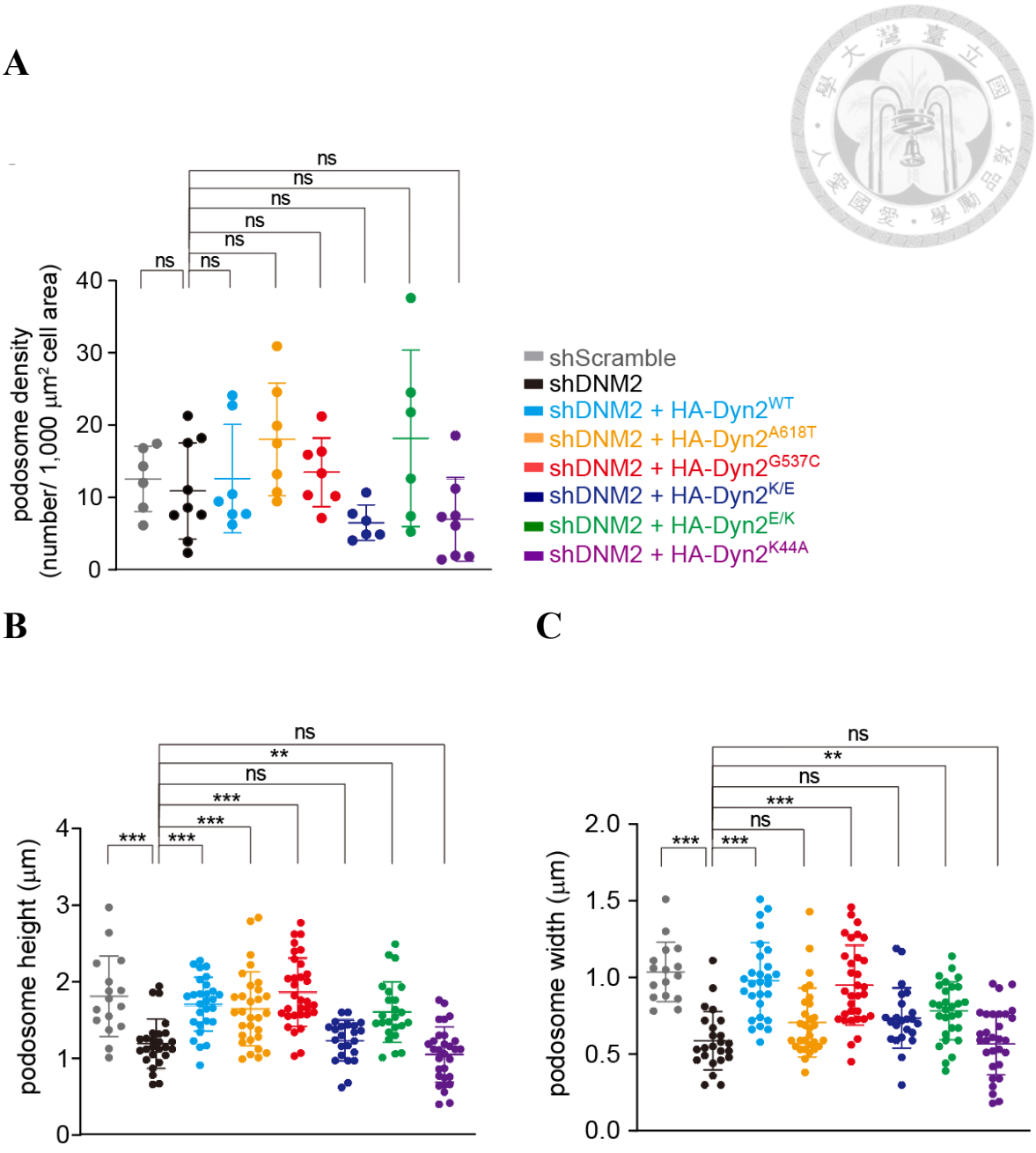

doi:10.6342/NTU202100043

Figure 24. Dyn2 is essential for podosome turnover

(A) Frequency distribution of podosome lifetime in myotubes expressing different Dyn2 mutants. Myoblasts were transfected with Lifeact-GFP and Dyn2-mCherry to visualize F-actin and Dyn2, respectively. Myotubes were imaged by inverted fluorescence microscopy at 37°C with 2 min frame intervals. Lifespans of individual podosomes were tracked and measured manually. For each condition, at least 68 podosomes for each mutant were analyzed. ns, not significant; $^{**}p < 0.01$; $^{***}p < 0.001$. **(B)** Snapshots of the time-lapse imaging of single podosomes with $Dyn2^{A618T}$-mCherry surrounding. Myoblasts were transfected with Lifeact-GFP and $Dyn2^{A618T}$-mCherry to visualize F-actin and $Dyn2^{A618T}$, respectively. Myoblasts were then seeded on laminin-coated glass-bottom dish, subjected to differentiation for 5-7 days and imaged with inverted fluorescence microscope at 37°C with 2 min frame intervals. Arrowhead at t = 10 min: appearance of podosome core; Arrowhead at t = 40 - 840 min: appearance of Dyn2 belt; Arrowhead at t = 910 min: disassembly of Dyn2 belt. Scale bar, 2 μm.

doi:10.6342/NTU202100043

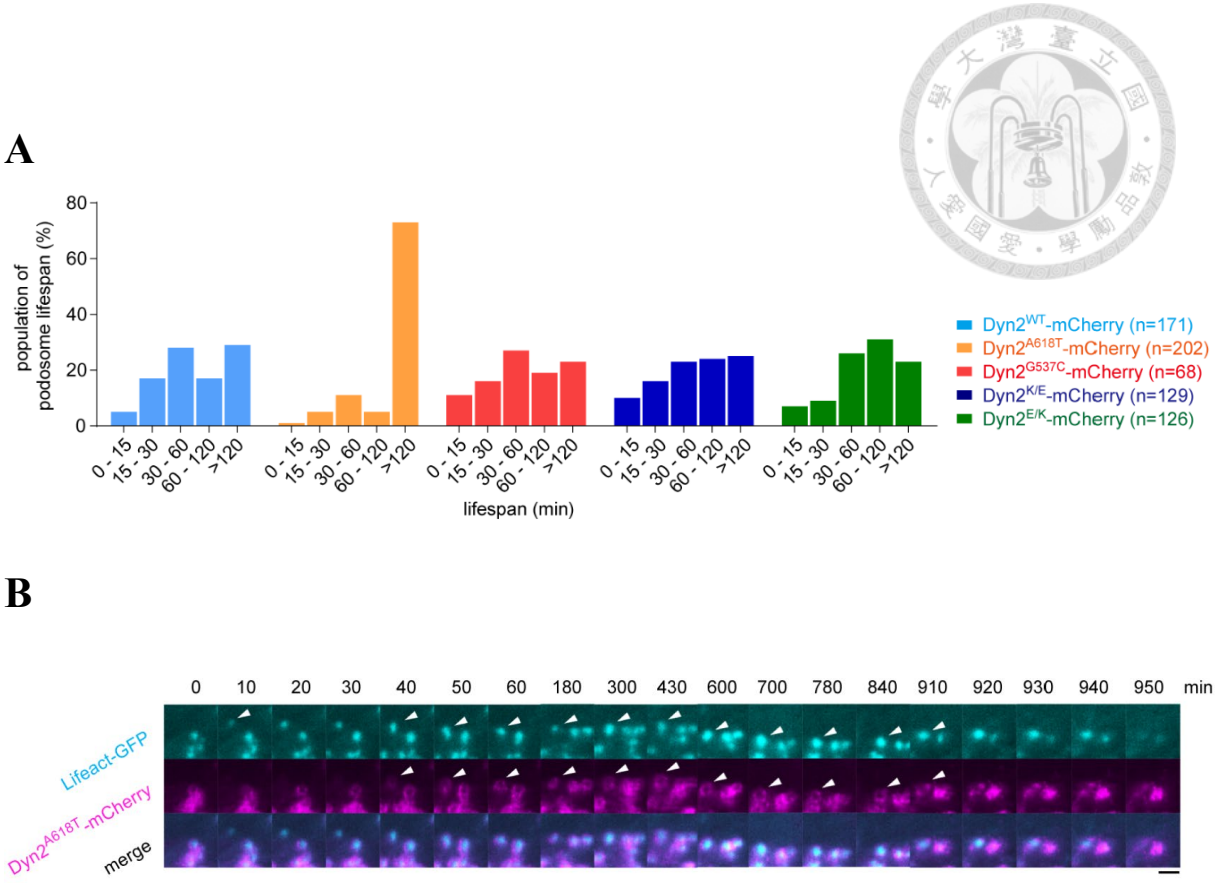

doi:10.6342/NTU202100043

Figure 25. Dyn2 is essential for podosome growth in c-Src transformed NIH3T3 cells

(A) Confocal microscopy images of Dyn2 distribution at podosome rosette. c-Src transformed NIH3T3 fibroblasts were stained and imaged with z-stack focal sectioning. Scale bars, 10 μm. **(B-C)** Effects of different Dyn2-mCherry mutants on the morphology of podosome rosette in c-Src-transformed NHI3T3 cells. Each dot represents one podosome rosette (n = 26~38 podosomes rosette per mutant).

doi:10.6342/NTU202100043

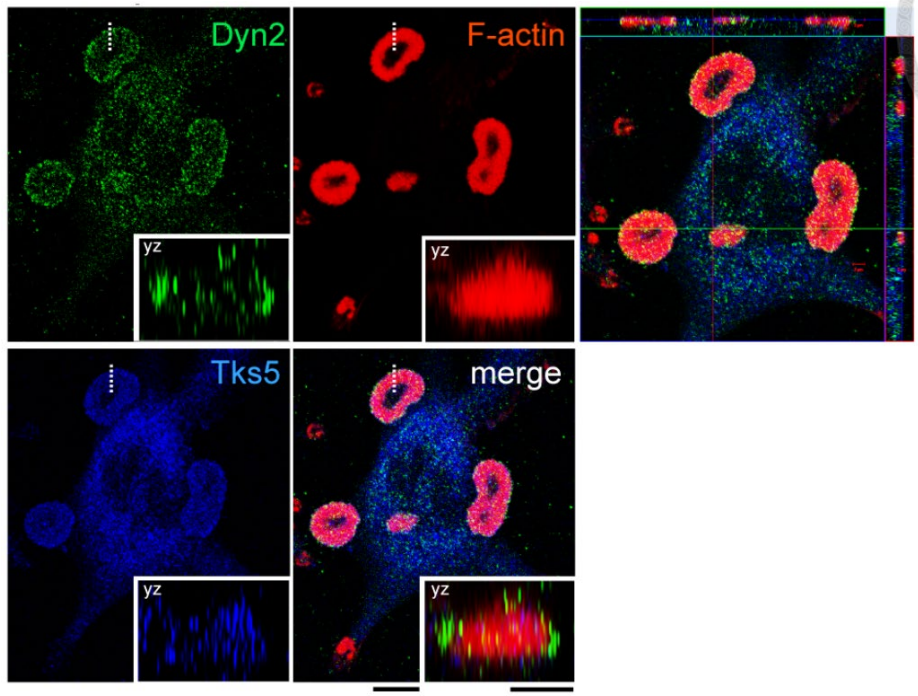

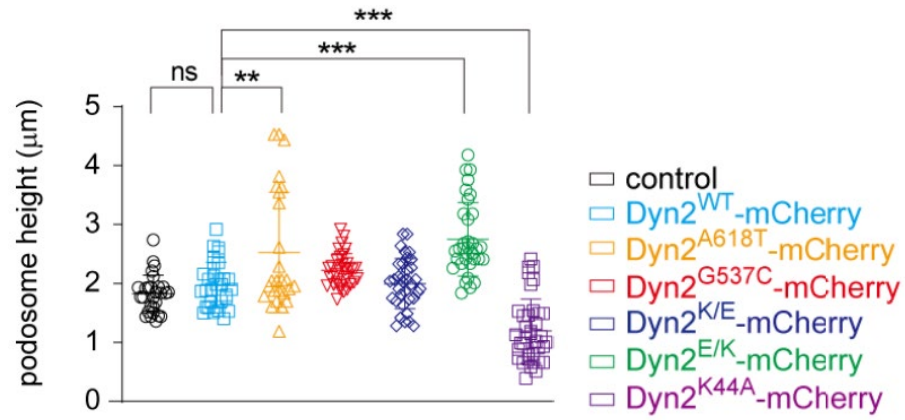

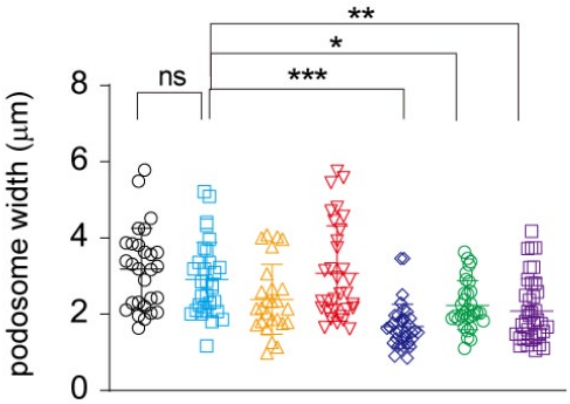

doi:10.6342/NTU202100043

Figure 26. Dyn2 is essential for podosome turnover in c-Src transformed NIH3T3 cells

Effects of different Dyn2-mCherry mutants on the lifespan of podosome rosette in c-Src-transformed NHI3T3 cells. c-Src-transformed NHI3T3 cells were transfected with Lifeact-GFP and Dyn2-mCherry to visualize F-actin and Dyn2, respectively and imaged by inverted fluorescence microscopy at 37°C. Scale bars, 10 μm.

doi:10.6342/NTU202100043

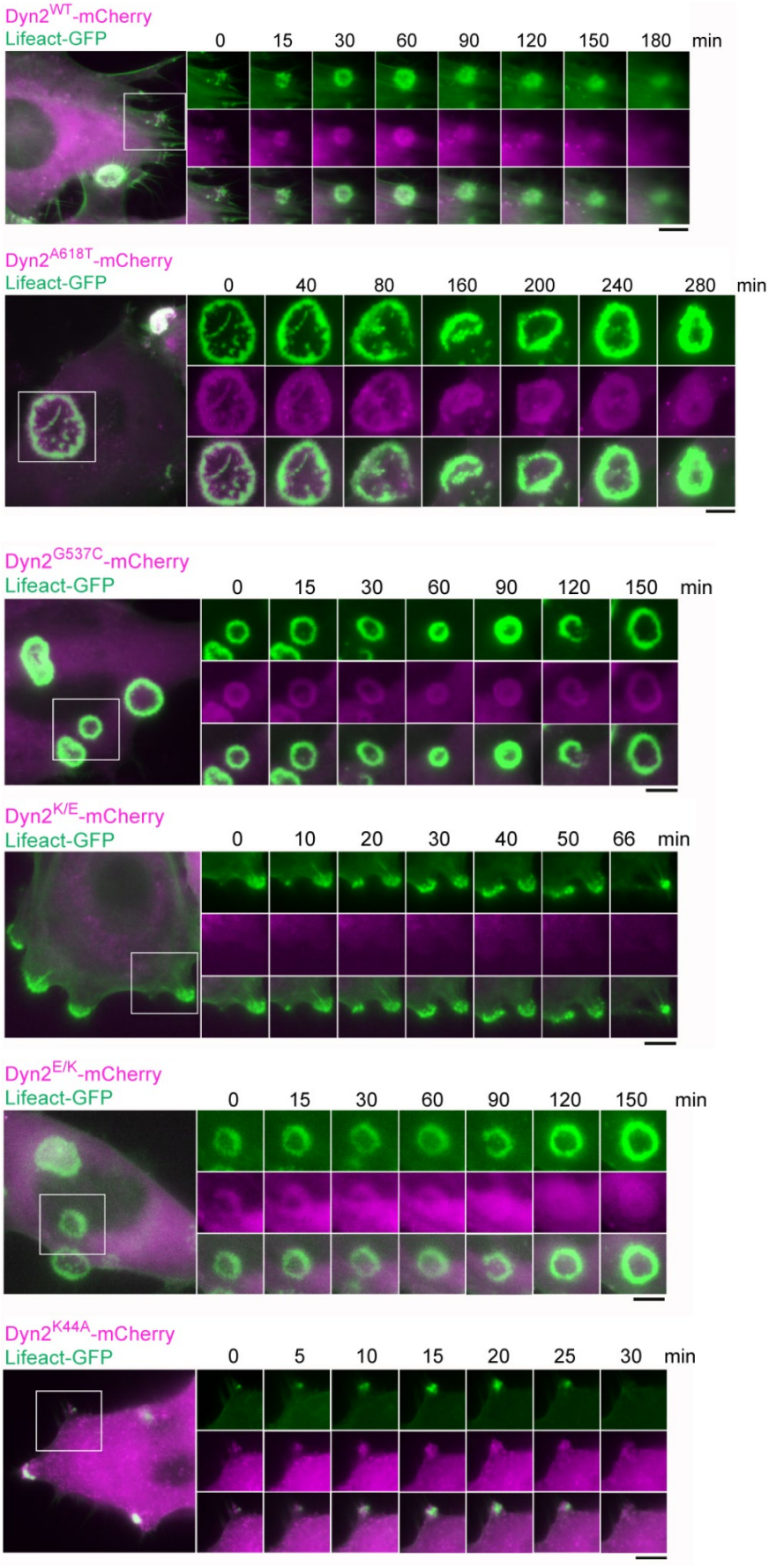

doi:10.6342/NTU202100043

Figure 27. Dyn2 regulates podosome lifespan in c-Src transformed NIH3T3 cells

Frequency distribution of podosome lifetime in c-Src-transformed NHI3T3 cells expressing different Dyn2 mutants. Lifespans of individual podosomes were tracked and measured manually.

doi:10.6342/NTU202100043

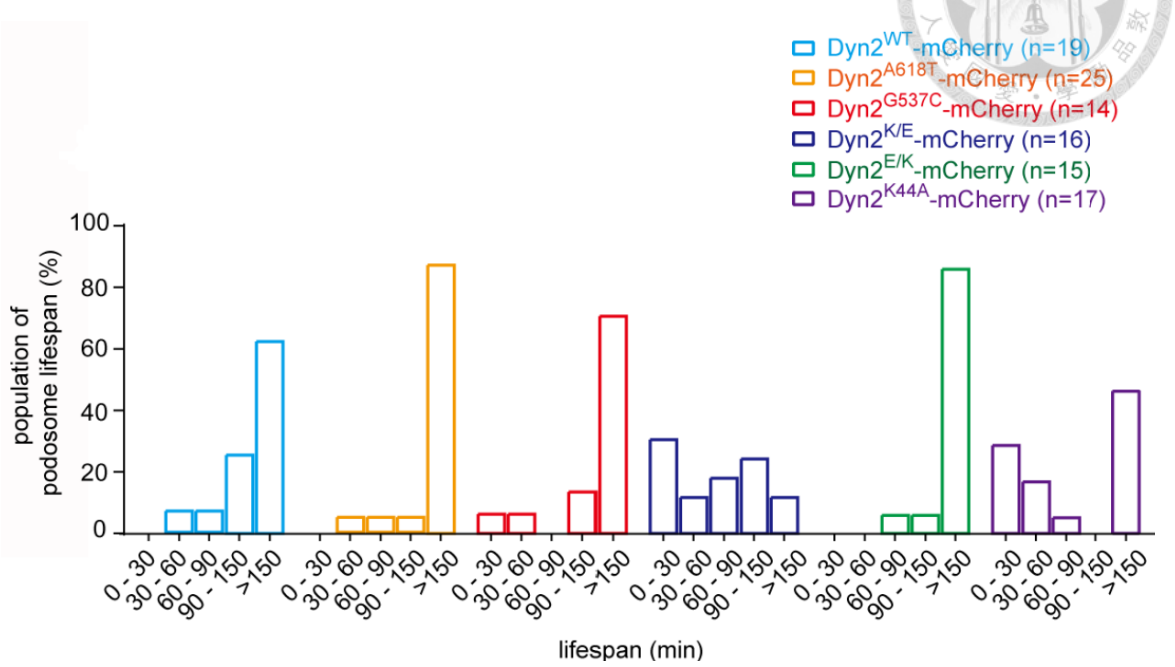

doi:10.6342/NTU202100043

Figure 28. Dyn2 regulates podosome-mediated matrix degradation

(A) Rescue effects of HA-tagged Dyn2 mutants on the ECM degradation activities of Dyn2-depleted myotubes. HA-tagged Dyn2 and F-actin in day-4 Dyn2 knockdown (KD) myotubes were stained and imaged under confocal microscopy after 16 h of induction and culturing on gelatin-fluorescein isothiocyanate (FITC)-coated coverslips. Dashed lines indicate cell boundaries. Scale bar, 10 μm. **(B)** Quantification of degraded area versus cell area. Each dot represents the percentage of degraded area in each cell. For each mutant, at least six cells were analyzed. ns, not significant; ***p <0.001.

doi:10.6342/NTU202100043

A

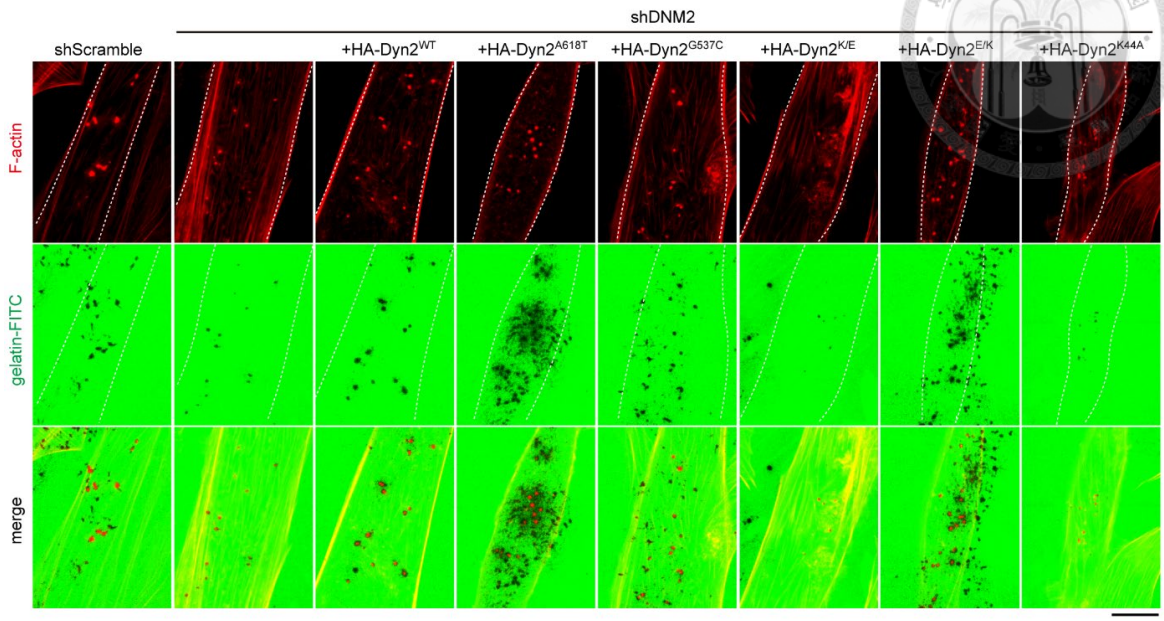

B

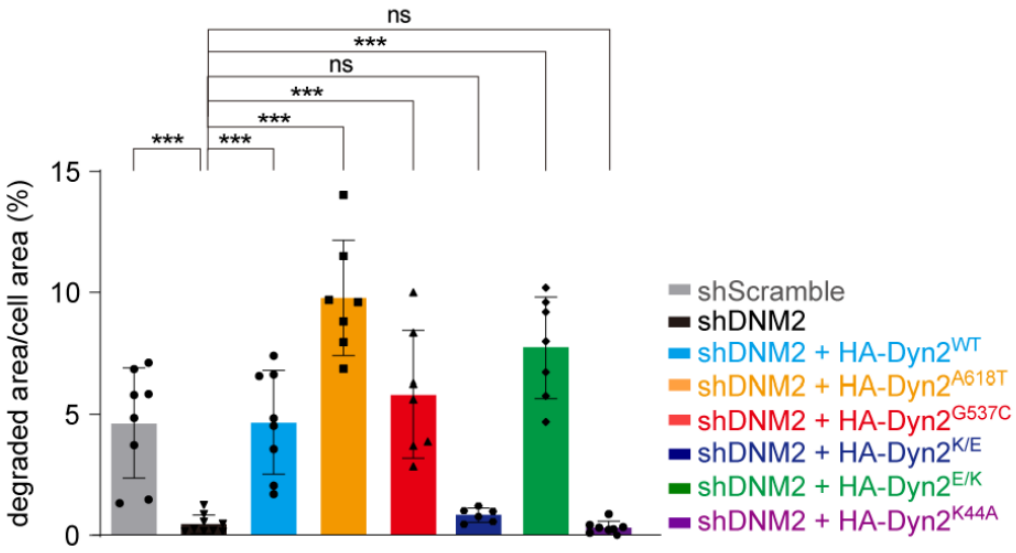

doi:10.6342/NTU202100043

Figure 29. Expressing Dyn2 hyper self-assembly mutant perturbs matrix degradation activity in wild type myotubes

(A) Effects of HA-tagged Dyn2 mutants on the ECM degradation activities in wild type myotubes. HA-tagged Dyn2 and F-actin in Day 4 myotubes were stained and imaged under confocal microscopy after 16 h of induction and culturing on gelatin-FITC coated coverslips. Dashed lines indicate cells boundaries. Scale bar, 10 μm. **(B)** Quantification of gelatin-FITC degraded area of HA-tagged Dyn2 mutants expressing wild-type myotubes. Each dot represents the percentage of degraded area in each cell. For each mutant, at least 15 cells were analyzed. ns, not significant; *p <0.05.

doi:10.6342/NTU202100043

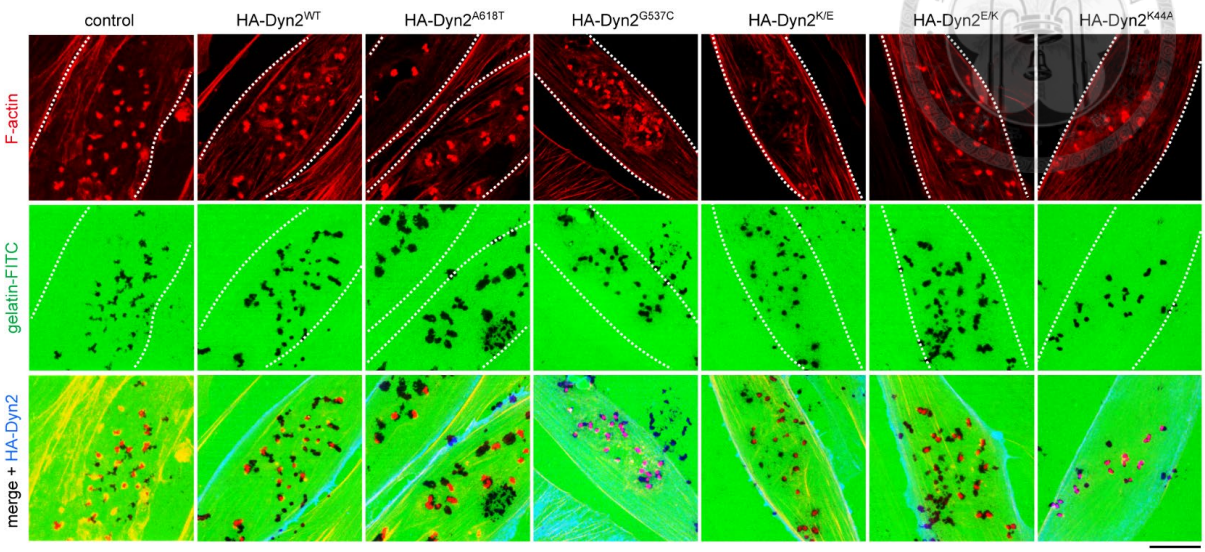

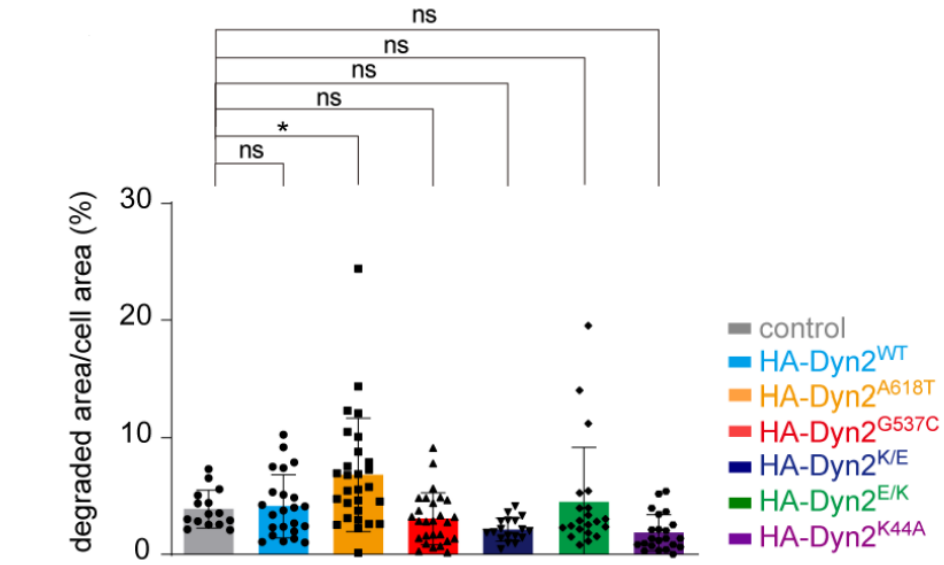

doi:10.6342/NTU202100043

Figure 30. Dyn2 mediates AChR cluster organization

(A) HA-tagged Dyn2, F-actin, and AChR (labeled by bungarotoxin) in day-6-differentiated myotubes cultured on Permanox slides were stained and imaged under z stack confocal microscopy after 16 h of induction. Dashed lines indicate cells expressing HA-tagged Dyn2 mutants. Scale bar, 10 μm. **(B-C)** Quantification of individual AChR area or total AChR area versus cell area. All data in this work are expressed as mean ± SD of at least three independent experiments. ns, not significant; $*p < 0.05$; $**p < 0.01$.

doi:10.6342/NTU202100043

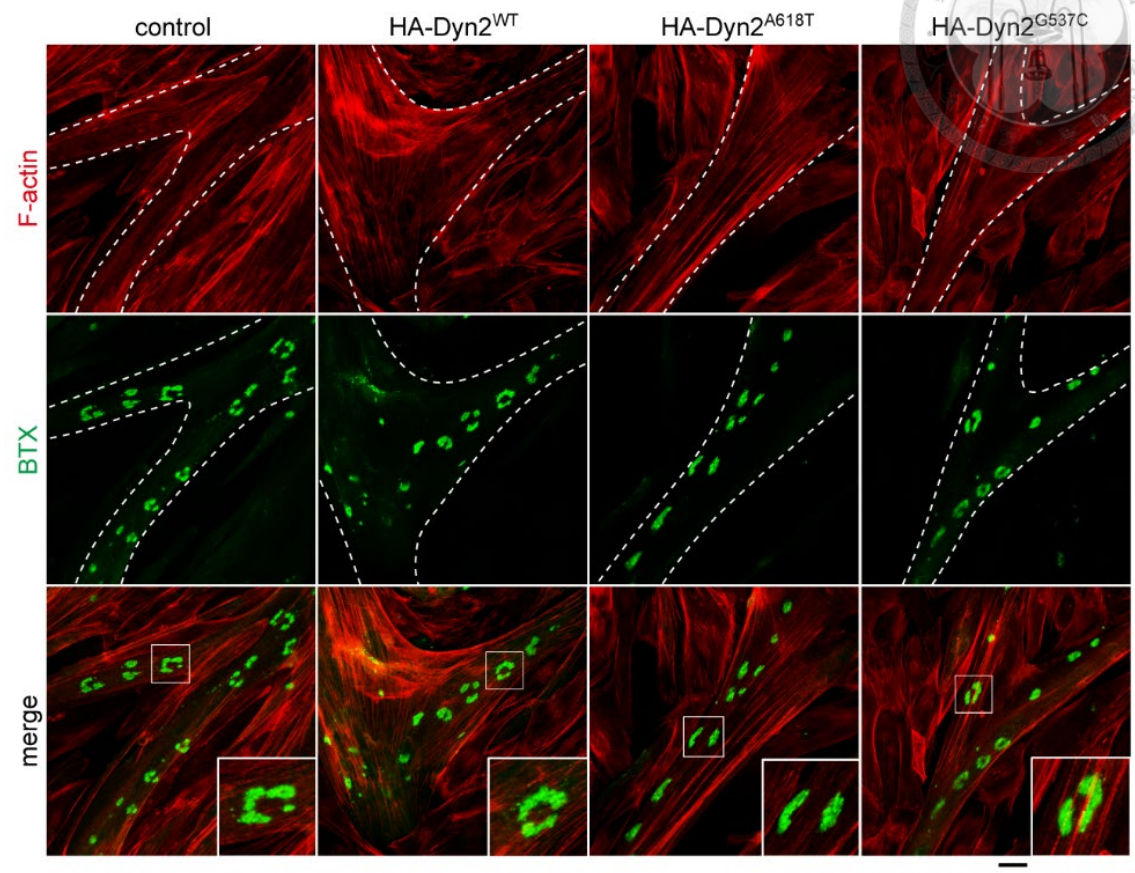

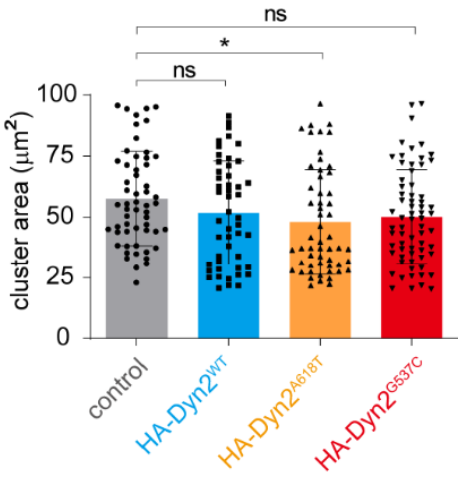

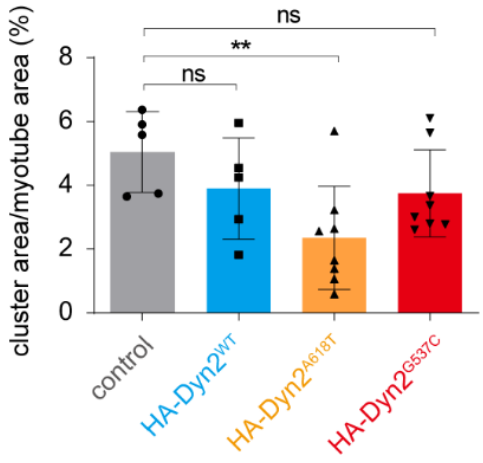

doi:10.6342/NTU202100043

Figure 31. Expressing Dyn2 hyper self-assembly mutant perturbs AChR perforation

HA-tagged Dyn2, F-actin, and AChR (labeled by Bungarotoxin) in Day 4-differentiated myotubes cultured on Permanox slides were stained and imaged under z-stack confocal microscopy after 16 h of induction. Scale bar, 10 μm.

doi:10.6342/NTU202100043

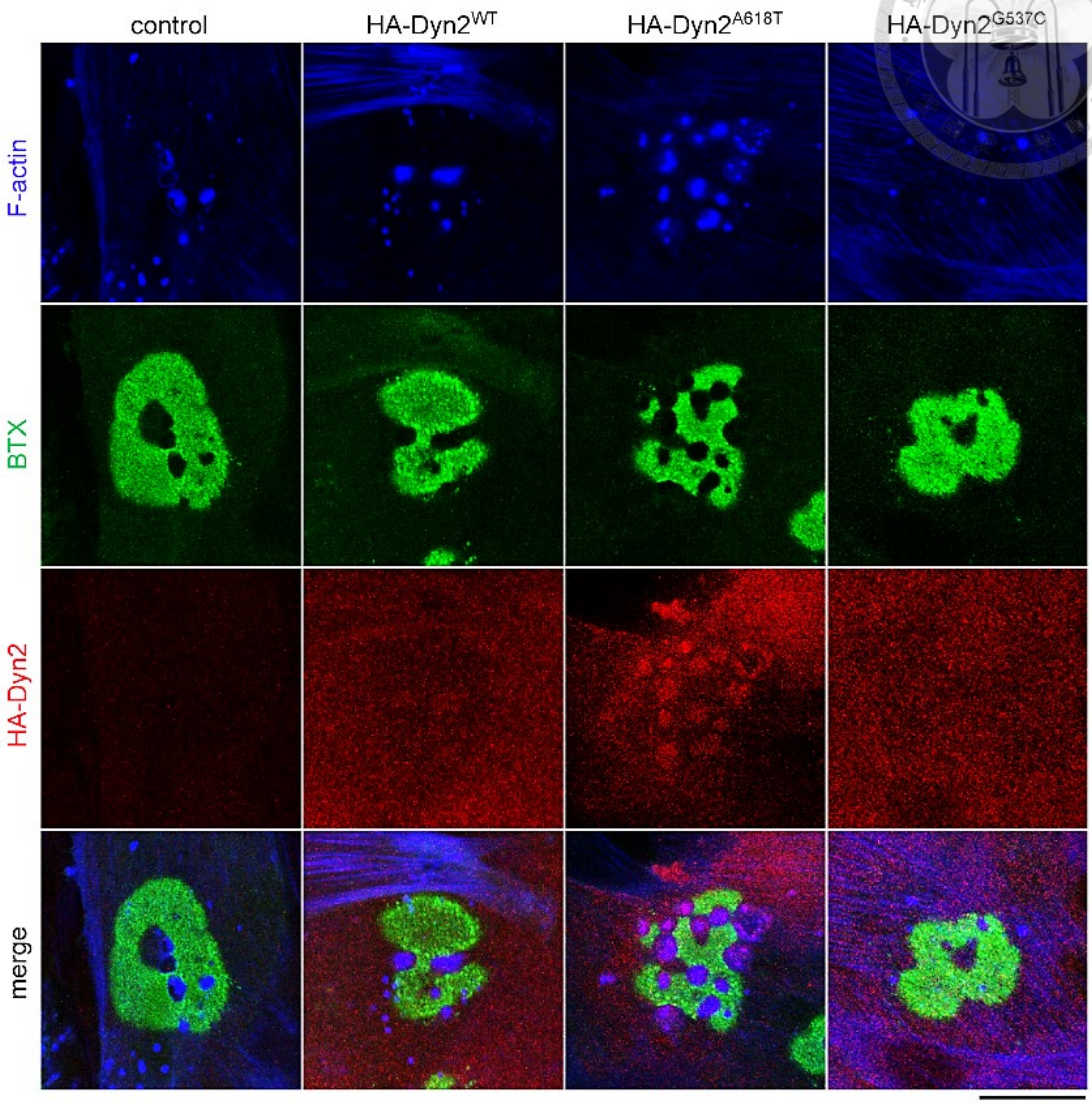

doi:10.6342/NTU202100043

Figure 32. Dyn2 bundles in vitro reconstituted actin filaments

(A-B) Both Dyn1 and Dyn2 bundle actin filaments. Reconstituted F-actin (5 μM) was incubated with Dyn at indicated concentrations for 30 min and subjected to 20 min of centrifugation at 14,000 × *g*. S, supernatant; P, pellet. **(C)** Dyn2 bundles actin filaments. Reconstituted F-actin (5 μM) was incubated with Dyn2 at indicated concentrations for 30 min and subjected to 20 min of centrifugation at 14,000 × *g*. S, supernatant; P, pellet. **(D)** Dyn2 (1 μM) shows significant actin-bundling activity. The percentage of sedimented actin was quantified in ImageJ as the ratio of actin in the pellet versus total actin. ns, not significant; $^{***}p < 0.001$.

doi:10.6342/NTU202100043

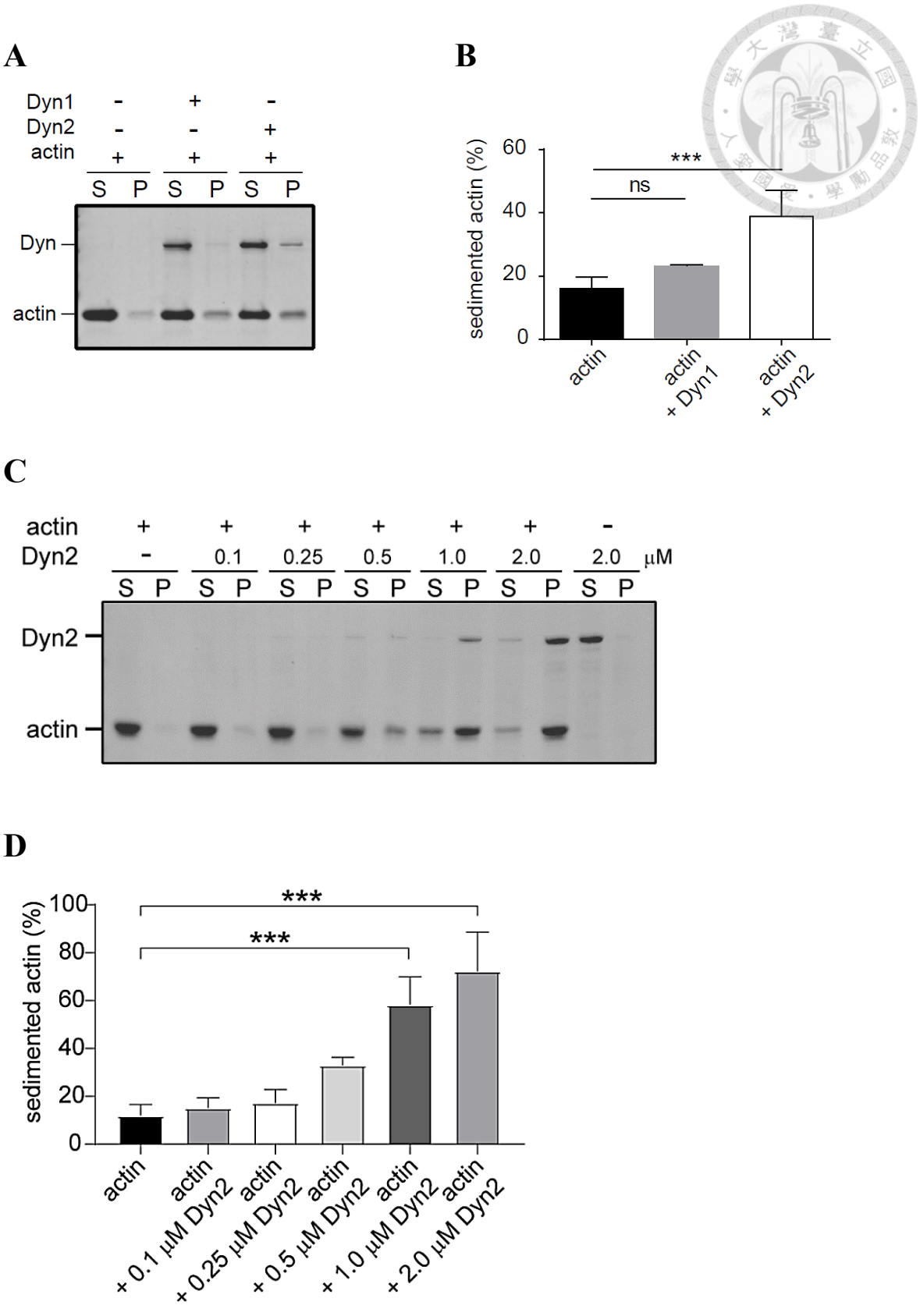

doi:10.6342/NTU202100043

Figure 33 GTP, GDP, and GTPγS addition reduced Dyn2-bundled actin

(A) Reconstituted F-actin (5 μM) was incubated with 1 μM Dyn2 for 30 min and subjected to addition of indicated nucleotides for 30 min then followed by centrifugation at 14,000 × *g*. S, supernatant; P, pellet. **(B)** Reconstituted F-actin (5 μM) was incubated with 1 μM Dyn2 for 30 min and subjected to addition of either GTP or GTPγS for indicated incubation time then followed by centrifugation at 14,000 × *g*. S, supernatant; P, pellet.

doi:10.6342/NTU202100043

A

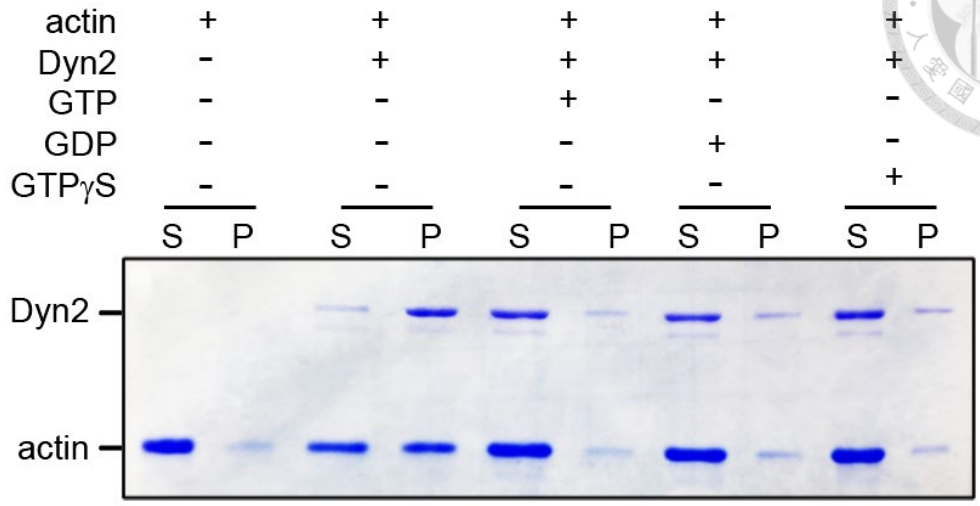

B

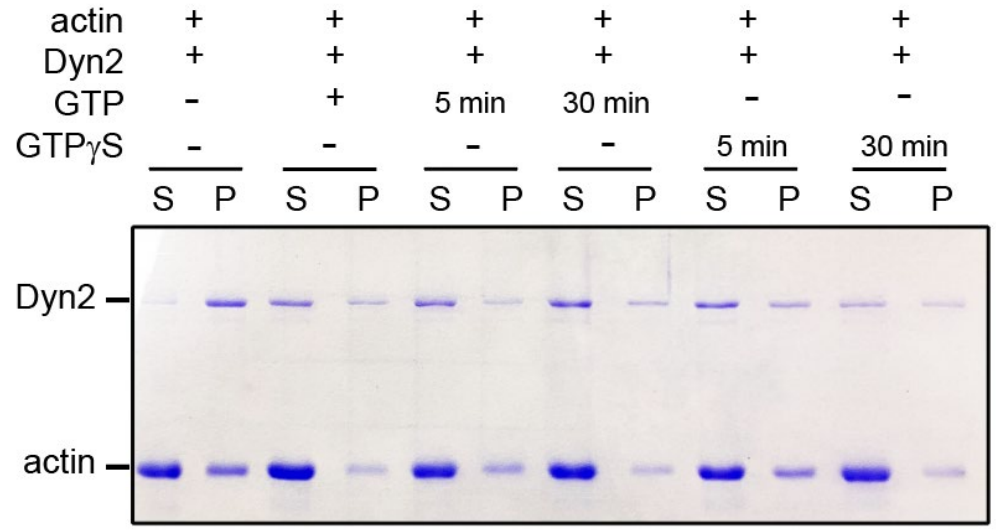

doi:10.6342/NTU202100043

Figure 34. GTP hydrolysis reduced Dyn2-bundled actin

(A-B) F-actin sedimentation assay and quantification result of Dyn2-bundling activity. Reconstituted F-actin (5 μM) was incubated with 1 μM Dyn2 for 30 min followed by 15 min of incubation with 1 mM GTP or GMPPCP. **(C)** Real-time visualization of the actin-bundling activity of Dyn2 under confocal microscopy. Scale bar, 10 μm. ns, not significant; $^{***}p < 0.001$.

doi:10.6342/NTU202100043

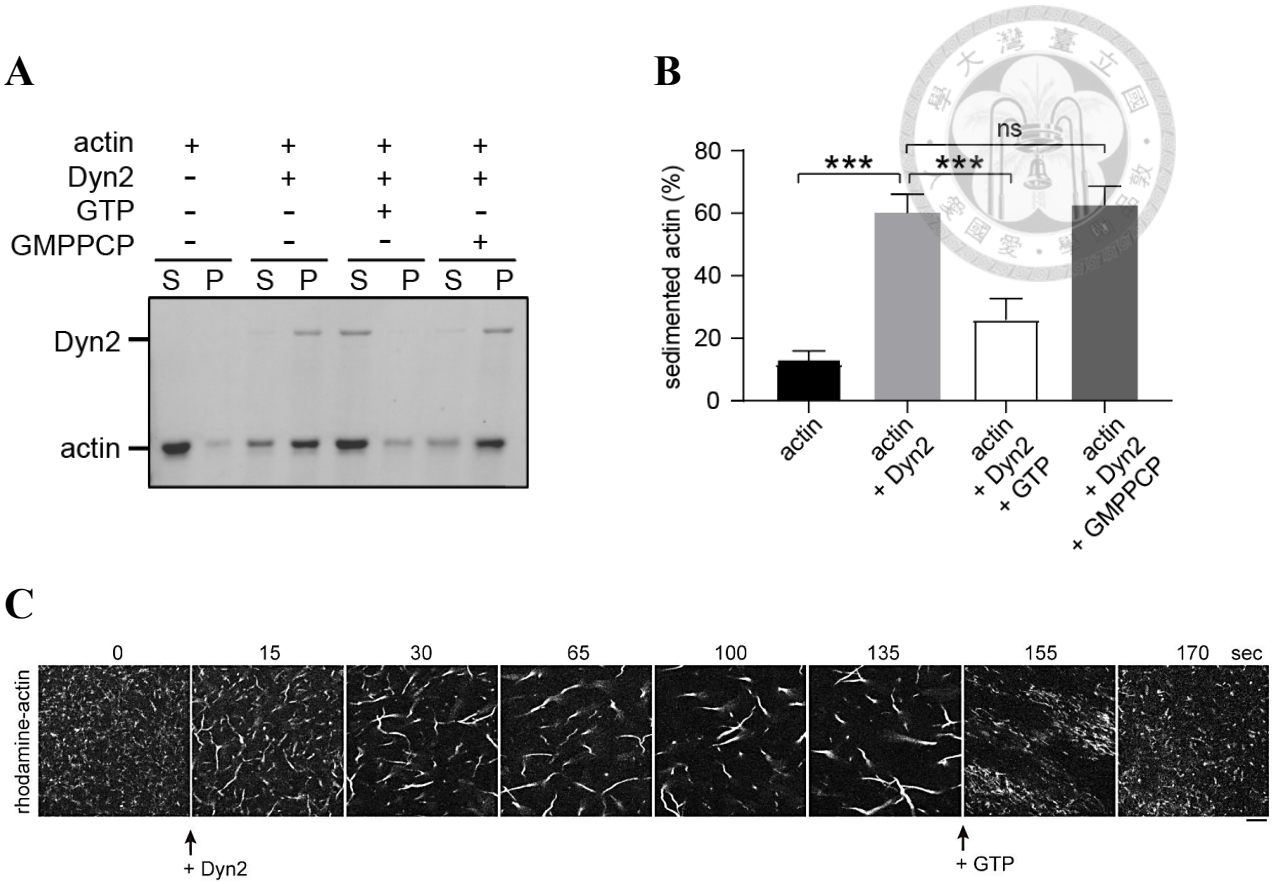

doi:10.6342/NTU202100043

Figure 35. GTP hydrolysis induced disassembly of Dyn2-bundled actin

(A) TEM images of negative-stained actin-Dyn2 bundles in the presence of different GTP analogs. Scale bar, 100 nm. **(B)** Quantification of width of single actin filament and minimum actin bundles.

doi:10.6342/NTU202100043

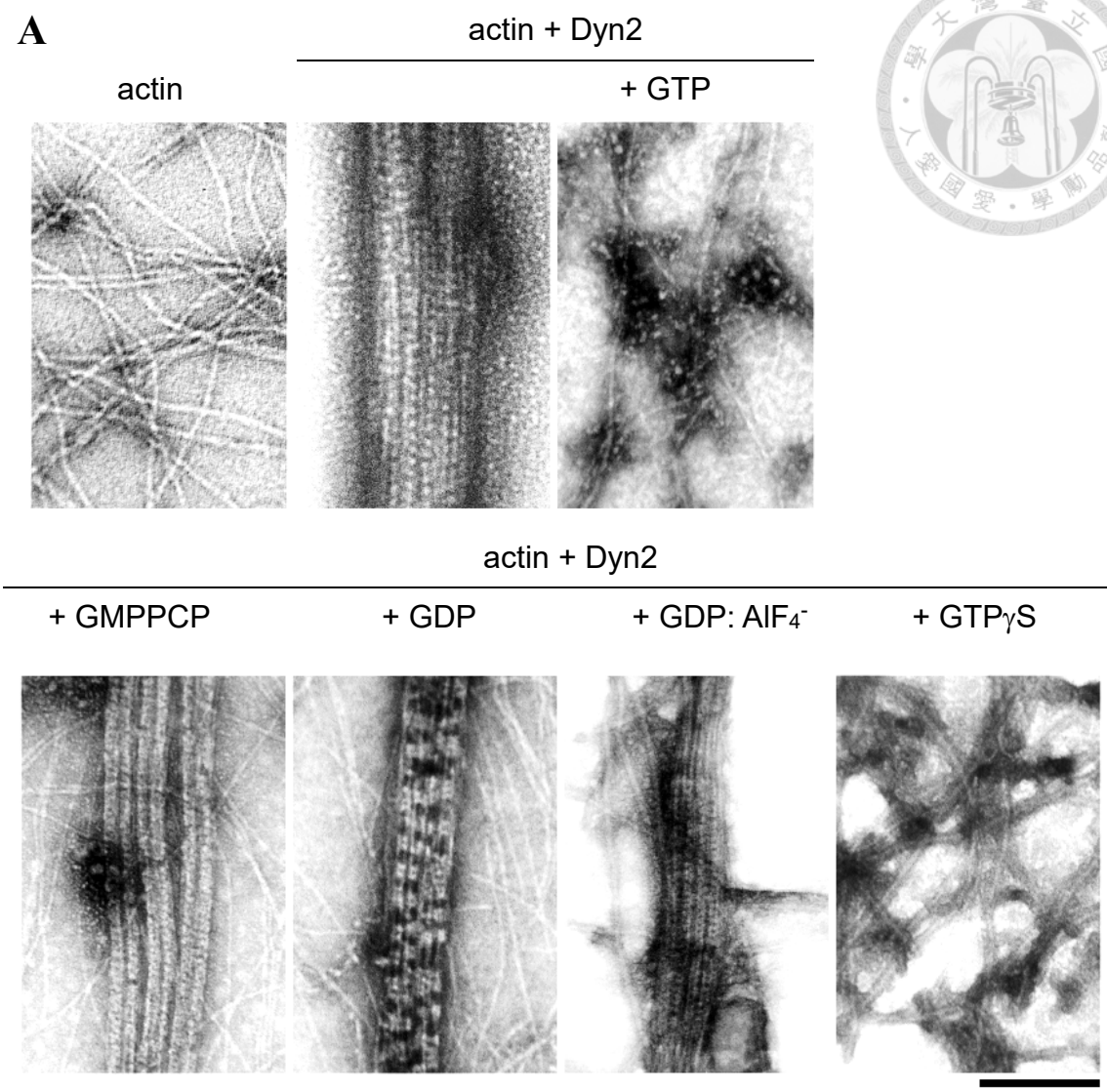

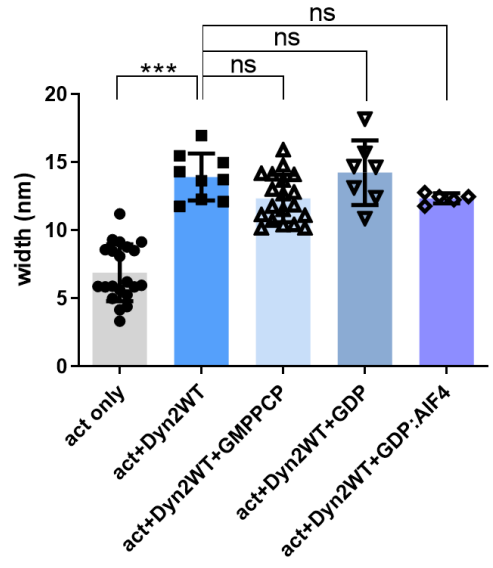

doi:10.6342/NTU202100043

Figure 36. PRD domain of Dyn2 is not required for its actin bundling activity

(A) TEM image of negative-stained actin filaments bundled by $Dyn2^{\Delta PRD}$. Scale bar, 100 nm. **(B)** Reconstituted F-actin (5 μM) was incubated with $Dyn2^{\Delta PRD}$ with indicated concentrations and subjected to centrifugation at 14,000 × *g*. S, supernatant; P, pellet. **(C)** Quantification of width of minimum actin bundles.

doi:10.6342/NTU202100043

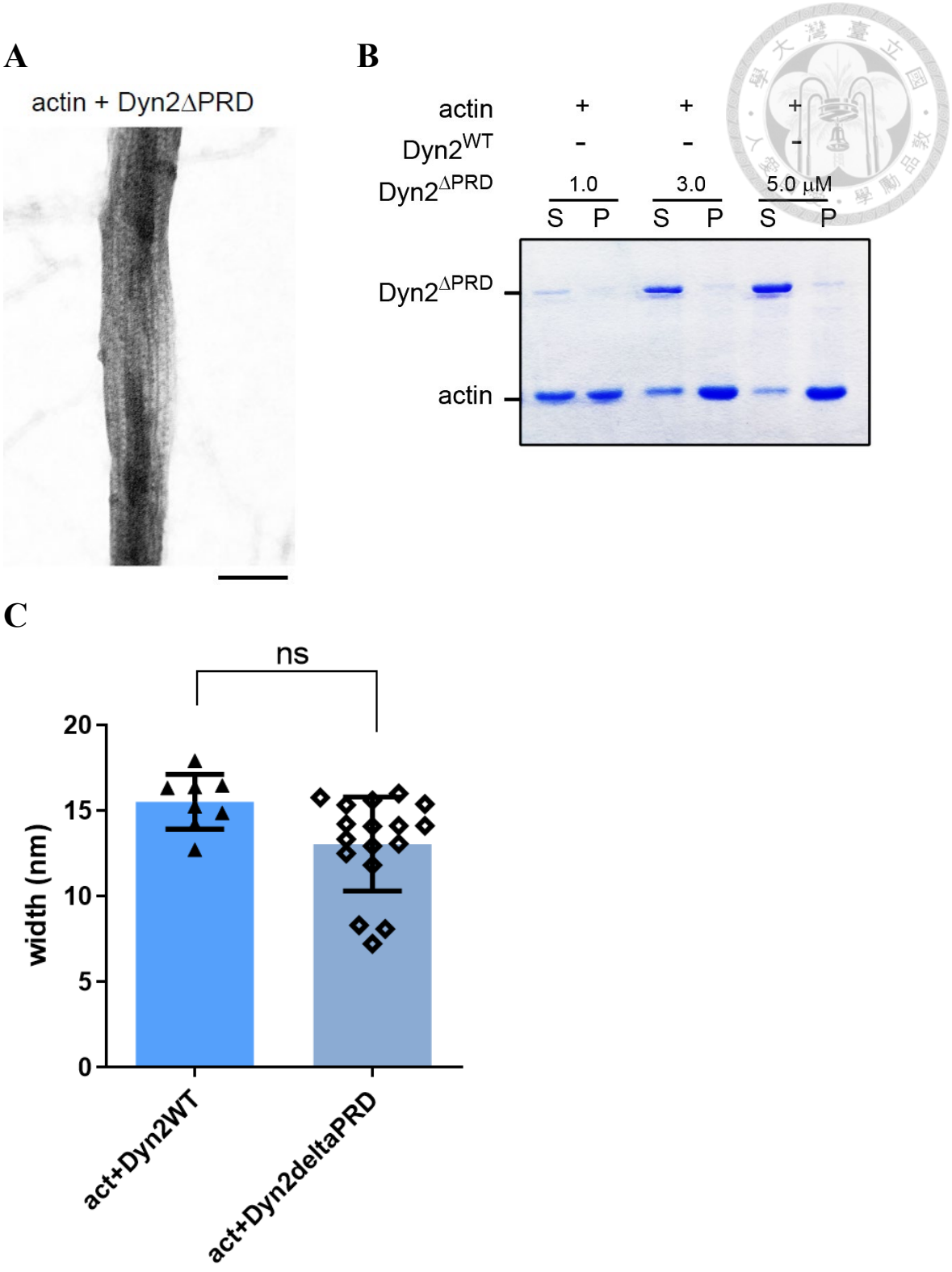

doi:10.6342/NTU202100043

Figure 37. Physical interruption failed to generate single actin bundles

Results of fractionation and different physical interruptions on Dyn2-bundled actin filaments (20% rhodamine labeled). Fractions 1 to 4 represent the top to bottom fraction of Dyn2-actin solution after centrifugation at 14,000 × *g*. The rhodamine labeled actin filaments were imaged under confocal microscopy. Scale bars, 20 μm.

doi:10.6342/NTU202100043

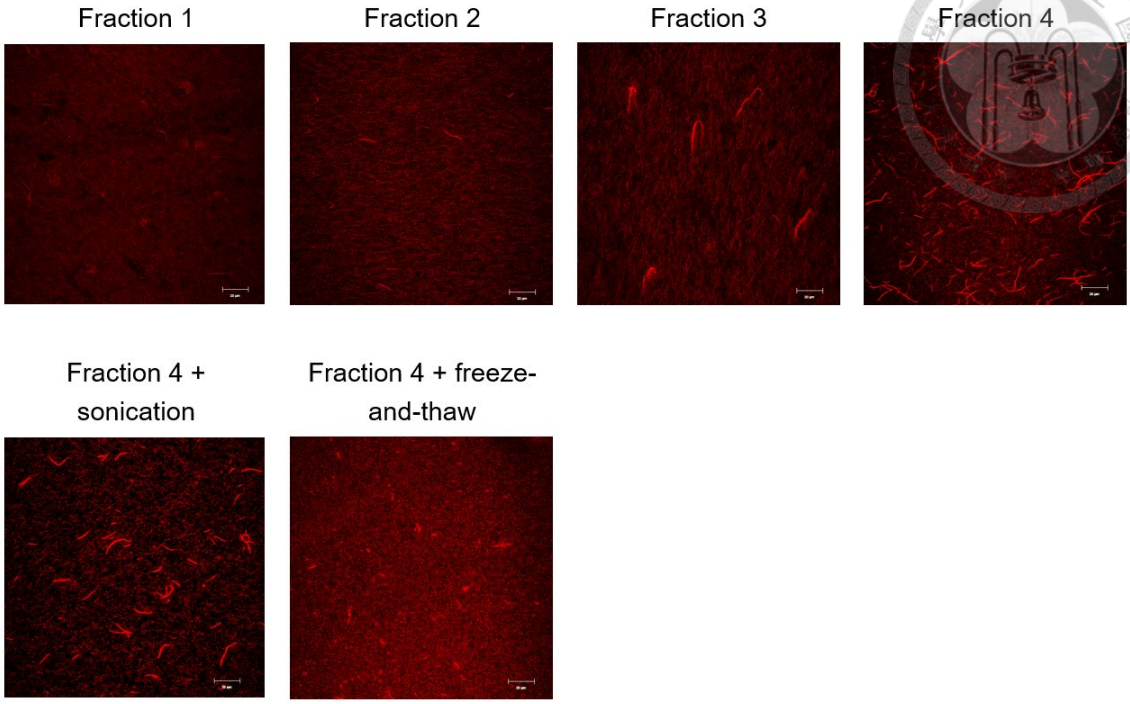

doi:10.6342/NTU202100043

Figure 38. Reducing temperature and Dyn2 concentration generated small actin bundles

(A) Negative stained TEM of actin bundles showed results from different incubation temperature and ratio between actin and Dyn2. Scale bars, 50 nm. **(B-E)** Removing Dyn2 aggregates prior to use and increasing the adsorption time provides better images (D-E compared with B-C) under CryoEM. Scale bars, 100 nm.

doi:10.6342/NTU202100043

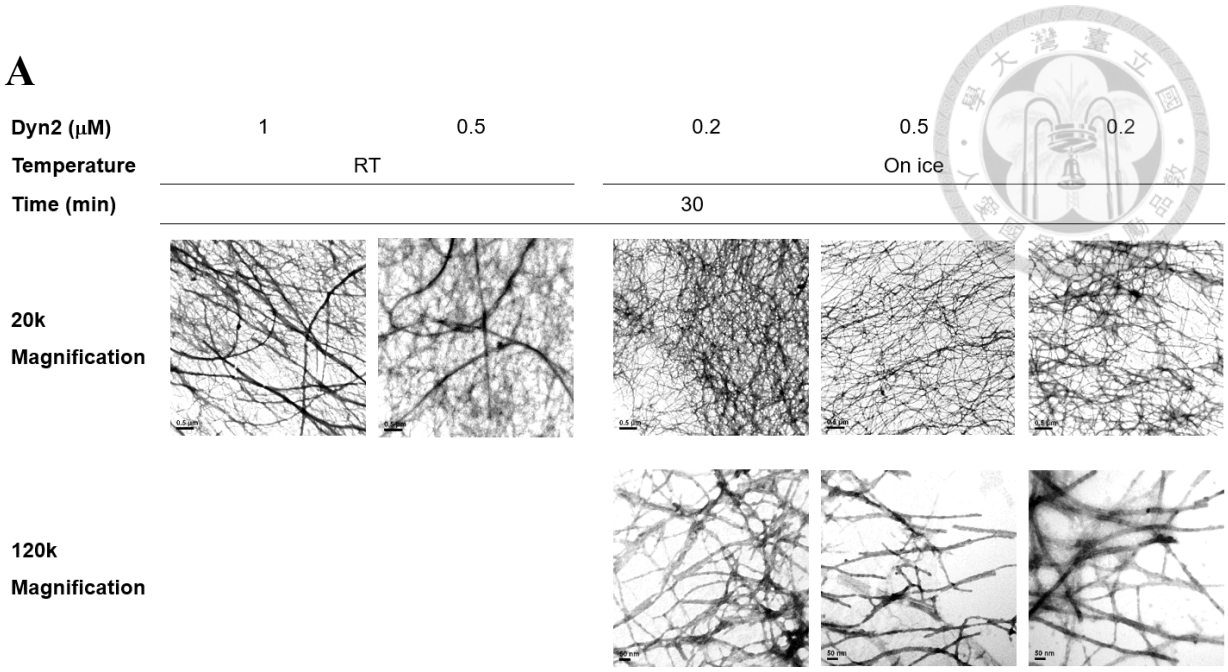

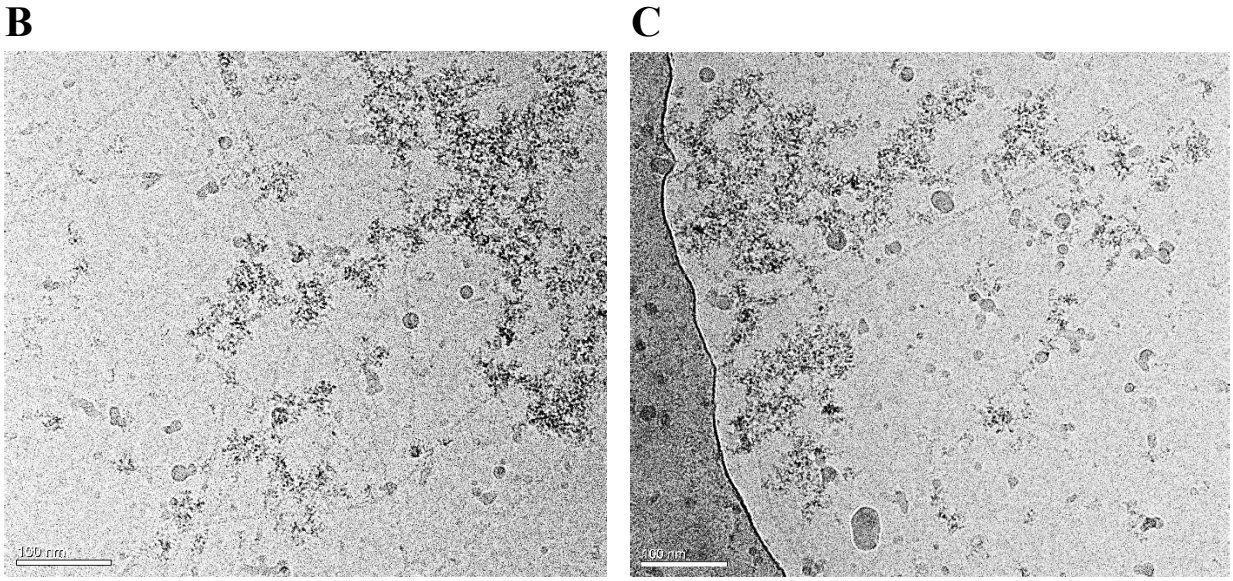

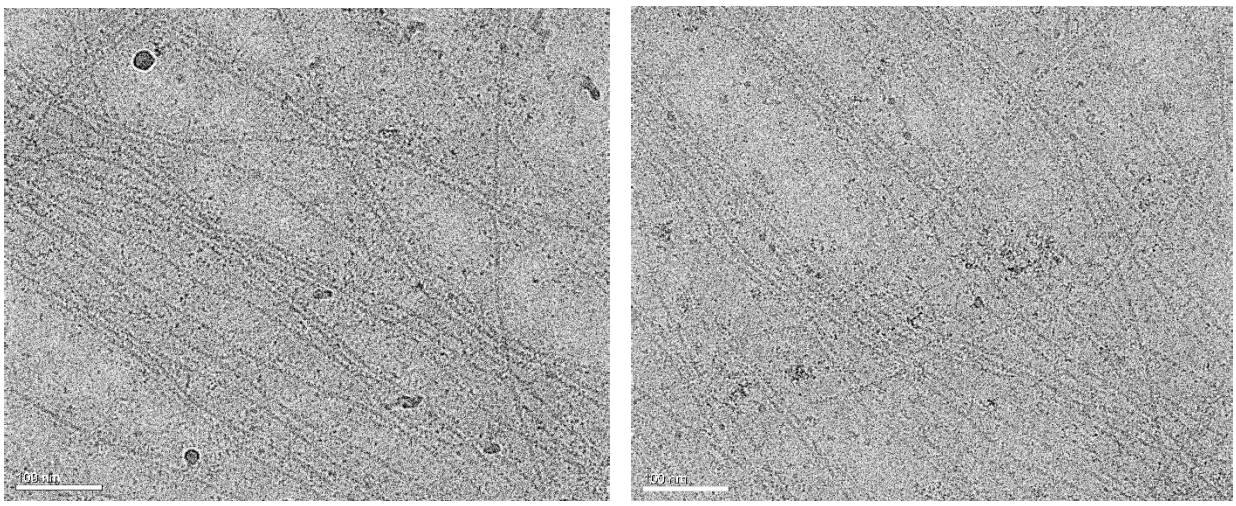

doi:10.6342/NTU202100043

Figure 39. Small actin bundles can be visualized under negative stain and CryoEM

(A-B) Negative stain TEM images of small actin bundles. Scale bar in **A**, 200nm. Scale bar in **B**, 100nm. **(C)** CryoEM images of actin filaments bundled by Dyn2. Scale bar, 100nm. **(D)** Examples of 2D classification results from 25classes of small Dyn2- actin bundles. Box size: 500*500px. **(E)** Examples of 2D classification results from 60 classes of single actin filaments. Box size: 100*100px. **(F)** Examples of 2D classification results from 30 classes of side-by-side actin filaments. Box size: 100*100px.

doi:10.6342/NTU202100043

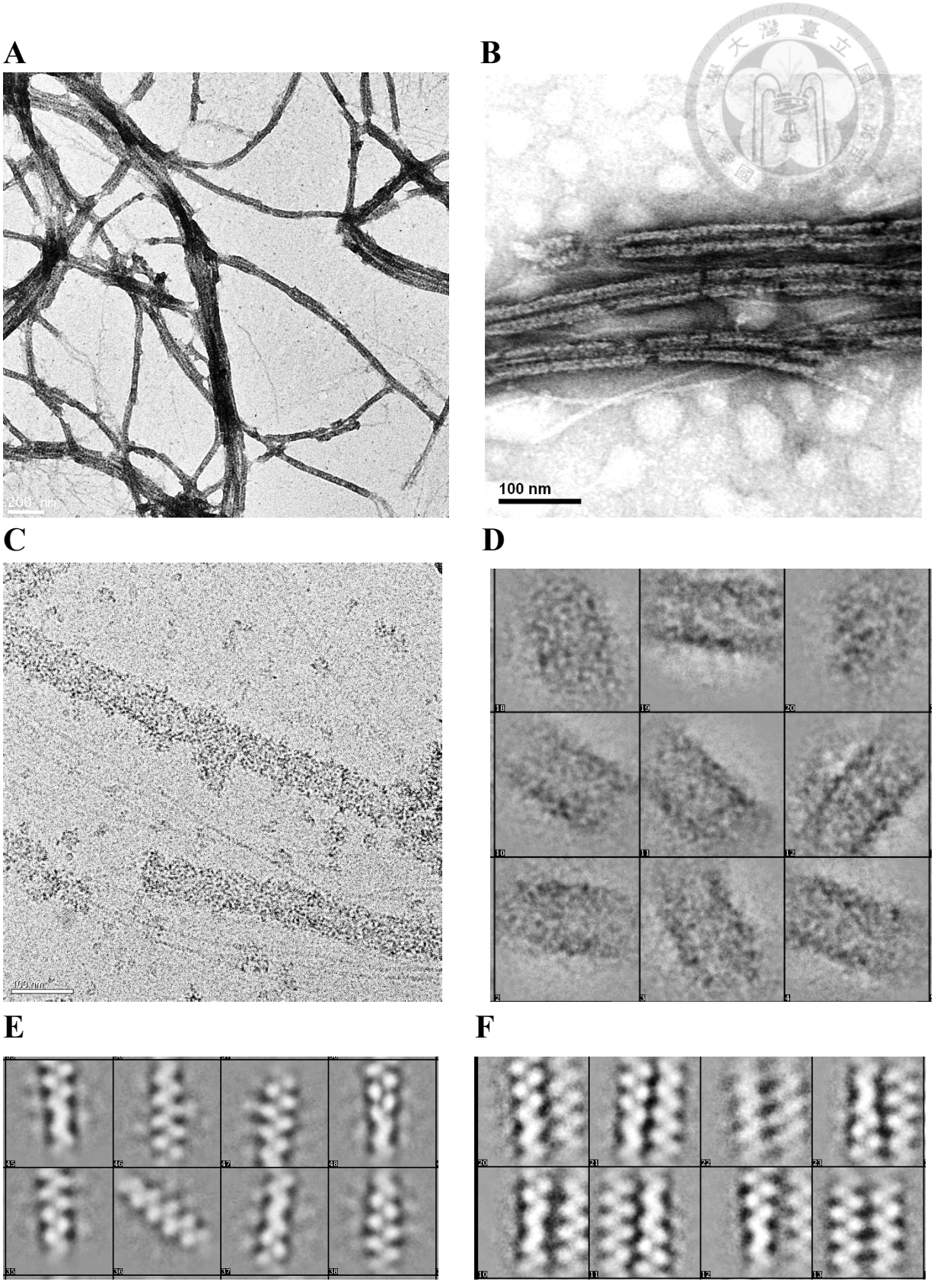

doi:10.6342/NTU202100043

Figure 40. Actin filaments packed inside the Dyn2 helix

(A) Negative stain TEM images of partially packed Dyn2 bundled actin filaments. **(B)** Upper, schematic diagram and EM tomography of partially packed actin-Dyn2 bundles. Lower, 3D tomography from negative stain TEM showing that actin filaments were packed inside the Dyn2 helix. Scale bars, 100 nm.

doi:10.6342/NTU202100043

A

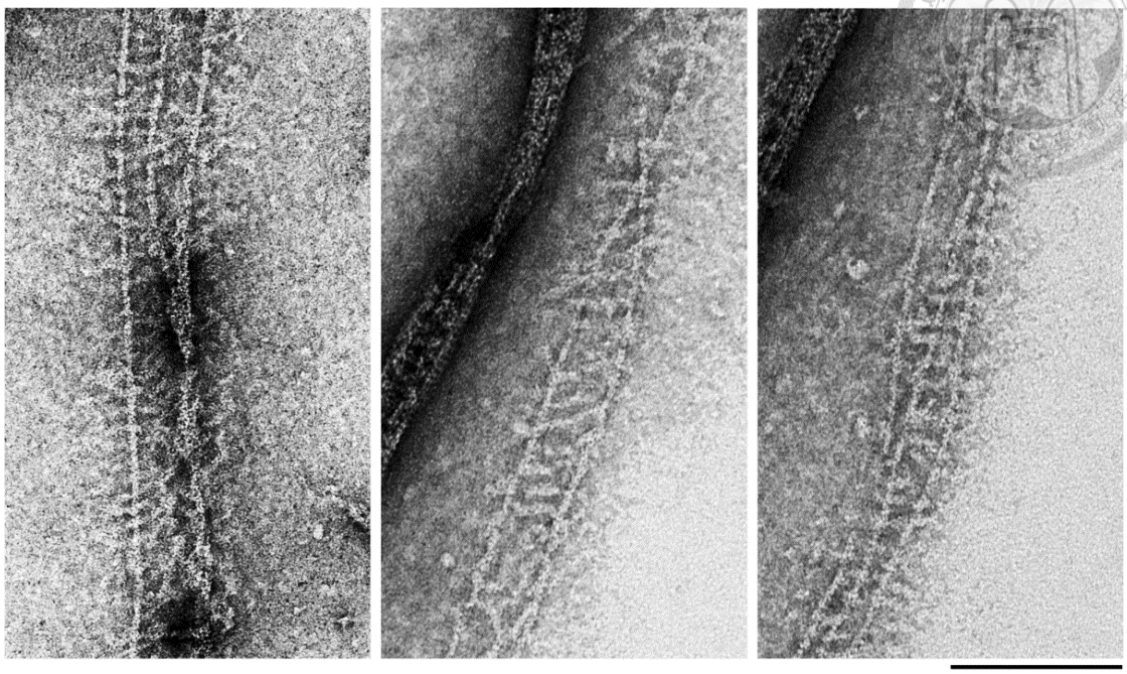

B

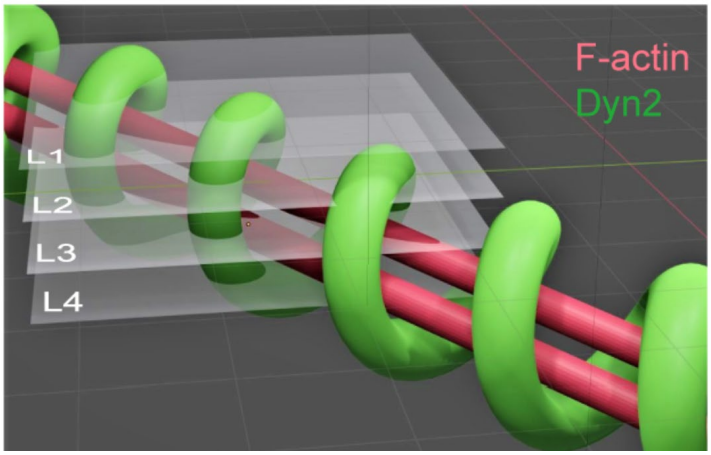

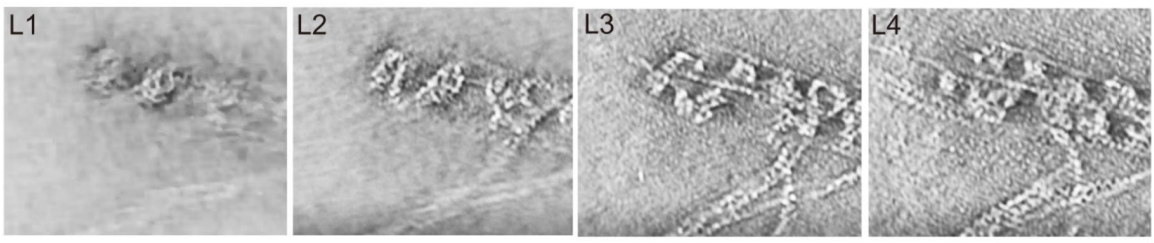

doi:10.6342/NTU202100043

Figure 41. Actin filaments bundled by hyper self-assembly Dyn2 mutant was less sensitive to GTP

(A) F-actin sedimentation assay and quantification result **(B)** of actin bundling activity of CNM-Dyn2 mutant, A618T, and CMT-Dyn2 mutant, G537C**.** ns, not significant; $^{*}p < 0.05$; $^{**}p < 0.01$; $^{***}p < 0.001$.

doi:10.6342/NTU202100043

A

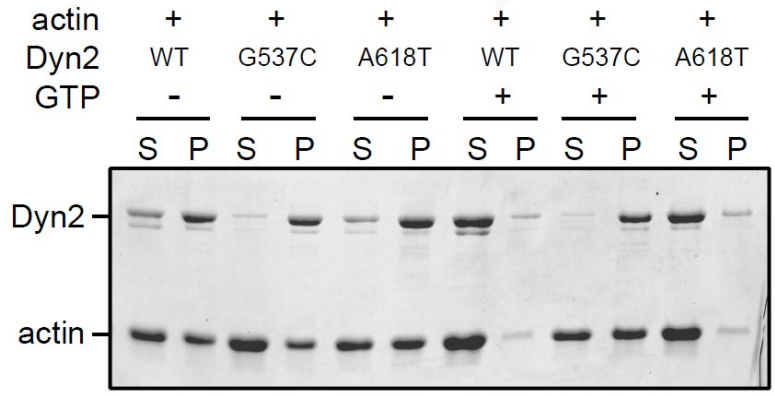

B

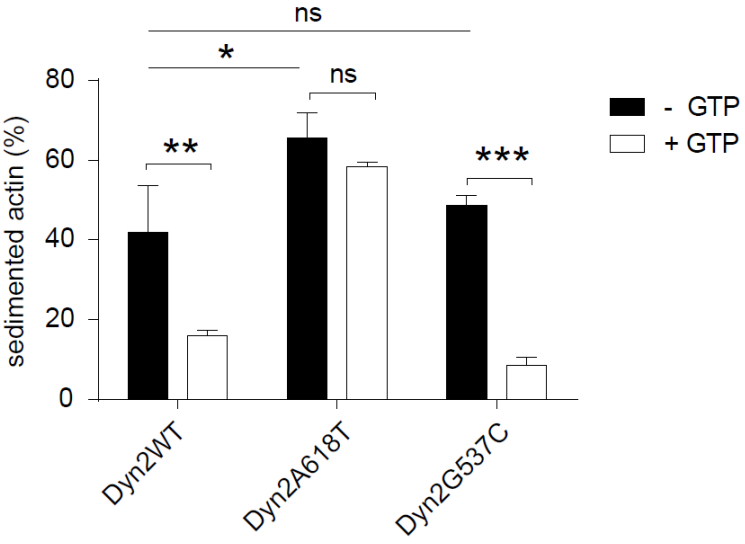

doi:10.6342/NTU202100043

Figure 42. Actin filaments bundled by CNM-Dyn2 mutant were less sensitive to GTP

(A-B) F-actin sedimentation assay and quantification of Dyn2 bundling activity in the absence of GTP. **(C)** TEM images of negative-stained actin-Dyn2 bundles. Scale bar, 100 nm. **(D-E)** F-actin sedimentation assay and quantification of Dyn2 bundling activity in the presence of GTP. $^{*}p < 0.05$; $^{**}p < 0.01$; $^{***}p < 0.001$.

doi:10.6342/NTU202100043

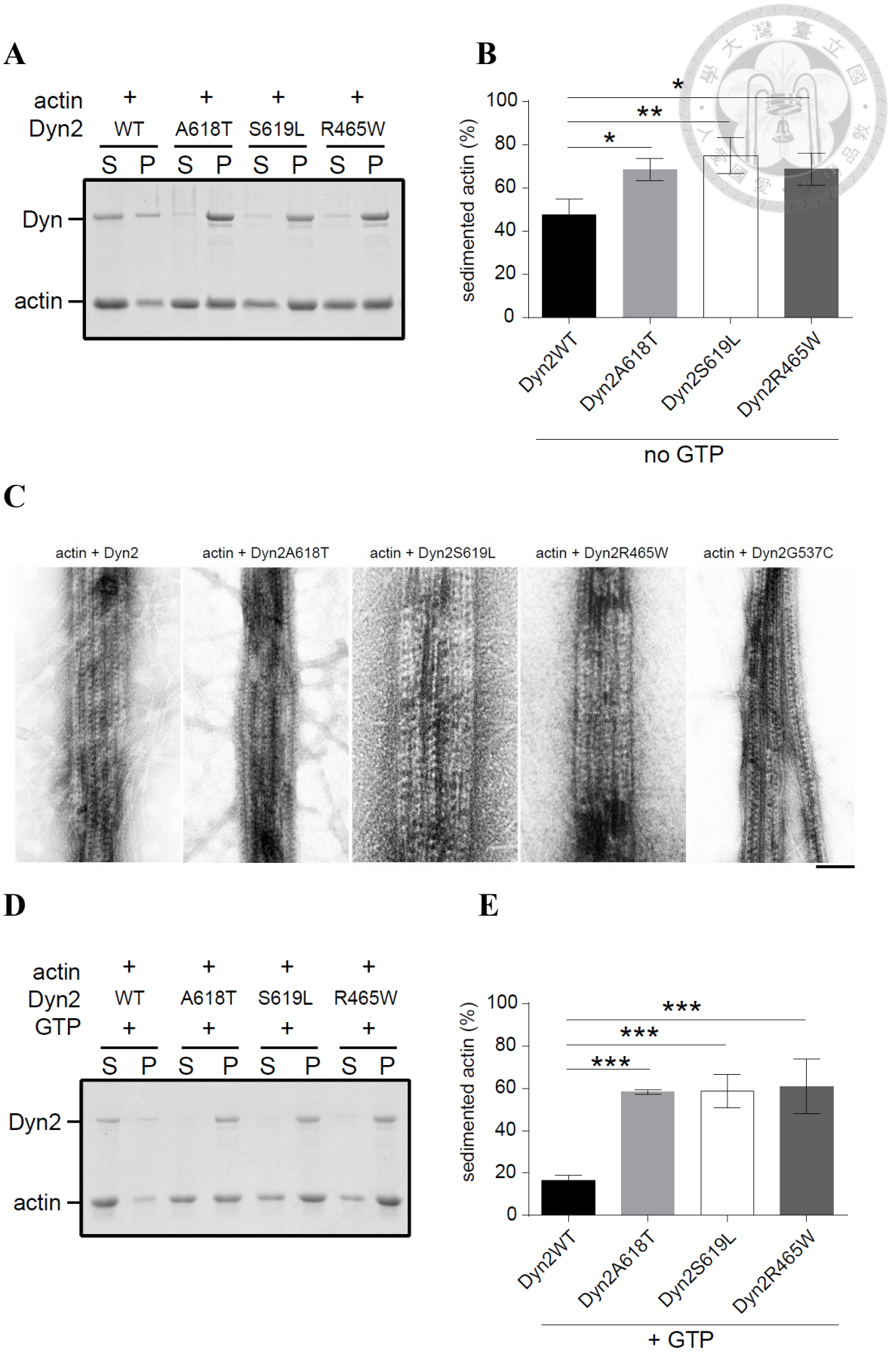

doi:10.6342/NTU202100043

Figure 43. Dyn2 bundles branched actin

(A-B) Branched F-actin sedimentation assay and quantification result of Dyn2-bundling activity. Concentrations of individual components were 5 μM actin, 1 μM Dyn2, 30 nM Arp2/3 complex, 80 nM VCA, and 1 mM GTP. **(C)** Morphology of Dyn2-bundled linear and branched actin under confocal microscopy. ns, not significant; *$p < 0.05$.

doi:10.6342/NTU202100043

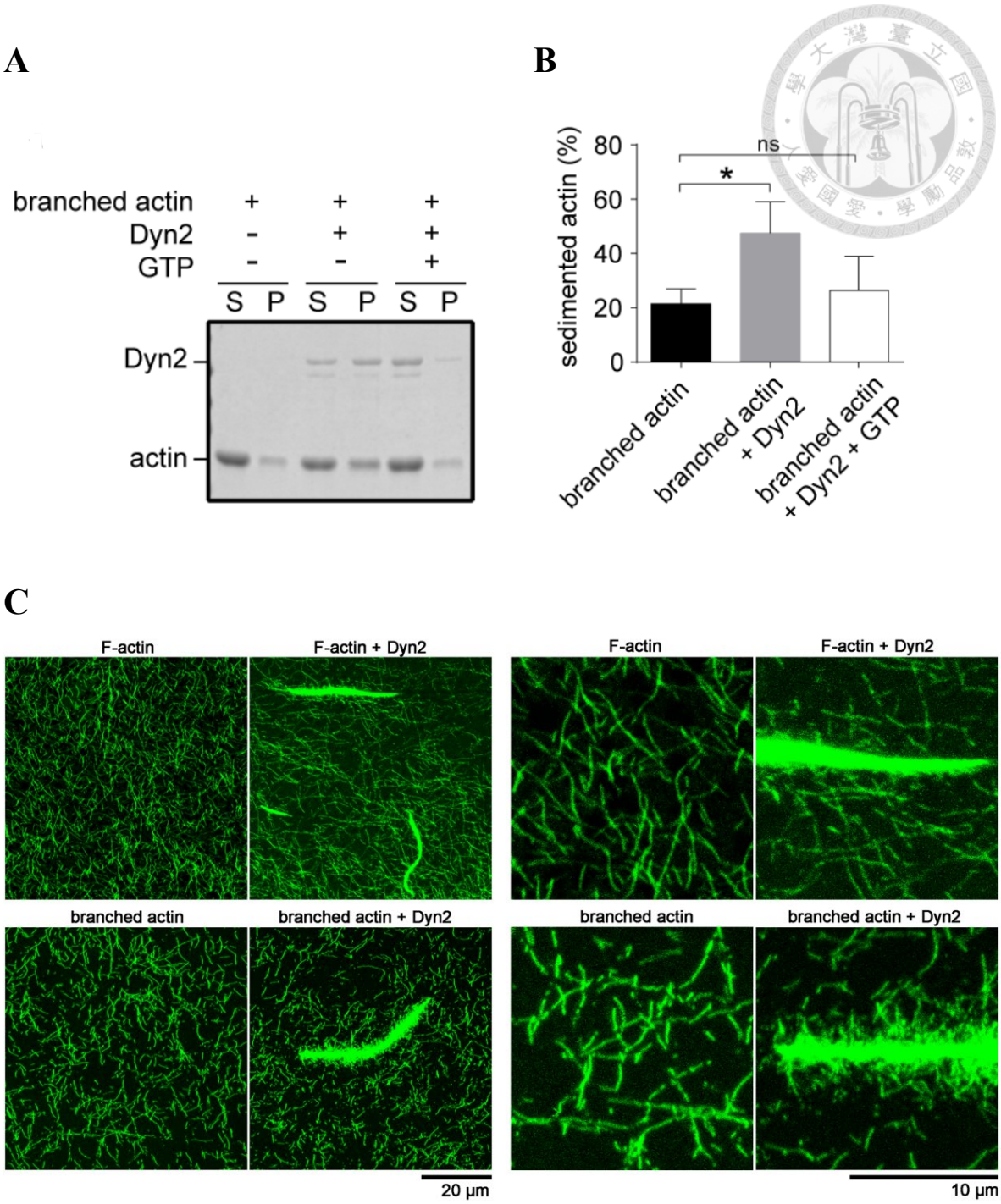

doi:10.6342/NTU202100043

Figure 44. GTP hydrolysis regulates disassembly of branched-actin bundles

(A-B) Branched F-actin sedimentation assay and quantification result of Dyn2-bundling activity. Concentrations of individual components were 5 μM actin, 1 μM Dyn2, 30 nM Arp2/3 complex, 80 nM VCA, and 1 mM GTP or GMPPCP. **(C)** Negative stain TEM images of branched actin in the presence of Dyn2, GTP, and GMPPCP. Scale bar, 100 nm. ns, not significant; *$p < 0.05$.

doi:10.6342/NTU202100043

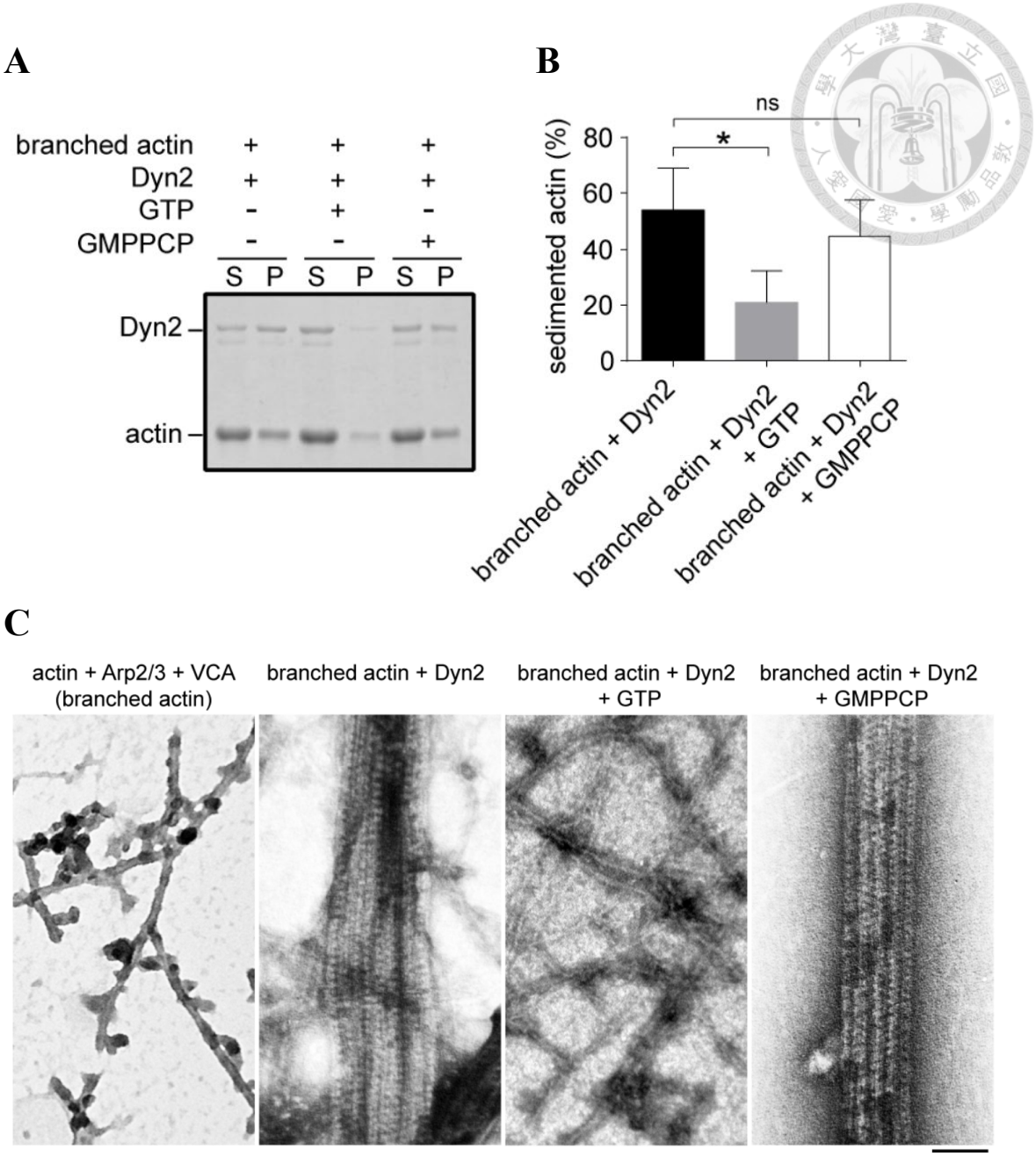

doi:10.6342/NTU202100043

Figure 45. branched-actin bundled by CNM-Dyn2 were less sensitive to GTP hydrolysis

(A-B) Branched-actin sedimentation assay and quantification of wild-type and CNM-Dyn2 bundling activity in the absence of GTP. **(C-D)** Branched-actin sedimentation assay and quantification of wild-type and CNM-Dyn2 bundling activity in the presence of GTP. ns, not significant; ***$p < 0.001$.

doi:10.6342/NTU202100043

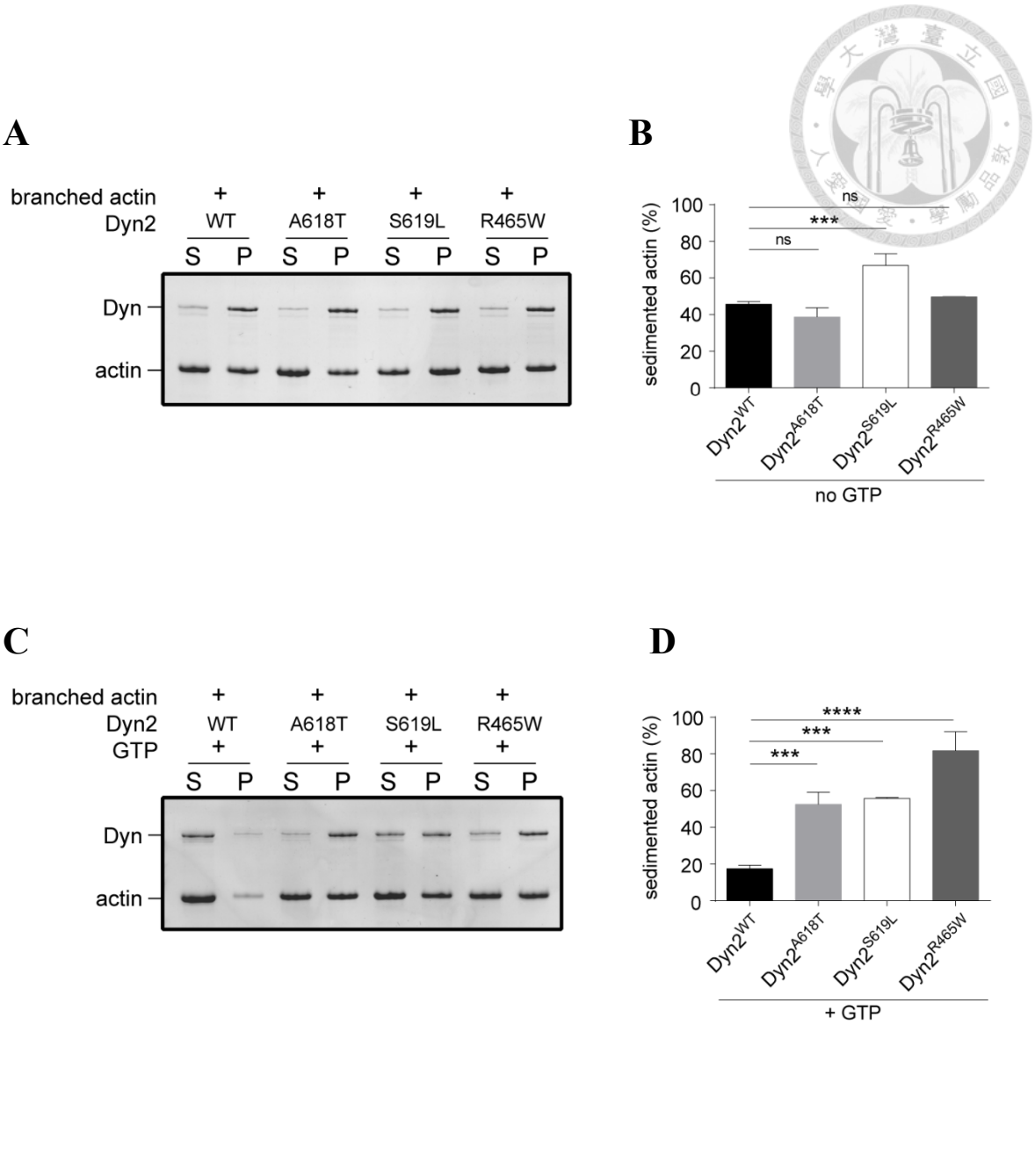

doi:10.6342/NTU202100043

Figure 46. Working model of Dyn2 in podosome turnover and its distinct role in pre- and postsynaptic NMJ

(A) Dyn2 functions as a molecular girdle and a checkpoint for podosome growth and turnover, respectively. (i and ii) Interactions between ECM and integrins initiate podosome formation. Actin polymerization proteins such as the Arp2/3 complex and cortactin drive podosome initiation. Tks5 is recruited to the nascent podosome and promotes podosome maturation. (iii) Phosphorylated Dyn2 is recruited to the podosome to bundle the actin core and facilitate its growth. Dyn2 forms a belt-like structure around the actin core to enhance the function of the podosome. (iv and v) GTP hydrolysis triggers Dyn2 dissociation from the podosome and induces its turnover. **(B)** Distinct roles of Dyn at pre- and postsynaptic NMJs. At the presynaptic membrane, Dyn functions as a membrane scission catalyzer to facilitate synaptic vesicle recycling. At the postsynaptic membrane, Dyn functions as a molecular girdle at synaptic podosomes and regulates actin organization during NMJ development.

doi:10.6342/NTU202100043

A

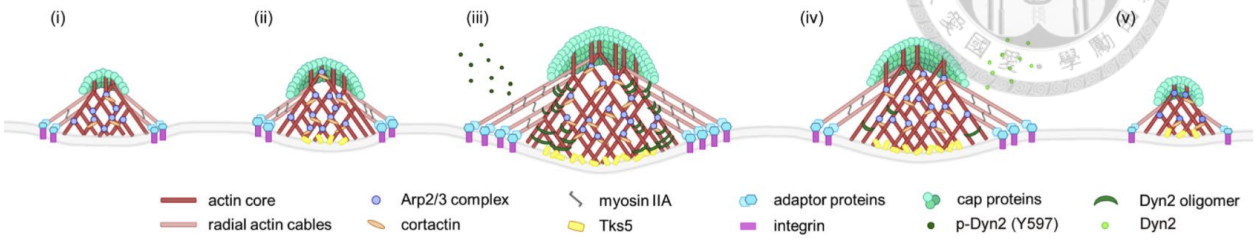

B

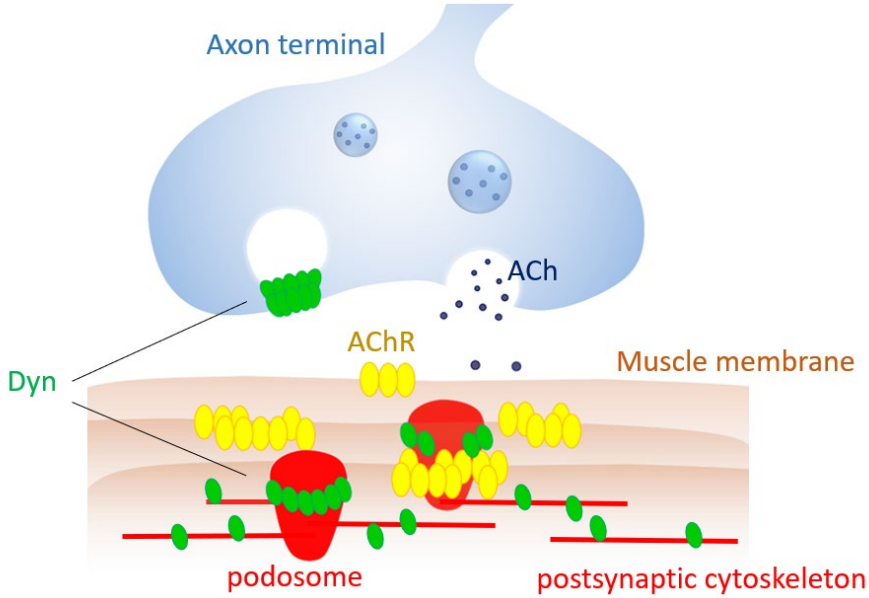

doi:10.6342/NTU202100043

Table 1. Plasmids used in this study

Plasmid	vector	source
Dyn2	pIEx-6	Schmid lab[#]
Dyn2^{A618T}	pIEx-6	(Chin et al., 2015)
Dyn2^{G537C}	pIEx-6	(Chin et al., 2015)
Dyn2^{R465W}	pIEx-6	(Chin et al., 2015)
Dyn2^{S619L}	pIEx-6	(Chin et al., 2015)
Dyn2^{Y597E}	pIEx-6	In this study
Dyn2^{Y597F}	pIEx-6	In this study
Dyn2-mCherry	pmCherry-N1	Addgene 27689
Dyn2^{A618T}-mCherry	pmCherry-N1	(Chin et al., 2015)
Dyn2^{G537C}-mCherry	pmCherry-N1	(Chin et al., 2015)
Dyn2^{K44A}-mCherry	pmCherry-N1	In this study
Dyn2$^{K/E}$-mCherry	pmCherry-N1	In this study
Dyn2$^{E/K}$-mCherry	pmCherry-N1	In this study
Dyn2^{Y597F}-mCherry	pmCherry-N1	In this study
Dyn2^{Y597E}-mCherry	pmCherry-N1	In this study
Lifeact-GFP	pEGFP	Schmid lab[#]
Tks5-GFP	pEGFP	Schmid lab[#]
Cortactin-mCherry		Addgene 27676
Dyn2	pADtet	Schmid lab[#]
Dyn2^{K44A}	pADtet	Schmid lab[#]
Dyn2^{G537C}	pADtet	(Chin et al., 2015)
Dyn2^{A618T}	pADtet	(Chin et al., 2015)
Dyn2$^{K/E}$	pADtet	(Chin et al., 2015)
Dyn2$^{E/K}$	pADtet	(Chin et al., 2015)

[#]Dr. Sandra Schmid in the Department of Cell Biology, University of Texas Southwestern Medical Center, Dallas, TX 75390, USA

doi:10.6342/NTU202100043

Table 2. Antibodies used in this study

REAGENT or RESOURCE	SOURCE	IDENTIFIER
Goat polyclonal anti-Dynamin-2	Santa Cruz	Cat#sc-6400; RRID: AB_639943
Rabbit polyclonal anti-Tks5	Santa Cruz	Cat#sc-30122; RRID: AB_2254551
Rabbit polyclonal anti-Cortactin	Santa Cruz	Cat#sc-11408; RRID: AB_2088281
Mouse monoclonal anti-Arp2	Abcam	Cat#ab49674; RRID: AB_867730
Mouse monoclonal anti-Vinculin	Sigma-Aldrich	Cat#V4505; RRID: AB_477617
Rabbit polyclonal anti-Myosin IIA	Sigma-Aldrich	Cat#M8064; RRID: AB_260673
Mouse monoclonal anti-HA	Biolegend	Cat#901513; RRID: AB_2565335
Rabbit polyclonal anti-HA	Santa Cruz	Cat#sc-805; RRID: AB_631618
Mouse monoclonal anti-Discs large	Developmental Studies Hybridoma Bank	Cat#4F3 anti-discs large; RRID: AB_528203
Mouse monoclonal anti-alpha spectrin	Developmental Studies Hybridoma Bank	Cat#3A9 (323 or M10-2); RRID: AB_528473
Mouse monoclonal anti-Brunchpilot	Developmental Studies Hybridoma Bank	Cat#nc82; RRID: AB_2314866
Mouse monoclonal anti-Glutamate receptor subunit, DGluR-IIA	Developmental Studies Hybridoma Bank	Cat#8B4D2 (MH2B); RRID: AB_528269
Rhodamine-conjugated rabbit polyclonal anti-horseradish peroxidase	Jackson ImmunoResearch	Cat#323-025-021; RRID: AB_2340257

doi:10.6342/NTU202100043

Rabbit monoclonal anti-Synaptophysin	Invitrogen	Cat#MA5-14532; RRID: AB_10983675
Alexa Fluor 488-conjugated donkey polyclonal anti-goat IgG	Invitrogen	Cat#A-11055; RRID: AB_2534102
Alexa Fluor 594-conjugated donkey polyclonal anti-goat IgG	Invitrogen	Cat#A-11058; RRID: AB_142540
Alexa Fluor 594-conjugated donkey polyclonal anti-rabbit IgG	Invitrogen	Cat#A-21207; RRID: AB_141637
Alexa Fluor 594-conjugated donkey polyclonal anti-mouse IgG	Invitrogen	Cat#A-21203; RRID: AB_141633
Alexa Fluor 405-conjugated donkey polyclonal anti-mouse IgG	Abcam	Cat#ab175659;

Chapter 6-References

Antonny, B., Burd, C., De Camilli, P., Chen, E., Daumke, O., Faelber, K., Ford, M., Frolov, V.A., Frost, A., Hinshaw, J.E., *et al.* (2016). Membrane fission by dynamin: what we know and what we need to know. The EMBO journal *35*, 2270-2284.

Au - Murray, L., Au - Gillingwater, T.H., and Au - Kothary, R. (2014). Dissection of the Transversus Abdominis Muscle for Whole-mount Neuromuscular Junction Analysis. JoVE, e51162.

Bashkirov, P.V., Akimov, S.A., Evseev, A.I., Schmid, S.L., Zimmerberg, J., and Frolov, V.A. (2008). GTPase cycle of dynamin is coupled to membrane squeeze and release, leading to spontaneous fission. Cell *135*, 1276-1286.

Bernadzki, K.M., Rojek, K.O., and Prószyński, T.J. (2014). Podosomes in muscle cells and their role in the remodeling of neuromuscular postsynaptic machinery. European Journal of Cell Biology *93*, 478-485.

Bezakova, G., and Ruegg, M.A. (2003). New insights into the roles of agrin. Nat Rev Mol Cell Biol *4*, 295-308.

Bitoun, M., Maugenre, S., Jeannet, P.Y., Lacene, E., Ferrer, X., Laforet, P., Martin, J.J., Laporte, J., Lochmuller, H., Beggs, A.H., *et al.* (2005). Mutations in dynamin 2 cause

doi:10.6342/NTU202100043

dominant centronuclear myopathy. Nature genetics *37*, 1207-1209.
Blunk, A.D., Akbergenova, Y., Cho, R.W., Lee, J., Walldorf, U., Xu, K., Zhong, G., Zhuang, X., and Littleton, J.T. (2014). Postsynaptic actin regulates active zone spacing and glutamate receptor apposition at the Drosophila neuromuscular junction. Mol Cell Neurosci *61*, 241-254.
Bruzzaniti, A., Neff, L., Sanjay, A., Horne, W.C., De Camilli, P., and Baron, R. (2005). Dynamin forms a Src kinase-sensitive complex with Cbl and regulates podosomes and osteoclast activity. Molecular biology of the cell *16*, 3301-3313.
Budnik, V., Koh, Y.H., Guan, B., Hartmann, B., Hough, C., Woods, D., and Gorczyca, M. (1996). Regulation of synapse structure and function by the Drosophila tumor suppressor gene dlg. Neuron *17*, 627-640.
Cervero, P., Wiesner, C., Bouissou, A., Poincloux, R., and Linder, S. (2018). Lymphocyte-specific protein 1 regulates mechanosensory oscillation of podosomes and actin isoform-based actomyosin symmetry breaking. Nature communications *9*, 515-515.
Chan, Z.C.-K., Kwan, H.-L.R., Wong, Y.S., Jiang, Z., Zhou, Z., Tam, K.W., Chan, Y.-S., Chan, C.B., and Lee, C.W. (2020). Site-directed MT1-MMP trafficking and surface insertion regulate AChR clustering and remodeling at developing NMJs. eLife *9*, e54379.
Chappie, J.S., Acharya, S., Leonard, M., Schmid, S.L., and Dyda, F. (2010). G domain dimerization controls dynamin's assembly-stimulated GTPase activity. Nature *465*, 435-440.
Chappie, J.S., Mears, J.A., Fang, S., Leonard, M., Schmid, S.L., Milligan, R.A., Hinshaw, J.E., and Dyda, F. (2011). A pseudoatomic model of the dynamin polymer identifies a hydrolysis-dependent powerstroke. Cell *147*, 209-222.
Chin, Y.H., Lee, A., Kan, H.W., Laiman, J., Chuang, M.C., Hsieh, S.T., and Liu, Y.W. (2015). Dynamin-2 mutations associated with centronuclear myopathy are hypermorphic and lead to T-tubule fragmentation. Human molecular genetics *24*, 5542-5554.
Chuang, M.C., Lin, S.S., Ohniwa, R.L., Lee, G.H., Su, Y.A., Chang, Y.C., Tang, M.J., and Liu, Y.W. (2019). Tks5 and Dynamin-2 enhance actin bundle rigidity in invadosomes to promote myoblast fusion. The Journal of cell biology *218*, 1670-1685.
Cowling, B.S., Toussaint, A., Amoasii, L., Koebel, P., Ferry, A., Davignon, L., Nishino, I., Mandel, J.L., and Laporte, J. (2011). Increased expression of wild-type or a centronuclear myopathy mutant of dynamin 2 in skeletal muscle of adult mice leads to structural defects and muscle weakness. Am J Pathol *178*, 2224-2235.
Destaing, O., Ferguson, S.M., Grichine, A., Oddou, C., De Camilli, P., Albiges-Rizo, C.,

doi:10.6342/NTU202100043

and Baron, R. (2013). Essential Function of Dynamin in the Invasive Properties and Actin Architecture of v-Src Induced Podosomes/Invadosomes. PLoS One *8*, e77956.

Destaing, O., Saltel, F., Géminard, J.-C., Jurdic, P., and Bard, F. (2002). Podosomes Display Actin Turnover and Dynamic Self-Organization in Osteoclasts Expressing Actin-Green Fluorescent Protein. Molecular Biology of the Cell *14*, 407-416.

Faelber, K., Gao, S., Held, M., Posor, Y., Haucke, V., Noe, F., and Daumke, O. (2013). Oligomerization of dynamin superfamily proteins in health and disease. Prog Mol Biol Transl Sci *117*, 411-443.

Ferguson, S.M., Brasnjo, G., Hayashi, M., Wolfel, M., Collesi, C., Giovedi, S., Raimondi, A., Gong, L.W., Ariel, P., Paradise, S.*, et al.* (2007). A selective activity-dependent requirement for dynamin 1 in synaptic vesicle endocytosis. Science *316*, 570-574.

Ferguson, S.M., and De Camilli, P. (2012). Dynamin, a membrane-remodelling GTPase. Nat Rev Mol Cell Biol *13*, 75-88.

Ferraro, E., Molinari, F., and Berghella, L. (2012). Molecular control of neuromuscular junction development. Journal of cachexia, sarcopenia and muscle *3*, 13-23.

Gibbs, E.M., Clarke, N.F., Rose, K., Oates, E.C., Webster, R., Feldman, E.L., and Dowling, J.J. (2013). Neuromuscular junction abnormalities in DNM2-related centronuclear myopathy. Journal of molecular medicine (Berlin, Germany) *91*, 727-737.

Gibbs, E.M., Davidson, A.E., Telfer, W.R., Feldman, E.L., and Dowling, J.J. (2014). The myopathy-causing mutation DNM2-S619L leads to defective tubulation in vitro and in developing zebrafish. Dis Model Mech *7*, 157-161.

Gu, C., Yaddanapudi, S., Weins, A., Osborn, T., Reiser, J., Pollak, M., Hartwig, J., and Sever, S. (2010). Direct dynamin-actin interactions regulate the actin cytoskeleton. The EMBO journal *29*, 3593-3606.

Guiet, R., Verollet, C., Lamsoul, I., Cougoule, C., Poincloux, R., Labrousse, A., Calderwood, D.A., Glogauer, M., Lutz, P.G., and Maridonneau-Parini, I. (2012). Macrophage mesenchymal migration requires podosome stabilization by filamin A. J Biol Chem *287*, 13051-13062.

Hinshaw, J.E. (2000). Dynamin and Its Role in Membrane Fission. Annual review of cell and developmental biology *16*, 483-519.

Hohendahl, A., Roux, A., and Galli, V. (2016). Structural insights into the centronuclear myopathy-associated functions of BIN1 and dynamin 2. J Struct Biol *196*, 37-47.

Jameson, D.M. (2014). Introduction to Fluorescence (CRC Press).

Kenniston, J.A., and Lemmon, M.A. (2010). Dynamin GTPase regulation is altered by

doi:10.6342/NTU202100043

PH domain mutations found in centronuclear myopathy patients. The EMBO journal *29*, 3054-3067.

Kishi, M., Kummer, T.T., Eglen, S.J., and Sanes, J.R. (2005). LL5beta: a regulator of postsynaptic differentiation identified in a screen for synaptically enriched transcripts at the neuromuscular junction. The Journal of cell biology *169*, 355-366.

Kong, L., Sochacki, K.A., Wang, H., Fang, S., Canagarajah, B., Kehr, A.D., Rice, W.J., Strub, M.P., Taraska, J.W., and Hinshaw, J.E. (2018). Cryo-EM of the dynamin polymer assembled on lipid membrane. Nature *560*, 258-262.

Kummer , T.T., Misgeld , T., Lichtman , J.W., and Sanes , J.R. (2004). Nerve-independent formation of a topologically complex postsynaptic apparatus. The Journal of cell biology *164*, 1077-1087.

Labernadie, A., Bouissou, A., Delobelle, P., Balor, S., Voituriez, R., Proag, A., Fourquaux, I., Thibault, C., Vieu, C., Poincloux, R.*, et al.* (2014). Protrusion force microscopy reveals oscillatory force generation and mechanosensing activity of human macrophage podosomes. Nat Commun *5*, 5343.

Lee, G., and Schwarz, T.L. (2016). Filamin, a synaptic organizer in Drosophila, determines glutamate receptor composition and membrane growth. eLife *5*, e19991.

Lin, S.-S., Chuang, M.-C., and Liu, Y.-W. (2019). F-actin Bundle Sedimentation Assay. Bio-protocol *9*, e3419.

Lin, S.-S., Hsieh, T.-L., Liou, G.-G., Li, T.-N., Lin, H.-C., Chang, C.-W., Wu, H.-Y., Yao, C.-K., and Liu, Y.-W. (2020). Dynamin-2 Regulates Postsynaptic Cytoskeleton Organization and Neuromuscular Junction Development. Cell Reports *33*, 108310.

Lin, W., Burgess, R.W., Dominguez, B., Pfaff, S.L., Sanes, J.R., and Lee, K.F. (2001). Distinct roles of nerve and muscle in postsynaptic differentiation of the neuromuscular synapse. Nature *410*, 1057-1064.

Linder, S. (2007). The matrix corroded: podosomes and invadopodia in extracellular matrix degradation. Trends in Cell Biology *17*, 107-117.

Linder, S., and Aepfelbacher, M. (2003). Podosomes: adhesion hot-spots of invasive cells. Trends in Cell Biology *13*, 376-385.

Linder, S., and Kopp, P. (2005). Podosomes at a glance. J Cell Sci *118*, 2079.

Linder, S., and Wiesner, C. (2016). Feel the force: Podosomes in mechanosensing. Experimental Cell Research *343*, 67-72.

Liu, Y.W., Neumann, S., Ramachandran, R., Ferguson, S.M., Pucadyil, T.J., and Schmid, S.L. (2011). Differential curvature sensing and generating activities of dynamin isoforms

doi:10.6342/NTU202100043

provide opportunities for tissue-specific regulation. Proc Natl Acad Sci U S A *108*, E234-242.

Luxenburg, C., Geblinger, D., Klein, E., Anderson, K., Hanein, D., Geiger, B., and Addadi, L. (2007). The architecture of the adhesive apparatus of cultured osteoclasts: from podosome formation to sealing zone assembly. PLoS One *2*, e179-e179.

Luxenburg, C., Winograd-Katz, S., Addadi, L., and Geiger, B. (2012). Involvement of actin polymerization in podosome dynamics. Journal of cell science *125*, 1666-1672.

Marques, M.J., Conchello, J.-A., and Lichtman, J.W. (2000). From Plaque to Pretzel: Fold Formation and Acetylcholine Receptor Loss at the Developing Neuromuscular Junction. The Journal of Neuroscience *20*, 3663.

Marrus, S.B., Portman, S.L., Allen, M.J., Moffat, K.G., and DiAntonio, A. (2004). Differential localization of glutamate receptor subunits at the Drosophila neuromuscular junction. J Neurosci *24*, 1406-1415.

McNiven, M.A., Kim, L., Krueger, E.W., Orth, J.D., Cao, H., and Wong, T.W. (2000). Regulated Interactions between Dynamin and the Actin-Binding Protein Cortactin Modulate Cell Shape. The Journal of cell biology *151*, 187.

Menon, M., and Schafer, D.A. (2013). Chapter Three - Dynamin: Expanding Its Scope to the Cytoskeleton. In International Review of Cell and Molecular Biology, K.W. Jeon, ed. (Academic Press), pp. 187-219.

Mooren, O.L., Kotova, T.I., Moore, A.J., and Schafer, D.A. (2009). Dynamin2 GTPase and cortactin remodel actin filaments. J Biol Chem *284*, 23995-24005.

Newton, A.J., Kirchhausen, T., and Murthy, V.N. (2006). Inhibition of dynamin completely blocks compensatory synaptic vesicle endocytosis. Proceedings of the National Academy of Sciences *103*, 17955-17960.

Obar, R.A., Collins, C.A., Hammarback, J.A., Shpetner, H.S., and Vallee, R.B. (1990). Molecular cloning of the microtubule-associated mechanochemical enzyme dynamin reveals homology with a new family of GTP-binding proteins. Nature *347*, 256-261.

Ochoa, G.-C., Slepnev, V.I., Neff, L., Ringstad, N., Takei, K., Daniell, L., Kim, W., Cao, H., McNiven, M., Baron, R.*, et al.* (2000). A Functional Link between Dynamin and the Actin Cytoskeleton at Podosomes. The Journal of cell biology *150*, 377.

Pan, Y.R., Chen, C.L., and Chen, H.C. (2011). FAK is required for the assembly of podosome rosettes. J Cell Biol *195*, 113-129.

Peng, J.-J., Lin, S.-H., Liu, Y.-T., Lin, H.-C., Li, T.-N., and Yao, C.-K. (2019). A circuit-dependent ROS feedback loop mediates glutamate excitotoxicity to sculpt the Drosophila

doi:10.6342/NTU202100043

motor system. eLife *8*, e47372.

Pęziński, M., Daszczuk, P., Pradhan, B.S., Lochmüller, H., and Prószyński, T.J. (2020). An improved method for culturing myotubes on laminins for the robust clustering of postsynaptic machinery. Scientific Reports *10*, 4524.

Pielage, J., Fetter, R.D., and Davis, G.W. (2006). A postsynaptic Spectrin scaffold defines active zone size, spacing, and efficacy at the Drosophila neuromuscular junction. The Journal of cell biology *175*, 491.

Proszynski, T.J., Gingras, J., Valdez, G., Krzewski, K., and Sanes, J.R. (2009a). Podosomes are present in a postsynaptic apparatus and participate in its maturation. Proceedings of the National Academy of Sciences *106*, 18373.

Proszynski, T.J., Gingras, J., Valdez, G., Krzewski, K., and Sanes, J.R. (2009b). Podosomes are present in a postsynaptic apparatus and participate in its maturation. Proceedings of the National Academy of Sciences of the United States of America *106*, 18373-18378.

Proszynski, T.J., and Sanes, J.R. (2013). Amotl2 interacts with LL5beta, localizes to podosomes and regulates postsynaptic differentiation in muscle. J Cell Sci *126*, 2225-2235.

Pucadyil, T.J., and Schmid, S.L. (2008). Real-time visualization of dynamin-catalyzed membrane fission and vesicle release. Cell *135*, 1263-1275.

Raimondi, A., Ferguson, S.M., Lou, X., Armbruster, M., Paradise, S., Giovedi, S., Messa, M., Kono, N., Takasaki, J., Cappello, V*., et al.* (2011). Overlapping role of dynamin isoforms in synaptic vesicle endocytosis. Neuron *70*, 1100-1114.

Romero, N.B. (2010). Centronuclear myopathies: a widening concept. Neuromuscul Disord *20*, 223-228.

Schafer, D.A. (2004). Regulating actin dynamics at membranes: a focus on dynamin. Traffic *5*, 463-469.

Seals, D.F., Azucena, E.F., Jr., Pass, I., Tesfay, L., Gordon, R., Woodrow, M., Resau, J.H., and Courtneidge, S.A. (2005). The adaptor protein Tks5/Fish is required for podosome formation and function, and for the protease-driven invasion of cancer cells. Cancer cell *7*, 155-165.

Shi, L., Fu, A.K., and Ip, N.Y. (2012). Molecular mechanisms underlying maturation and maintenance of the vertebrate neuromuscular junction. Trends Neurosci *35*, 441-453.

Sidiropoulos, P.N., Miehe, M., Bock, T., Tinelli, E., Oertli, C.I., Kuner, R., Meijer, D., Wollscheid, B., Niemann, A., and Suter, U. (2012). Dynamin 2 mutations in Charcot-

doi:10.6342/NTU202100043

Marie-Tooth neuropathy highlight the importance of clathrin-mediated endocytosis in myelination. Brain *135*, 1395-1411.

Tinelli, E., Pereira, J.A., and Suter, U. (2013). Muscle-specific function of the centronuclear myopathy and Charcot–Marie–Tooth neuropathy-associated dynamin 2 is required for proper lipid metabolism, mitochondria, muscle fibers, neuromuscular junctions and peripheral nerves. Human molecular genetics *22*, 4417-4429.

Van Audenhove, I., Debeuf, N., Boucherie, C., and Gettemans, J. (2015). Fascin actin bundling controls podosome turnover and disassembly while cortactin is involved in podosome assembly by its SH3 domain in THP-1 macrophages and dendritic cells. Biochimica et Biophysica Acta (BBA) - Molecular Cell Research *1853*, 940-952.

van den Dries, K., Bolomini-Vittori, M., and Cambi, A. (2014). Spatiotemporal organization and mechanosensory function of podosomes. Cell Adh Migr *8*, 268-272.

van den Dries, K., Meddens, M.B.M., de Keijzer, S., Shekhar, S., Subramaniam, V., Figdor, C.G., and Cambi, A. (2013). Interplay between myosin IIA-mediated contractility and actin network integrity orchestrates podosome composition and oscillations. Nature Communications *4*, 1412.

van der Bliek, A.M., and Meyerowitz, E.M. (1991). Dynamin-like protein encoded by the Drosophila shibire gene associated with vesicular traffic. Nature *351*, 411-414.

Wu, H., Xiong, W.C., and Mei, L. (2010). To build a synapse: signaling pathways in neuromuscular junction assembly. Development *137*, 1017-1033.

Yang, X., Arber, S., William, C., Li, L., Tanabe, Y., Jessell, T.M., Birchmeier, C., and Burden, S.J. (2001). Patterning of Muscle Acetylcholine Receptor Gene Expression in the Absence of Motor Innervation. Neuron *30*, 399-410.

Zhang, R., Lee, D.M., Jimah, J.R., Gerassimov, N., Yang, C., Kim, S., Luvsanjav, D., Winkelman, J., Mettlen, M., Abrams, M.E.*, et al.* (2020). Dynamin regulates the dynamics and mechanical strength of the actin cytoskeleton as a multifilament actin-bundling protein. Nature Cell Biology.

Zhao, M., Maani, N., and Dowling, J.J. (2018). Dynamin 2 (DNM2) as Cause of, and Modifier for, Human Neuromuscular Disease. Neurotherapeutics *15*, 966-975.

Zuchner, S., Noureddine, M., Kennerson, M., Verhoeven, K., Claeys, K., De Jonghe, P., Merory, J., Oliveira, S.A., Speer, M.C., Stenger, J.E.*, et al.* (2005). Mutations in the pleckstrin homology domain of dynamin 2 cause dominant intermediate Charcot-Marie-Tooth disease. Nature genetics *37*, 289-294.

doi:10.6342/NTU202100043